

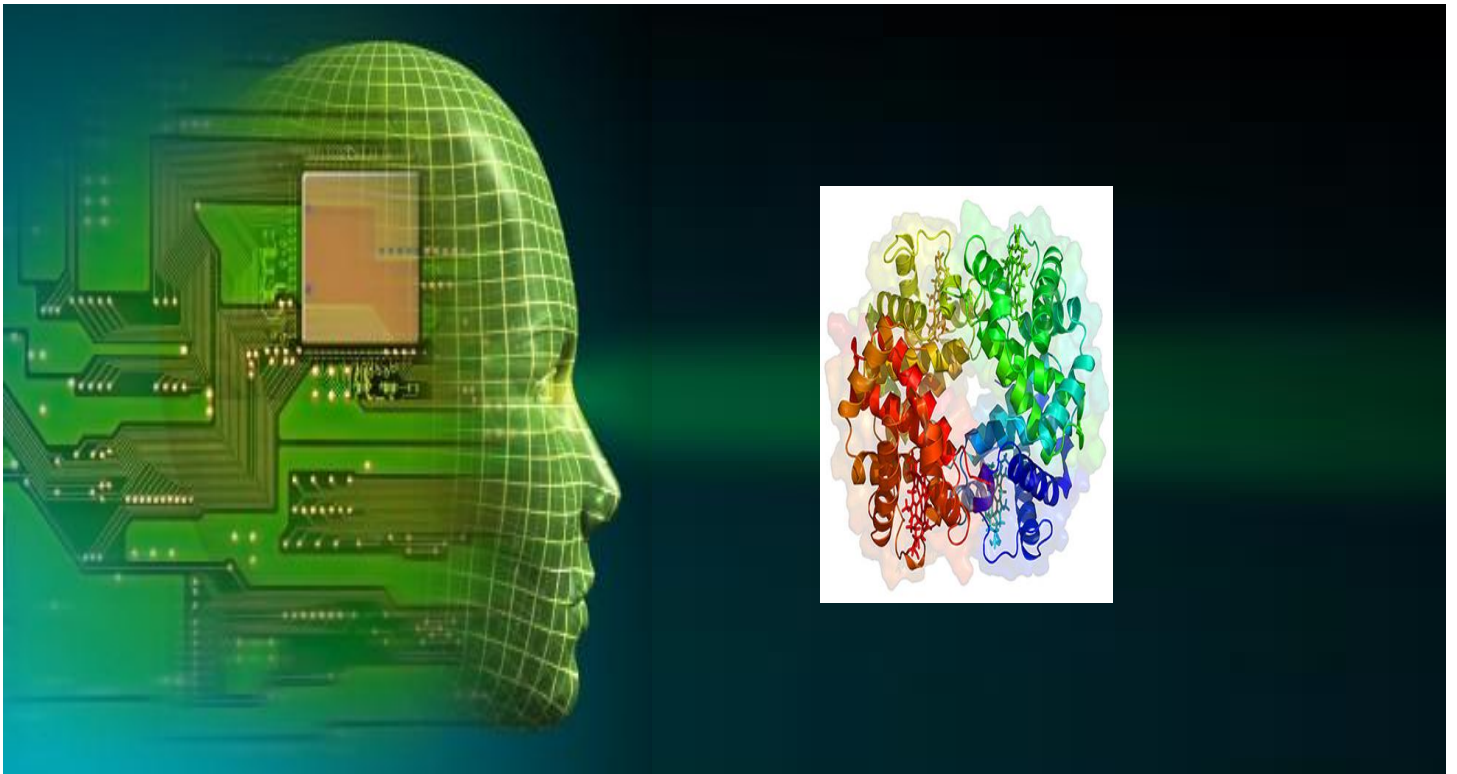
Fuzzy Logic Hemoglobin Sensors

Zur Erlangung des akademischen Grades eines

DOKTOR-INGENIEURS

von

M. Sc. Eng. Kawther Abo Alam



Karlsruhe Institute of Technology

Fuzzy Logic Hemoglobin Sensors

Zur Erlangung des akademischen Grades eines

DOKTOR-INGENIEURS

von der Fakultät für

Elektrotechnik und Informationstechnik

des Karlsruher Instituts für Technologie (KIT)

vorgelegte

DISSERTATION

von

M. Sc. Eng. Kawther Abo Alam

Geb. in: El-Minoufia,

Ägypten.

Tag der mündlichen Prüfung: 10.05.2011

Hauptreferent: Prof. Dr. rer. nat. Armin Bolz

Korreferent: Prof. Dr. rer. nat. Josef Guttman



Karlsruhe Institute of Technology

INSTITUT FÜR BIOMEDIZINISCHE TECHNIK

KARLSRUHER INSTITUT FÜR TECHNOLOGIE (KIT)

List of Contents:

Introduction	14
1.1 Motivation	14
1.2 Research objectives	16
1.2.1 Non-invasive measuring	16
1.2.2 Invasive measuring	16
1.3 Thesis outline	17
Part I: Background and Current State of the Art	18
Physiological Foundations	20
2.1 Preliminaries	20
2.2 Blood composition and functions	20
2.2.1 Blood composition	20
2.2.2 Blood functions	21
2.3 Hemoglobin	22
2.3.1 Hemoglobin function	23
2.3.2 Hemoglobin structure	24
2.3.3 Hemoglobinopathy	25
2.3.4 Hemoglobin test	26
Pulse Oximetry	28
3.1 Preliminaries	28
3.2 Photoplethysmography	29
3.2.1 The photoplethysmography waveform	31
3.3 Light absorbance basics	32
3.4 Light absorbance in pulse oximetry and estimation of oxygen saturation	34
3.4.1 Light absorbance in pulse oximetry	34
3.4.2 Estimation of functional arterial oxygen saturation	36
3.5 Pulse oximetry limitations	40
3.5.1 Physiological limitations	40
3.5.2 Interference from substances	41
3.5.3 Limitation in the signal processing	43
3.5.4 Physical factors	45

3.6	Current state of the art.....	46
3.6.1	The previous work towards the non-invasive determination of the fractional oxygen saturation and the total hemoglobin concentration	46
3.6.2	Artificial intelligent applications for PPG signal	47
3.6.3	Non-invasive tHb concentration devices in the market.....	50
Part II: Methodology.....		52
Optoelectronic System Set-Up for Non-Invasive Measuring		54
4.1	Preliminaries	54
4.2	PPG signals extraction.....	54
4.2.1	Transimpedance amplifier circuit	56
4.2.2	LEDs drive circuit and control.....	58
4.3	Proposed low perfusion signal processing module	60
4.3.1	Functional block diagram of the proposed signal processing module.....	61
4.3.2	The proposed signal processing module evaluation.....	65
4.4	Flow chart of the software processing outline	67
4.5	Overview of the optoelectronic system output	68
Proposed Estimation Approaches for Non-Invasive Measuring.....		70
5.1	Preliminaries	70
5.2	PPGs main distinctive features extracting	70
5.3	Proposed algorithm based on modified Lambert-Beer law	74
5.3.1	Modified Lambert-Beer law	74
5.3.2	Modified Lambert-Beer law revisited for PPG signals	75
5.3.3	Extinction coefficients of the four hemoglobin components	79
5.3.4	Proposed indication for Δd applying.....	80
5.3.5	Recommended strategy of estimation based on modified Lambert-Beer law	82
5.4	Proposed algorithm based on fuzzy logic systems	87
5.4.1	Introduction to fuzzy logic	87
5.4.3.1	Architecture of fuzzy logic systems	87
5.4.2	Reasons behind using fuzzy logic system	89
5.4.3	Building the fuzzy logic expert system	90
5.4.3.1	Defining the crisp inputs and outputs of the fuzzy system	90
5.4.3.2	Employing the fuzzy inference scheme	91
5.4.3.3	Fuzzy rule base generation.....	93
5.4.3.4	Data flow of the proposed fuzzy expert system	94
Proposed Estimation Algorithm for Invasive Measuring		96
6.1	Preliminaries	96
6.2	Building the fuzzy expert system.....	96

LIST OF CONTENTS

6.2.1	Defining the crisp inputs and outputs of the fuzzy expert system	96
6.2.2	Employing the fuzzy inference scheme.....	98
6.2.3	Fuzzy rule base generation	98
6.3	The whole fuzzy expert system.....	98
Part III: Results and Conclusions		100
Results and Discussion.....		102
7.1	Preliminaries	102
7.2	Results: non-invasive measuring	102
7.2.1	Results of the method that is based on modified Lambert-Beer law.....	104
7.2.2	Results of fuzzy expert system algorithm.....	111
7.3	Results: invasive measuring	115
7.4	Discussion of the results	121
7.4.1	Non-invasive measuring results	121
7.4.2	Invasive measuring results	123
Conclusions and Future Work.....		125
8.1	Preliminaries	125
8.2	Contributions and conclusions	125
8.2.1	Non-invasive measuring.....	125
8.2.2	Invasive measuring	127
8.3	Future work.....	128
Appendix : The printed circuit layouts		129
References		131
Acknowledgements		141
Publications list and Awards.....		142
Curriculum Vitae.....		145

List of Figures:

Figure 2-1: Red blood cells and hemoglobin [Lom11].	22
Figure 2-2: 3-D Ribbon Structure of the hemoglobin molecule. Each of the 4 globin chains is represented in a different color. The heme molecule is shown in red [Psc11].	24
Figure 2-3: Heme molecule. Porphyrin ring with iron atom ligand bound inside [Oml11].	25
Figure 3-1: Several plethysmographic vein occlusion sensors and systems: strain gauge and fiber sensor (a), water plethysmograph (b), impedance plethysmograph (c), air plethysmograph sensor (d), Computer supported gravimetric plethysmograph (e), and microwave plethysmograph (f) [Nop01].	30
Figure 3-2: Transmission photoplethysmography (left) versus reflective photoplethysmography (right).	31
Figure 3-3: The pulsatile (AC) component of the PPG signal and corresponding electrocardiogram (ECG) [All07].	31
Figure 3-4: Absorbed light in living tissue [Web09].	32
Figure 3-5: Description of Lambert-Beer's law that controls the absorption of light travelling through a uniform substance.	33
Figure 3-6: Color difference between oxygenated and deoxygenated hemoglobin [Alt11].	35
Figure 3-7: Extinction coefficients of RHb and O ₂ Hb (a) and the interesting wavelength regions of the red light and the infrared light by pulse oximetry (b) [Web06] [Adv11].	35
Figure 3-8: A sketch of a finger pulse oximeter (a) and a generated PPG signal (b).	37
Figure 3-9: Lambert-Beer's law in pulse oximetry [Wie97] [Bol02].	37
Figure 3-10: Typical calibration curves for pulse oximeters [Wie97].	39
Figure 3-11: Oxyhemoglobin dissociation curve, i.e., the relationship between arterial oxygen saturation and arterial partial pressure [Wik11].	40
Figure 3-12: SpO ₂ and O ₂ Hb versus carboxyhemoglobin (COHb). SpO ₂ consistently overestimates saturation in the presence of COHb. At COHB= 70%, SpO ₂ is still roughly 90%, while O ₂ Hb has fallen to 30% [Bar87-].	41
Figure 3-13: Nellcor SpO ₂ readings (circles) and invasive SaO ₂ (squares) versus MetHb%. Line shown is SaO ₂ =100-MetHb% [Bar89].	42
Figure 4-1: Block diagram of the developed optoelectronic circuit.	55
Figure 4-2: The functional block diagram of ADUC7020 (Analog Devices) [Dat08].	56
Figure 4-3: Schematic diagram of the utilized transimpedance amplifier circuit.	56
Figure 4-4: Simulation of the transimpedance amplifier circuit output before adding a negative feedback capacitor [Zab08].	57

LIST OF FIGURES

Figure 4-5: Simulation of the transimpedance amplifier circuit output after adding a negative feedback capacitor [Zab08]..	58
Figure 4-6: Functional block diagrams of the LEDs drive circuit and control	59
Figure 4-7: Timing diagram of the LEDs synchronized illumination.	59
Figure 4-8: Flowchart of the LEDs intensity control loop.	60
Figure 4-9: The functional block diagram of the proposed signal processing module.	62
Figure 4-10: The analog differential amplifier circuit diagram.	62
Figure 4-11: Non-inverting amplifier circuit diagram.	63
Figure 4-12: Schematic diagram of the developed optoelectronic printed circuit for the PPG signals	64
Figure 4-13: Original PPG Signal (a1), Amplified PPG One (a2), their FFT in Different Ranges of Frequencies (b, c, d).	66
Figure 4-14: Flowchart of the software processing outline	67
Figure 4-15: The printed circuit of the optoelectronic system.	68
Figure 4-16: PPG signals separation in LabVIEW.	69
Figure 5-1: Peaks and valleys Detection by Peaks/Valleys detection VI.	71
Figure 5-2: Block diagram of the developed peaks and valleys detection algorithm in LabVIEW.	72
Figure 5-3: Desired peaks and valleys detection by the improved algorithm the ratios filter. ..	73
Figure 5-4: Relative visitation probabilities based on a Monte-Carlo random walk of photons are shown for red light transmitted through a simulated homogeneous tissue in (a) the absence of absorption and (b) with absorption consistent with human tissues [Man07].	75
Figure 5-5: PPG signal (transmitted light).	76
Figure 5-6: AC component and DC component of PPG signal (transmitted light).	78
Figure 5-7: The extinction coefficients of the four hemoglobin components [Web98].	79
Figure 5-8: Absorption coefficients of the hemoglobin versus water.	80
Figure 5-9: Seven extracted PPG signals using the developed optoelectronic system.	83
Figure 5-10: Functional block diagram of estimating tHb concentration process.	84
Figure 5-11: Functional block diagram of estimation the four hemoglobin ratios process.	86
Figure 5-12: Basic components of a fuzzy logic system	88
Figure 5-13: Mamdani's fuzzy inference scheme graphical interpretation for multi-inputs single-output system, as an example.	91
Figure 5-14: Data flow block diagram of the developed fuzzy expert system.	94
Figure 6-1: Extinction coefficients: ϵ_{O_2Hb} , ϵ_{RHb} , ϵ_{COHb} , and ϵ_{Met-Hb} at wavelengths between 600 nm and 1000 nm [Web98].	97
Figure 7-1: The LabVIEW front panel of the non-invasive measuring system.	104
Figure 7-2: Plot of tHb (g/dl) estimated vs. reference laboratory (RL) tHb (g/dl) measurements (Method-1-part1).	108
Figure 7-3: Plot of tHb (g/dl) estimated vs. reference laboratory (RL) tHb (g/dl) measurements (Method-1-part2).	110

Figure 7-4: Plot of tHb (g/dl) estimated vs. reference laboratory (RL) tHb (g/dl) measurements (Method-2).....	114
Figure 7-5: Plot of tHb (g/dl) estimated vs. Reference laboratory (RL) tHb (g/dl) measurements (D-Patch-1).	116
Figure 7-6: Plot of RHb% estimated vs. Reference laboratory (RL) RHb% measurements (D-Patch-1).	117
Figure 7-7: Plot of O ₂ Hb% estimated vs. Reference laboratory (RL) O ₂ Hb% measurements (D-Patch-1).	117
Figure 7-8: Plot of COHb% estimated vs. Reference laboratory (RL) COHb% measurements (D-Patch-1).	117
Figure 7-9: Plot of MetHb% estimated vs. Reference laboratory (RL) MetHb% measurements (D-Patch-1).	118
Figure 7-10: Plot of tHb (g/dl) estimated vs. reference laboratory (RL) tHb (g/dl) measurements of the training stage (D-Patch-2).....	119
Figure 7-11: Plot of O ₂ Hb% estimated vs. reference laboratory (RL) O ₂ Hb% measurements of the training stage (D-Patch-2).	119
Figure 7-12: Plot of RHb% estimated vs. reference laboratory (RL) RHb% measurements of the training stage (D-Patch-2).....	119
Figure 7-13: Plot of COHb% estimated vs. reference laboratory (RL) COHb% measurements of the training stage (D-Patch-2).	120
Figure 7-14: Plot of MetHb% estimated vs. reference laboratory (RL) MetHb% measurements of the training stage (D-Patch-2).....	120
Figure 7-15: Plot of tHb (g/dl) estimated vs. reference laboratory (RL) tHb (g/dl) measurements (Test-D-Patch-2).	121

List of Tables:

Table 5-1: Extinction coefficients of the four hemoglobin components at the employed wavelengths.	80
Table 5-2: Reference laboratory invasive measurements.	84
Table 5-3: Reference laboratory invasive measurements (four Hb components ratios)	86
Table 7-1: Root Mean Square error (RMS) of the results of the offline training stage (Method-1).	105
Table 7-2: Root Mean Square error (RMS) of the online test results (Method-1).	106
Table 7-3: Reference laboratory COHb% and its non-invasive value (Method-1-part1).	106
Table 7-4: Reference laboratory O2Hb% and its non-invasive value (Method-1-part1).	106
Table 7-5: Reference laboratory MetHb% and its non-invasive value (Method-1-part1).	107
Table 7-6: Reference laboratory RHb% and its non-invasive value (Method-1-part1).	107
Table 7-7: Reference laboratory tHb (g/dl) and its non-invasive value (Method-1-part1).	107
Table 7-8: Reference laboratory COHb% and its non-invasive value (Method-1-part2).	108
Table 7-9: Reference laboratory MetHb% and its non-invasive value (Method-1-part2).	109
Table 7-10: Reference laboratory RHb% and its non-invasive value (Method-1-part2).	109
Table 7-11: Reference laboratory tHb (g/dl) and its non-invasive value (Method-1-part2).	109
Table 7-12: Reproducibility test of (Method-1).	110
Table 7-13: Root mean square error (RMS) of the results of the offline training stage (method-2).	111
Table 7-14: Correlation (R) and root mean square (RMS) error of the online test results (Method-2).	111
Table 7-15: Reference laboratory COHb% and its non-invasive value (Method-2).	112
Table 7-16: Reference laboratory O2Hb% and its non-invasive value (Method-2).	112
Table 7-17: Reference laboratory MetHb% and its non-invasive value (Method-2).	112
Table 7-18: Reference laboratory RHb% and its non-invasive value (Method-2).	113
Table 7-19: Reference laboratory tHb (g/dl) and its non-invasive value (Method-2).	113
Table 7-20: Reproducibility test of (Method-2).	115
Table 7-21: Correlation and Root Mean Square error (RMS) of (D-Patch-1).	116
Table 7-22: Correlation and Root Mean Square error values of the training stage (D-Patch-2).	118

Table 8-1: Root Mean Square error (RMS) of the online test results for the proposed non-invasive methods.....126

**I dedicate this thesis to,,, my Father, my Mother, all my family,
soul of 25 January Egyptain revolution martyrs, and my lovely
persons in this world.**

1. Introduction

1.1 Motivation

Anaemia is common throughout the world. It is a condition that occurs when the hemoglobin level in the blood is low. Therefore, the red blood cells do not carry enough oxygen to the tissues of the body, as the hemoglobin is a protein-based component of the red blood cells that is responsible for transferring oxygen throughout the body's circulatory system. Anaemia affects all population groups. However, the most susceptible groups are pregnant women and young children. In the severe form, anaemia is associated with fatigue, weakness, dizziness and drowsiness. Without treatment, anaemia can worsen and becomes an underlying cause of chronic ill health, such as impaired fetal development during pregnancy, delayed cognitive development and increased risk of infection in young children, as well as reduced physical capacity in all people [WHO01].

Nine out of ten anaemia sufferers live in developing countries [WHO00]. The World Health Organization (WHO) reported that 1.6 billion people worldwide suffer from anaemia, although many more are suspected of being undiagnosed, with women and children at the highest risk [WHO02]. Anaemia may contribute up to 20% of maternal deaths [WHO01].

The current treatment of anaemia is dependent on measuring the total hemoglobin (tHb) concentration by invasive laboratory or Point-of-Care (POC) methods, using blood drawn from venipuncture or a finger stick. The test of tHb concentration is one of the most frequently requested tests in both acute care and outpatient settings, as anaemia is the most common amongst blood disorders.

Pulse oximeters measure the functional oxygen saturation of hemoglobin in arterial blood (SpO₂). Currently, these are widespread in operating rooms, recovery rooms, intensive

care, emergency medical aids, sleep medicine, home and other fields of medical care [Hil00] [Wuk88]. In spite of their wide applications for monitoring the SpO_2 , pulse oximeters have a lot of shortcomings, as demonstrated in detail in section 5.3. The most serious disadvantage of these devices is that the pulse oximetry will not detect carbon monoxide hemoglobin (COHb) and methemoglobin (MetHb). This leads to incorrect measurement of oxygen saturation by carbon monoxide poisoning and methemoglobinemia [Bar87] [Bar89]. Therefore, the fractional arterial oxygen saturation, which is the ratio of oxygenated hemoglobin concentration (O_2Hb) to the total hemoglobin concentration, has to be calculated. In these cases, the invasive measuring of the arterial oxygen saturation is conducted to measure the fractional oxygen saturation using the blood gas analyzers.

The invasive measurements either for tHb concentration or for the fractional arterial oxygen saturation have many disadvantages, unlike blood loss that can be briefly demonstrated as follows:

- The invasive measurements are time consuming and should be conducted in a laboratory. Therefore, it cannot be available at the place of the medical care like the intensive care unit and also the real-time (continuous monitoring) patient monitoring cannot be conducted.
- The invasive measurements may increase the risk of infection due to blood drawn and may expose the patient and the healthcare provider to blood-borne pathogens.
- The invasive measurements cause pain to many patients especially children and neonates during the blood drawn.

The accessibility of non-invasive measuring for tHb concentration by measuring the concentrations of its four hemoglobin components (COHb, MetHb, O_2Hb , and reduced hemoglobin (RHb)) will offer relevant advantages over the current invasive measuring methods to caregivers in intensive care units (ICUs), operating rooms, neonatal intensive care units, ambulatory care centers, blood donation centers, and general hospital wards. If tHb concentration and O_2Hb concentration are measured non-invasively, the fractional oxygen can be measured.

Measuring of the tHb concentration and the ratios of its four components (COHb, MetHb, O_2Hb , RHb) using a few drops of blood helps in overcoming some disadvantages of the traditional invasive laboratory measuring method, such as blood loss, time consumption and its availability at the point of care.

1.2 Research objectives

1.2.1 Non-invasive measuring

The main objective of this study is measuring the total hemoglobin concentration and the ratios of the oxyhemoglobin, carboxyhemoglobin, methemoglobin, and reduced hemoglobin non-invasively to overcome the disadvantages of the invasive measuring of these physiological variables. This objective can be achieved by investigating a new version of pulse oximetry devices that has the ability to measure these variables non-invasively. To achieve this objective some tasks should be conducted as follows:

- Proposing non-invasive measuring methods, two different methods are employed for that purpose. The two methods are based on photoplethysmography PPG signals with different wavelengths. The first method is based on modified Lambert-Beer law and the principles of the pulse oximetry. This method is applied by two different essential equations. Therefore, this method comprises two methods. The second method is based on the intelligent algorithms and the photoplethysmography technology. It is considered a new trend to measure these physiological variables using the intelligent algorithms like fuzzy expert systems.
- A reliable non-invasive optoelectronic measuring system should be developed according to the proposed methods. This measuring system provides non-invasive online measurements.
- Reliable algorithms are proposed to extract the main features of the PPG signals that are processed during the calculation and to improve the quality of the PPG signals.

1.2.2 Invasive measuring

Developing new fast algorithms to measure the total hemoglobin concentration and the ratios of the oxyhemoglobin, carboxyhemoglobin, methemoglobin and reduced hemoglobin using a compact hemoglobin analyzer that uses a few drops of blood is also one of the thesis objectives.

For this purpose, the intelligent algorithms are employed. A whole fuzzy expert system is developed, consisting of two fuzzy expert systems: one considers the accuracy and the other considers the interpretability of the measuring operation.

1.3 Thesis outline

Part I introduces the background and the current state of the art:

Chapter 2 introduces physiological foundations of hemoglobin including its function and test.

Chapter 3 discusses the principles of the pulse oximetry including the calculation method and its limitations. The final part of this chapter gives an overview about the current state of the art.

Part II is devoted to the methodology applied in this work:

Chapter 4 describes the developed optoelectronic system, the signal processing module that is proposed for the low-amplitude signals, and the overall software flowchart.

Chapter 5 introduces a reliable algorithm in order to extract the main distinctive features of the PPG signals and proposing the non-invasive calculation methods. Two methods are described in this chapter.

Chapter 6 presents the invasive calculation method that is based on the fuzzy expert systems.

Part III shows the results and the conclusions:

Chapter 7 demonstrates the results of the two non-invasive measuring methods and the results of the invasive measuring method. The final part of this chapter includes the results discussion.

Chapter 8 concludes the thesis by summarizing the contributions made and presents suggestions for future work.

Part I

Background and Current State of the Art

2. Physiological Foundations

2.1 Preliminaries

Blood is the medium in which dissolved gases, hormones, nutrients and waste products are transported. Blood, together with the heart and the blood vessels (e.g. veins and arteries), comprises the circulatory system of the body. The circulatory system is responsible for maintaining balanced conditions within the body (i.e. homeostasis).

This chapter introduces general considerations of human blood physiology, including a brief overview about the blood composition and functions. Special emphasis is placed upon hemoglobin, as the thesis concerns estimating the total hemoglobin concentration as well as the ratio of its components. The hemoglobin structure and function are described and also the hemoglobinopathy is demonstrated. The hemoglobin test is one of the most frequently requested laboratory measurements. The purpose, the precautions and the normal results of the hemoglobin test are described in detail in the final part of this chapter.

2.2 Blood composition and functions

2.2.1 Blood composition

The composition of blood is quite complex. Blood accounts for 8% of the human body weight [Alb07]. With an average density of approximately 1060 kg/m^3 , it is very close to pure water's density of 1000 kg/m^3 [Shu06]. The average adult has a blood volume of roughly 5 liters (1.3 gal), composed of plasma and several kinds of cells (occasionally called *corpuscles*); these formed elements of the blood are erythrocytes (red blood cells), leukocytes (white blood cells), and thrombocytes (platelets). By volume, the red blood cells constitute about 45% of whole blood, the plasma about 54.3%, and white cells about 0.7% [Alb07].

Whole blood (plasma and cells) exhibits non-Newtonian, viscoelastic fluid dynamics; its flow properties are adapted to flow effectively through tiny capillary blood vessels with less resistance than plasma by itself. In addition, if all human hemoglobin were free in the plasma rather than being contained in RBCs, the circulatory fluid would be too viscous for the cardiovascular system to function effectively [Gan03].

Blood cells

One microliter of blood contains:

4.7 to 6.1 million (male), 4.2 to 5.4 million (female) erythrocytes [Gan03]:

In most mammals, mature red blood cells lack a nucleus and organelles. They contain the blood's hemoglobin and distribute oxygen. The red blood cells (together with endothelial vessel cells and other cells) are also marked by glycoproteins that define the different blood types. The proportion of blood occupied by red blood cells is referred to as the hematocrit, and is normally about 45%. The combined surface area of all red blood cells of the human body would be roughly 2,000 times as great as the body's exterior surface [Tall06].

4,000–11,000 leukocytes: white blood cells are part of the immune system; they destroy and remove old or aberrant cells and cellular debris, as well as attack infectious agents (pathogens) and foreign substances. The cancer of leukocytes is called leukemia [Gan03].

200,000–500,000 thrombocytes: thrombocytes, also called platelets, are responsible for blood clotting (coagulation). They change fibrinogen into fibrin. This fibrin creates a mesh onto which red blood cells collect and clot, which then stops more blood from leaving the body and also helps to prevent bacteria from entering the body [Gan03].

Plasma

About 55% of whole blood is blood plasma, a fluid that is the blood's liquid medium, which by itself is straw-yellow in color. The blood plasma volume totals 2.7–3.0 liters (2.8–3.2 quarts) in an average human. It is essentially an aqueous solution containing 92% water, 8% blood plasma proteins, and traces of other materials. Plasma circulates dissolved nutrients, such as glucose, amino acids, and fatty acids (dissolved in the blood or bound to plasma proteins), and removes waste products, such as carbon dioxide, urea, and lactic acid. Other important components include: serum albumin, blood-clotting factors (to facilitate coagulation), immunoglobulins (antibodies), lipoprotein particles, various other proteins, various electrolytes (mainly sodium and chloride) [Gan03].

2.2.2 Blood functions

The primary function of red blood cells, or erythrocytes, is to carry oxygen and carbon dioxide. Hemoglobin (Hb) is an important protein in the red blood cells that carries oxygen from the lungs to all parts of our body. The primary function of white blood cells, or

leukocytes, is to fight infection. There are several types of white blood cells and each has its own role in fighting bacterial, viral, fungi, and parasitic infections. Types of white blood cells that are most important for helping protect the body from infection and foreign cells include the following: Neutrophils, Eosinophils, Lymphocytes, Monocytes, and Platelets. The primary function of platelets, or thrombocytes, is blood clotting. Platelets are much smaller in size than the other blood cells. They group together to form clumps, or a plug, in the hole of a vessel to stop bleeding [Guy06].

2.3 Hemoglobin

Hemoglobin is found in the red blood cells of the body (see Figure 2-1). Each red blood cell (RBC) contains approximately 280 million hemoglobin molecules [sea99]. The main function of hemoglobin is to transport oxygen from the lungs to the tissues and then transport CO₂ back from the tissues to the lungs. One hemoglobin molecule has the ability to transport up to 4 oxygen molecules. There are two main forms of hemoglobin: oxyhemoglobin, which is saturated with oxygen molecules and deoxyhemoglobin (also called reduced hemoglobin), which is desaturated with oxygen molecules [sea99]. Oxyhemoglobin has a higher affinity for oxygen than deoxyhemoglobin, and deoxyhemoglobin has a higher affinity for CO₂ than oxyhemoglobin. Therefore, oxygen binds to oxyhemoglobin in the lungs and is then transported through the blood stream until it reaches the tissues. There, the oxygen is released to myoglobin, which then transports it to the mitochondria where it is used for aerobic respiration. In exchange, deoxyhemoglobin picks up 2 protons and 2 molecules of CO₂ and returns to the lungs, where the CO₂ is released through exhalation [Pre78].

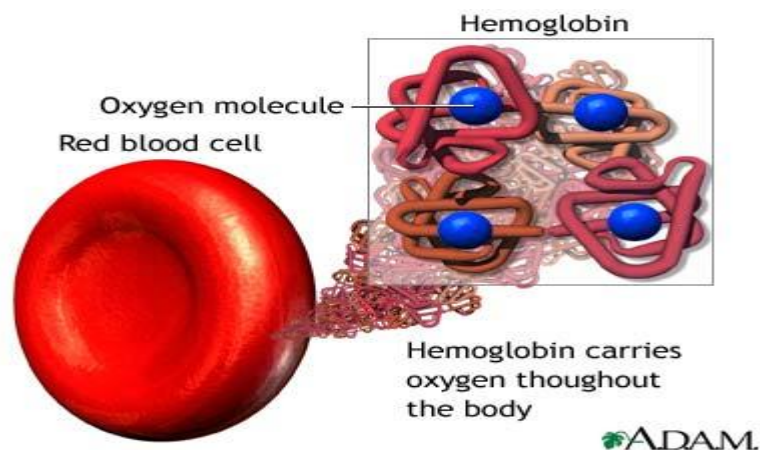


Figure 2-1: Red blood cells and hemoglobin [Lom11].

Hemoglobin may also be in the forms of dysfunctional hemoglobins (or dyshemoglobins) that do not support the transport of oxygen to the tissues. They are either unable to bind reversibly to oxygen or interfere with the ability of oxyhemoglobin to release its oxygen to

the tissue. The four most common dyshemoglobins are methemoglobin (MetHb), carboxyhemoglobin (COHb), sulfhemoglobin, and carboxysulfhemoglobin [Wie97].

Methemoglobin is oxidized hemoglobin. It is a result of oxidation of a free heme iron instead of the reversible binding of oxygen to heme inserted into globin subunits. Oxidized hemoglobin subunits are not capable of binding oxygen and altering the oxygen binding of the remaining ferrous hemes. Therefore, the functionality of hemoglobin is highly affected by methemoglobin. Under physiological circumstances the amount of methemoglobin remains below 0.6% of the total hemoglobin.

Carboxyhemoglobin is hemoglobin that has carbon monoxide (CO) instead of the normal oxygen bound to it. The carbon atom of carbon monoxide is bonded to the iron atom of heme. The affinity of hemoglobin binding with carbon monoxide is approximately 210 times larger than that of oxygen. Therefore, the presence of a high level of carbon monoxide will reduce the amount of oxygenated hemoglobin significantly. The source of the carbon monoxide may be exhaust (such as from a car, truck, boat or generator), smoke from a fire, or tobacco smoke. The level of carboxyhemoglobin is a measure of the degree of carbon monoxide exposure. In non-smokers the level of COHb is usually below 2% but this value varies with the local environment [WuK88].

Sulfhemoglobin is produced by the reaction of oxyhemoglobin and hydrogen sulphide. The oxygen affinity of the heme iron in sulfhemoglobin is 100-fold lower than the oxygen affinity of unmodified hemoglobin [Wie97].

Carboxysulfhemoglobin results from a reaction of sulfhemoglobin with carbon monoxide.

The concentrations of sulfhemoglobin and carboxysulfhemoglobin in human blood are usually not significant [Wie97].

2.3.1 Hemoglobin function

The ability of hemoglobin to take up oxygen molecules in the lungs and then release them in the tissues is regulated by several factors both within the hemoglobin molecule itself and through external chemical factors. One of the biggest regulators of the oxygen affinity of the hemoglobin is the presence of oxygen itself. In the lungs, where the oxygen levels are high, the hemoglobin has a higher affinity for oxygen and this affinity increases disproportionately with the number of molecules it already has bound to it [Sea99]. In other words, after the oxyhemoglobin binds one molecule of oxygen its affinity for oxygen increases until the hemoglobin is fully saturated. In the same way, deoxyhemoglobin has a lower affinity for oxygen and this affinity decreases disproportionately with the number of molecules it already has bound [Sea99]. Thus, the loss of one oxygen molecule from

deoxyhemoglobin lowers the affinity for the remaining oxygen. This regulation is known as cooperativity and is essential to the functioning of the hemoglobin because it allows the oxyhemoglobin to carry the maximum amount of oxygen to the tissues and then allows deoxyhemoglobin to release the maximum amount of oxygen into the tissues [Sea99]. Cooperativity is a function of the hemoglobin's unique structural characteristics, and it was found that the cooperative effects of the hemoglobin totally disappear if the hemoglobin is split in half [Pre78]. Essentially, hemoglobin is an allosteric protein that has more than one shape and can undergo conformational changes in its structure based on environment conditions [Sea99].

There are two alternative structures of hemoglobin; the relaxed structure (R) which has a greater oxygen affinity, and the tense structure (T) which has lower affinity for oxygen [Pre78]. The change between the T and R structures is the result of a rotation of 15 degrees between the two alpha-beta dimers [Kea04].

2.3.2 Hemoglobin structure

Hemoglobin is a tetramer composed of 4 globin molecules; 2 alpha globins and 2 beta globins (see Figure 2-2). The alpha globin chain is composed of 141 amino acids and the beta globin chain is composed of 146 amino acids [Pre78]. Both alpha and beta globin proteins share similar secondary and tertiary structures, each with 8 helical segments (labeled helix A-G). Each globin chain also contains one heme molecule. The heme molecule is composed of a porphyrin ring, which contains 4 pyrrole molecules cyclically linked together, and an iron ion ligand bound in the center. The heme molecule is located between helix E and helix F of the globin protein. The alpha and beta subunits of the globin chains exist in two dimers which are bonded together strongly [Kea04].

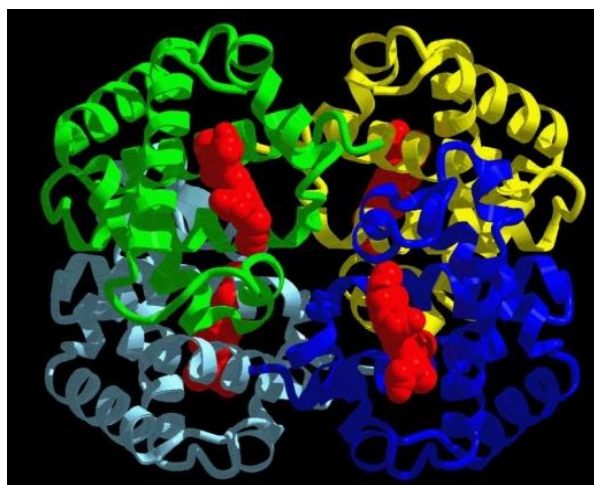


Figure 2-2: 3-D Ribbon Structure of the hemoglobin molecule. Each of the 4 globin chains is represented in a different color. The heme molecule is shown in red [Psc11].

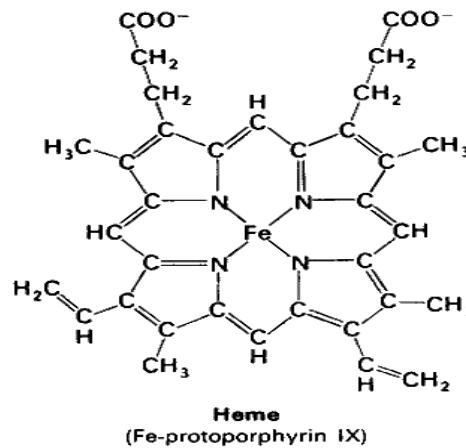


Figure 2-3: Heme molecule. Porphyrin ring with iron atom ligand bound inside [Oml11].

Oxygen binds to the iron ion tightly, and if two heme molecules come together in the presence of oxygen the iron atoms will oxidize and irreversibly bind to the oxygen (see Figure 2-3). This irreversible binding would not be of use in the hemoglobin molecule because oxygen needs to be released in the tissues. The globin chain prevents this irreversible binding by folding the protein around the heme molecule, creating a pocket to isolate the heme molecule from other heme molecules. Therefore, the globin molecules allow the iron atom to form loose bonds with the oxygen, and therefore, the ability to bind to oxygen and then release it into the tissues without becoming permanently oxidized in the process [Pre78].

2.3.3 Hemoglobinopathy

It is to have hemoglobin different from the normal hemoglobin. The hemoglobinopathies are among the most common monogenic diseases, with more than 1,000 different mutant alleles having been identified on the molecular level [Old07]. The most significant of these from a clinical point of view are the sickle-cell diseases (SCD) and β thalassemia which affect populations with origins in Africa, the Mediterranean region, Southeast Asia, the Middle East and the Far East [Kha06]. Around 1-2% of the global populations are heterozygous for hemoglobin S and 3% are heterozygous for β thalassemia [The07].

Historically, the majority of children who were carriers of these diseases died during their first 10 years of life from complications. However, recent important advances have extended the average life of patients and significantly improved their quality of life. Improved understanding of the etiology and mechanisms of anaemia, earlier diagnosis, new therapeutic approaches and better management of transfusion iron overload have dramatically improved the clinical picture [Old07].

The inherited disorders of hemoglobin are classified into three groups:

1. Structural variants.
2. Thalassemias.
3. Hereditary persistence of fetal hemoglobin (HPFH).

The first group is characterized by the presence of abnormal hemoglobins with different structures, but no alterations in the rate of globin production. Approximately 1000 Hb variants have been identified, of which Hbs S, C, D, and E are the most frequent worldwide [Beu06]. The second group, thalassemias, is characterized by a reduced rate or lack of synthesis of one or more globin chains. The two main types are α and β thalassemias. α -thal is classified as type 1, where both $\alpha 1$ and $\alpha 2$ genes are deleted (or mutated), and type 2, where only one α gene is deleted (or mutated). β -thals are divided into β^{+-} thal, with a low β globin chain production, and β^0 -thal, in which the β chain synthesis is null [Wea06]. The last group, HPFH, is a benign condition in which synthesis of Hb Fetal (Hb F) persists beyond the neonatal period. Hemoglobinopathies constitute the most common monogenic disease group in the world. The World Health Organization estimates that about 370,000 infants are born each year with a hemoglobinopathy, and approximately 5% of the world's population carries a genetic mutation for this pathology [Wea01].

2.3.4 Hemoglobin test

Definition

A hemoglobin test reveals how much hemoglobin is in an individual's blood. This information can be used to help physician's diagnose and monitor anaemia [a low hemoglobin level] and polycythemia vera [a high hemoglobin level] [Che01].

Purpose

A hemoglobin test is performed to determine the amount of hemoglobin in an individual's red blood cells (RBCs). This is important because the amount of oxygen available to tissues depends upon how much oxygen is in the RBCs, and local perfusion of the tissues. Without sufficient hemoglobin, the tissues lack oxygen and the heart and lungs must work harder to compensate. A low hemoglobin measurement usually means the individual has anaemia. Anaemia results from a decrease in the number, size, or function of RBCs. Common causes include excessive bleeding, a deficiency of iron, and vitamin B12, or folic acid, destruction of red cells by antibodies or mechanical trauma, and structurally abnormal hemoglobin. Hemoglobin levels are also decreased due to cancer, kidney diseases, other chronic diseases, and excessive IV fluids. An elevated hemoglobin level may be caused by dehydration (decreased water), hypoxia (decreased oxygen), or polycythemia vera. Hypoxia may result from high altitudes, smoking, chronic obstructive lung diseases (such as

emphysema), and congestive heart failure. Hemoglobin levels are also used to determine if a person needs a blood transfusion. Usually a person's hemoglobin must be below 7–8 g/dl before a transfusion is considered, or higher if the person has heart or lung disease. The hemoglobin concentration is also used to determine how many units of packed red blood cells should be transfused. A common rule of thumb is that each unit of red cells should increase the hemoglobin by approximately 1.0–1.5 g/dl [Kee01].

Precautions

Fluid volume in the blood affects hemoglobin values. Accordingly, the blood sample should not be taken from an arm receiving IV fluid. It should also be noted that pregnant women and people with cirrhosis, a type of permanent liver disease, have extra fluid, which dilutes the blood, decreasing the hemoglobin. Dehydration, a decreased amount of water in the body, concentrates the blood, which may cause an increased hemoglobin result. Certain drugs such as antibiotics, aspirin, antineoplastic drugs, doxapram, indomethacin, sulfonamides, primaquine, rifampin, and trimethadione, may also decrease the hemoglobin level. A nurse or phlebotomist usually collects the sample by inserting a needle into a vein, after cleaning the skin, which helps prevent infections [Che01].

Normal results

Normal values vary with age and sex, with women generally having lower hemoglobin values than men. Normal results for men range from 13–18 g/dl. For women the normal range is 12–16 g/dl. Critical limits (panic values) for both males and females are below 5.0 g/dl or above 20.0 g/dl. A low hemoglobin value usually indicates the person has anaemia. Different tests are done to discover the cause and type of anaemia. Dangerously low hemoglobin levels put a person at risk of a heart attack, congestive heart failure, or stroke. A high hemoglobin value indicates the body may be making too many red blood cells. Other tests are performed to differentiate the cause of the abnormal hemoglobin level. Laboratory scientists perform hemoglobin tests using automated laboratory equipment. Critically high or low levels should be immediately called to the attention of the patient's doctor [Kje00].

3. Pulse Oximetry

3.1 Preliminaries

Pulse oximetry is considered one of the most significant technological advances in clinical patient monitoring over the last two decades that decreases the cost of care [Men92] [Web97]. It provides information about functional arterial oxygen saturation non-invasively. Pulse oximetry became known as the fifth vital sign along with blood pressure, heart rate, temperature, and respiration rate [Sam09] [Coh05] [Nef8] [Yel83].

It is now routinely used in many clinical applications and in all types of health settings [Sam09] [Dem07]. Outpatient sites of service typically include the emergency department, pulmonary function laboratory, clinic, physician's office, pulmonary rehabilitation programs, and the patient's home. Inpatient pulse oximetry is performed in operating rooms, intensive care units (ICUs), neonatal intensive care units and on general hospital wards. Pulse oximetry is also used in alternative settings such as skilled nursing facilities and long-term acute care facilities.

In recent years, many research groups have employed the principles of the conventional pulse oximetry to measure more clinical physiological variables unlike the arterial oxygen saturation and the heart rate, such as total hemoglobin (tHb) concentration, blood pressure and blood glucose. This thesis concerns measuring tHb concentration and the ratios of oxyhemoglobin, carboxyhemoglobin, methemoglobin, and reduced hemoglobin, according to the principles of the pulse oximetry. Therefore, it is very important to introduce an overview about pulse oximetry technology foundations.

This chapter presents the essential theoretical background for pulse oximetry including information about photoplethysmography, general physical basics of light absorbance, and

physical basics of light absorbance in pulse oximetry. The method of calculating the functional arterial oxygen saturation by pulse oximetry is explained after the theoretical introduction. The sources of inaccuracy in pulse oximeters are briefly discussed in section 3.5 to optimize the usage of these devices. The final section of this chapter demonstrates a literature review of estimating tHb concentration non-invasively and the artificial application for the photoplethysmography signal to show the current state of the art of utilizing the principles of the pulse oximetry to measure tHb concentration and its four components ratios.

3.2 Photoplethysmography

Plethysmography (PG) is a set of non-invasive techniques to measure changes in blood flow or air volume in different parts of the body. It can be employed to detect blood clots in arms and legs, or to estimate how much air can be drawn into the lungs. The commonly detected volume changes are those caused by breathing, blood being forced into vessels, and in the heart as it pumps. PG can be conducted by different means, such as strain gauge plethysmography, water plethysmography, impedance plethysmography, air plethysmography, gravimetric plethysmography, microwave plethysmography, and photoplethysmography [Nop10] [Gra96]. Several plethysmographic vein occlusion sensors and systems are shown in Figure 3-1. In the following, photoplethysmography is introduced in detail, as it is the cornerstone of the pulse oximetry devices.

Photoplethysmography (PPG), also called photoelectric plethysmography, is not a new technology. The principles of photoelectric plethysmography were first described in 1935 by K. Mattes, K. Kramer and also F. Gross who followed photoelectrically the reduction of oxyhemoglobin in the blood in vitro and in vivo as reported by A. B. Hertzman in 1938 [Her38] [Mat35] [Gal89]; however, A. B. Hertzman and C. R. Spielman were the first to use the term “Photoplethysmograph” and suggested that the resultant “Plethysmogram” represents volumetric changes in the blood vessels of the skin [Kam89].

PPG refers to an optical measurement technique that can be applied to detect changes in blood flow and blood volume in the microvascular bed of tissue [Cha74]. Valuable information about the cardiovascular system can be supplied non-invasively by PPG [Kam89]. The basic system of Photoplethysmography technology consists of a few optoelectronic components: a light source (most commonly light emitting diode (LED)) to illuminate the tissue and a light detector (photodetector) to measure the small variations of the light intensity. The detector can be placed either directly across from the light source for transmission photoplethysmography or next to the light source for reflective

photoplethysmography, as illustrated in Figure 3-2. PPG is applied non-invasively and often operates in red and near infrared light wavelengths regions.

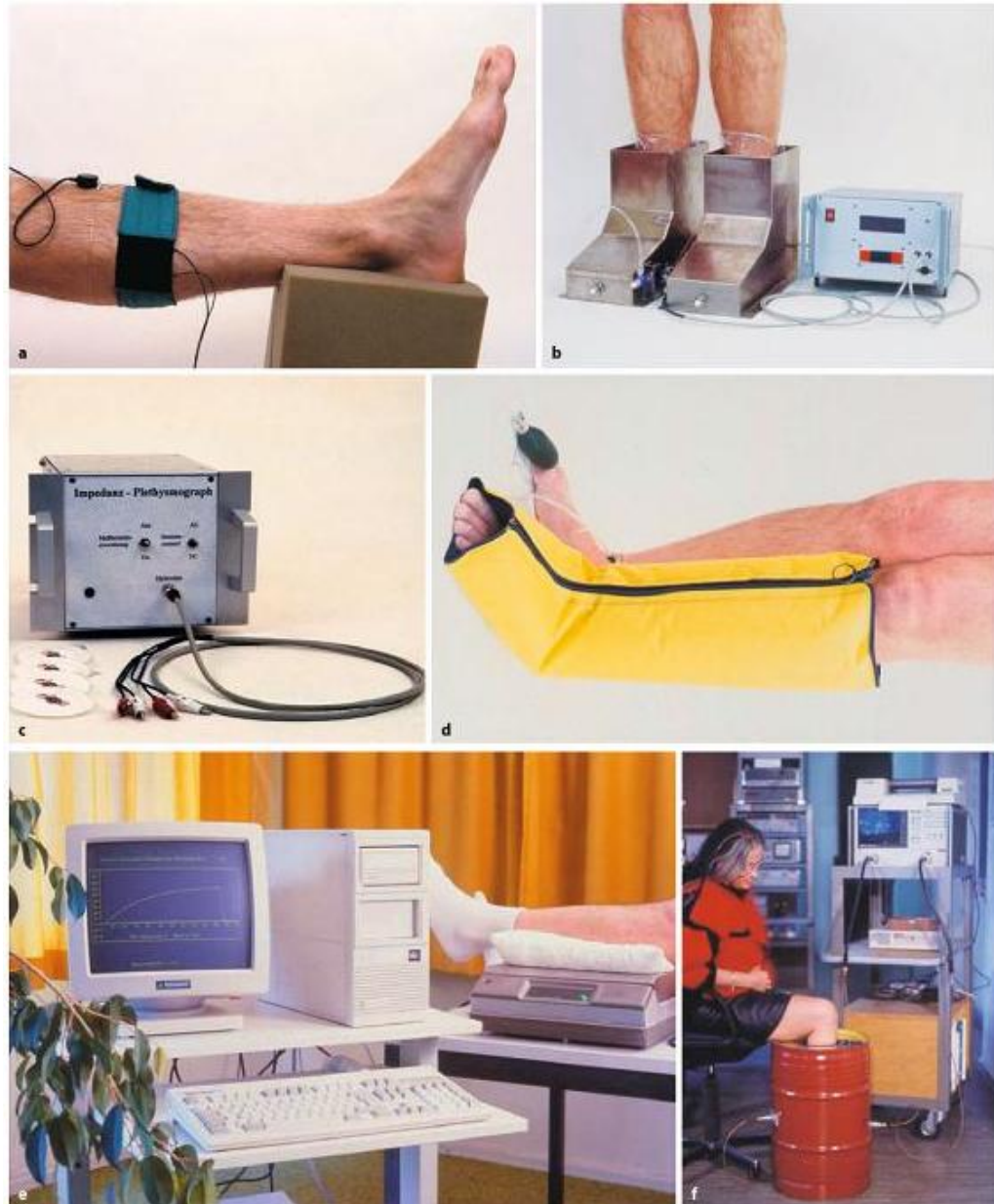


Figure 3-1: Several plethysmographic vein occlusion sensors and systems: strain gauge and fiber sensor (a), water plethysmograph (b), impedance plethysmograph (c), air plethysmograph sensor (d), Computer supported gravimetric plethysmograph (e), and microwave plethysmograph (f) [Nop01].

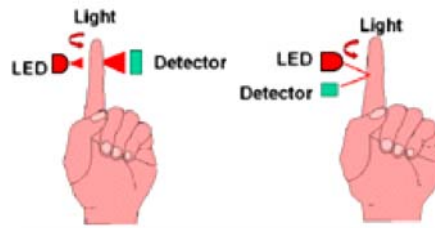


Figure 3-2: Transmission photoplethysmography (left) versus reflective photoplethysmography (right).

The Photoplethysmography technology has been used in a wide range of commercially available medical devices for measuring oxygen saturation, cardiac output, blood pressure, respiration monitoring, and assessing autonomic function and also detecting peripheral vascular diseases [All07].

3.2.1 The photoplethysmography waveform

The PPG waveform comprises a pulsatile (alternating part AC) physiological waveform attributed to cardiac synchronous changes in the blood volume and usually has its fundamental frequency, typically around 1 Hz according to heart beat, as shown by Figure 3-3. The AC pulsatile is superimposed on a slowly varying (static part DC) baseline. This DC component varies slowly with various lower frequency components attributed to respiration, sympathetic nervous system activity and thermoregulation.

Figure 3-4 shows the amount of the absorbed light in the living tissue as a function of time. The amount of the absorbed light is correlated with the pulsation of arterial blood. A constant amount of light is absorbed by the skin pigmentation, bone, other tissue, venous blood and the non-pulsating part of the arterial blood. More blood is present in the arteries during systole and therefore more light is absorbed.



Figure 3-3: The pulsatile (AC) component of the PPG signal and corresponding electrocardiogram (ECG) [All07].

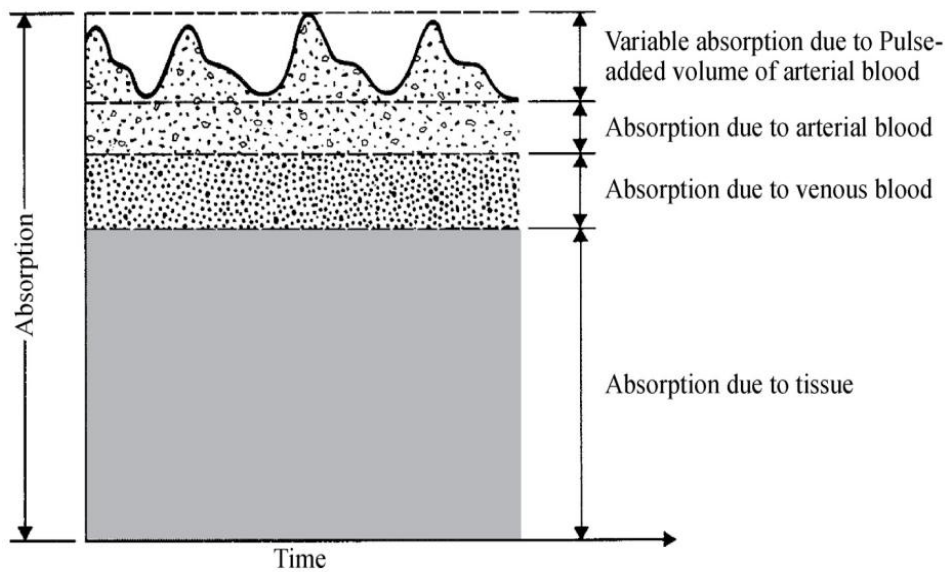


Figure 3-4: Absorbed light in living tissue [Web09].

3.3 Light absorbance basics

This section describes the basic principles of light absorption in substances to understand the important theoretical concepts of the operation of the pulse oximeter [Wie97] [Dem98] [Pee01].

The determination of the concentration of a light-absorbing substance in a medium using a spectrophotometer is based on Lambert-Beer's law (also referred to as Beer's or Bouguer's law). Lambert-Beer's law identifies the attenuation of light entering a sample of a uniform medium that contains an absorbing substance due to the absorption. If monochromatic incident light of an intensity I_o enters the medium, a part of this light is transmitted through the medium while another part is absorbed. As illustrated in Figure 3-5, the intensity I of light travelling through the medium decreases exponentially with distance and can be expressed by the following equation.

$$I = I_o e^{-\varepsilon(\lambda)cd} \quad (3.1)$$

where $\varepsilon(\lambda)$ is the absorbability or the extinction coefficient of the absorbing substance at a particular wavelength, c is the concentration of the absorber that is constant in the medium, and d is the absorption optical path length through the medium. The concentration c is measured in mmol L^{-1} , the distance is expressed in cm , and the extinction coefficient is measured in $\text{L mmol}^{-1}\text{cm}^{-1}$.

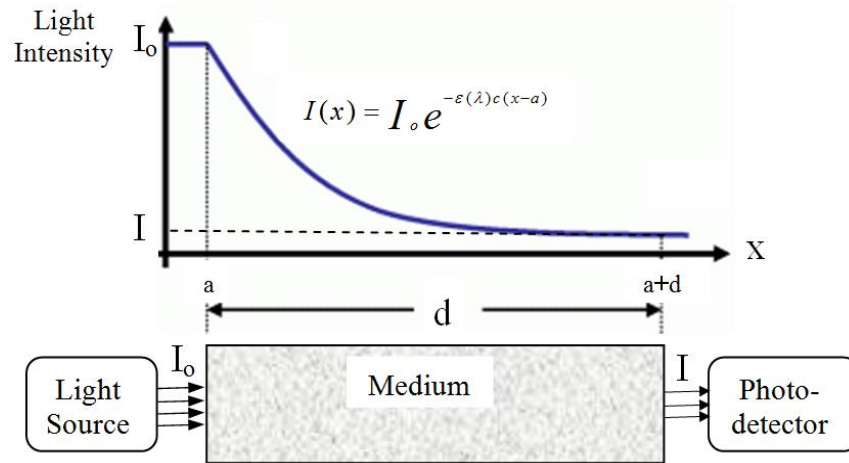


Figure 3-5: Description of Lambert-Beer's law that controls the absorption of light travelling through a uniform substance.

The atoms of all molecules vibrate in a particular pattern that is unique for every substance. As the light is passed through a substance, the frequency of the light similar to the vibration frequency of the substance is absorbed while all the other frequencies are transmitted or reflected. The absorbance is sometimes referred to as the optical density of a medium. The extinction coefficient of a substance can be graphed at various wavelengths as a spectrum. This spectrum is specific for each substance.

It is necessary to mention some of the other useful definitions:

The transmittance (T) of light is defined as the ratio of the transmitted light I to the incident light I_0 that travels through a medium with an absorbing substance.

$$T = \frac{I}{I_0} = e^{-\epsilon(\lambda)cd} \quad (3.2)$$

The unscattered absorbance (A) of this process is defined as the negative natural logarithm of the transmittance of light.

$$A = -\ln T = \epsilon(\lambda)cd \quad (3.3)$$

The absorption coefficient ($\alpha(\lambda)$) of this process is a measure of the rate of decrease in the intensity of the light as it passes through a given substance. It depends on the wavelength of the incident light and can be calculated by the following equation.

$$\alpha(\lambda) = \epsilon(\lambda)c \quad (3.4)$$

What is the case if there is more than one substance that absorbs light in the same medium? The properties of Lambert-Beer's law are also valid in this case. The mathematical representation of such system of absorbers is a superposition of the individual absorbing processes. The resulting total absorbance A and total absorption coefficient $\alpha(\lambda)$ of light in a medium with n absorbing substances are the sum of their n independent absorbencies and absorption coefficients, respectively, as demonstrated by the following two equations.

$$A = \varepsilon_1(\lambda)c_1d_1 + \varepsilon_2(\lambda)c_2d_2 + \dots + \varepsilon_n(\lambda)c_nd_n = \sum_{i=1}^n \varepsilon_i(\lambda)c_id_i \quad (3.5)$$

$$\alpha(\lambda) = \varepsilon_1(\lambda)c_1 + \varepsilon_2(\lambda)c_2 + \dots + \varepsilon_n(\lambda)c_n = \sum_{i=1}^n \varepsilon_i(\lambda)c_i \quad (3.6)$$

where $\varepsilon_i(\lambda)$, c_i , and d_i are the extinction coefficient, concentration of the substance i , and the optical path length through the absorbing substance, respectively.

According to Eq. (3.4), Lambert-Beer's law allows us to determine n unknown concentrations of n different absorbing substances in a homogenous medium if the absorbance of light is measured at n different wavelengths, the extinction coefficients of the substances are known, and the optical path lengths, which may differ from substance to substance in the medium, are estimated.

3.4 Light absorbance in pulse oximetry and estimation of oxygen saturation

This section demonstrates the theoretical background for the measurement of light absorbance in pulse oximetry as a basis for estimating the arterial oxygen saturation.

3.4.1 Light absorbance in pulse oximetry

Hemoglobin is a respiratory pigment contained within red blood cells. One oxygenated hemoglobin molecule can carry four molecules of oxygen. Hemoglobin changes color when oxygenated. A deoxygenated hemoglobin molecule is dull red; hence, it absorbs most of any red light passing through it. An oxygenated hemoglobin molecule is bright red, as shown by Figure 3-6. It absorbs less amount of red light and transmits most of it. Pulse oximetry uses this color change to measure hemoglobin oxygen saturation [Cla97].

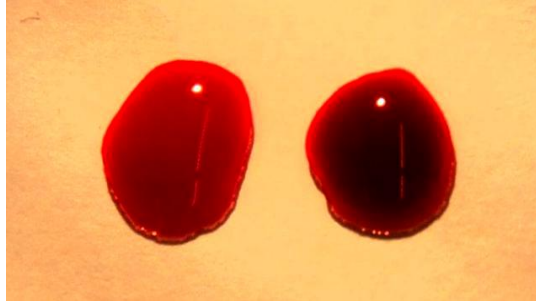


Figure 3-6: Color difference between oxygenated and deoxygenated hemoglobin [Alt11]

Figure 3-7a shows the extinction coefficients of the reduced hemoglobin (RHb or Hb) and oxyhemoglobin O_2Hb at wavelengths in the range of 650 nm and 1000 nm and Figure 3-7b demonstrates the interesting wavelength regions of the red light and the infrared light by pulse oximetry. The absorbing characteristics of hemoglobin change with its chemical binding and the wavelength of the incident light. The absorbance of light in the red region of the spectrum is much higher for RHb than for O_2Hb . In the infrared region, RHb is slightly more transparent to light than O_2Hb .

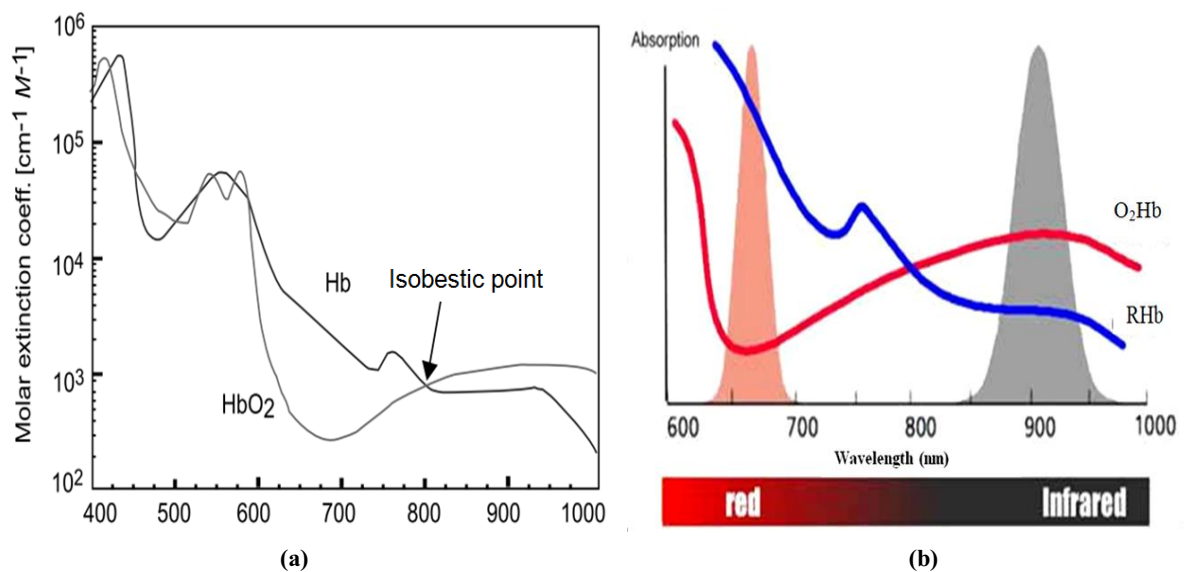


Figure 3-7: Extinction coefficients of RHb and O_2Hb (a) and the interesting wavelength regions of the red light and the infrared light by pulse oximetry (b) [Web06] [Adv11].

Pulse oximetry utilizes two wavelengths to determine the arterial oxygen saturation. One of them is in the red light region and the other in the infrared light region. The most common choice for the two wavelengths is 660 nm and 940 nm. At these wavelengths, hemoglobin is the main light absorber in human blood. There are different reasons that lead to this choice. They can be described as follows:

- There is a large difference in the extinction coefficients of RHb and O₂Hb at the wavelength of 660 nm that changes light absorbance significantly, even when the oxygen saturation changes slightly.
- The light emitting diodes (LEDs) are available at these wavelengths. That is considered an important factor for cost reduction in commercial pulse oximeters.
- The flatness of the absorption spectra around the chosen wavelength, so that the shifts in the peak wavelength of the LEDs, (due to the temperature or the manufacture), do not result in large errors [Moy94]. The flatness of the absorption spectra around the wavelength of 940 nm is more obvious than at the wavelength of 660 nm, as depicted in Figure 3-7.

3.4.2 Estimation of functional arterial oxygen saturation

Measuring at two wavelengths allows distinguishing the concentrations of only two different absorbers (RHb and O₂Hb), which are called the functional hemoglobins, as they are able to bind reversibly with oxygen molecular, which is considered the main purpose of the hemoglobin. Most of the hemoglobins in healthy individuals are functional hemoglobins. The functional arterial oxygen saturation (functional S_aO₂) is measured according to the values of the functional hemoglobins only, as shown by the following equation.

$$\text{Functional } S_aO_2 = \frac{C_{O_2Hb}}{C_{RHb} + C_{O_2Hb}} \times 100\% \quad (3.5)$$

where C_{O₂Hb} and C_{RHb} are the concentration of O₂Hb and RHb, respectively.

According to Eq. (3.5), the concentrations of RHb and O₂Hb can be expressed in terms of the functional arterial oxygen saturation (S_aO₂) by equations (3.6) and (3.7).

$$C_{RHb} = (1 - S_aO_2) \times (C_{RHb} + C_{O_2Hb}) \quad (3.6)$$

$$C_{O_2Hb} = S_aO_2 \times (C_{RHb} + C_{O_2Hb}) \quad (3.7)$$

By shining red or infrared light (I₀) onto a fingertip and detecting the intensity of the transmitted light (I) by a photodetector circuit, a photoplethysmography (PPG) signal will be generated, as shown by Figure 3-8 (a). Light travelling through biological tissue, such as the finger or earlobe, is absorbed by different absorbing substances. Bones, skin

pigmentation, and the arterial and venous blood are the primary absorbers of light in the region of interest.

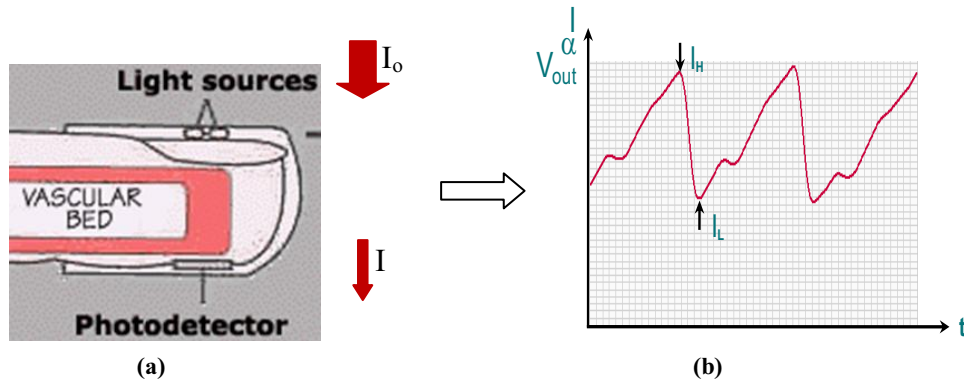


Figure 3-8: A sketch of a finger pulse oximeter (a) and a generated PPG signal (b)

Pulse oximeters use the advantage of the arterial pulsation. The arteries contain more blood during systole than during diastole, and therefore, their diameter increases due to the increased pressure. This effect occurs only in the arteries but not in the veins. As illustrated by Figure 3-9, which describes Lambert-Beer’s law in pulse oximetry, the amount of the transmitted light correlates with the pulsation of arterial blood. The transmitted light decreases during systole mainly because of the larger amount of absorbing substances (hemoglobin) and has a low peak (I_L), due to the fact that the optical path length d in the arteries increases and can be expressed as d_{max} . During diastole, the diameter of the arterial vessels is minimal (d_{min}) and thus the absorbance due to arterial hemoglobin is minimal and the amount of the transmitted light has a high peak (I_H).

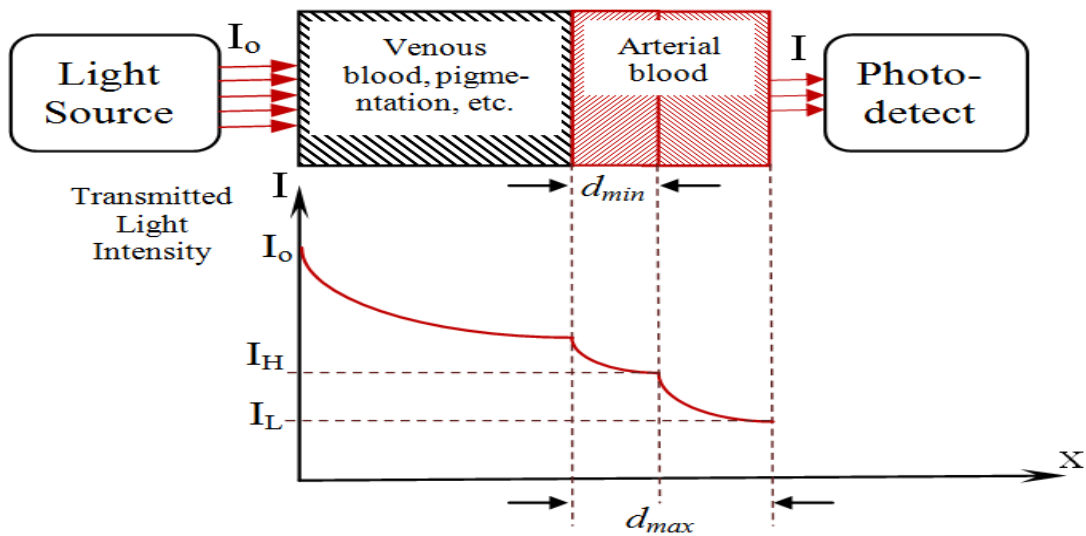


Figure 3-9: Lambert-Beer’s law in pulse oximetry [Wie97] [Bol02].

According to Lambert-Beer's law, the transmitted red light can be expressed during both cases of the diastole and the systole by Eq. (3.8) and Eq. (3.9), respectively.

$$I_{H,R} = I_{o,R} e^{-\alpha(\lambda_R)d_{R\min}} \quad (3.8)$$

$$I_{L,R} = I_{o,R} e^{-\alpha(\lambda_R)d_{R\max}} \quad (3.9)$$

By dividing the transmitted red light during diastole $I_{H,R}$ by the transmitted red light during systole $I_{L,R}$ and applying natural logarithm (ln) to both sides of Eq. (3.10), Eq. (3.11) will be derived, which can also be written for the transmitted infrared light, as depicted in Eq. (3.12).

$$\frac{I_{H,R}}{I_{L,R}} = \frac{e^{-\alpha(\lambda_R)d_{R\min}}}{e^{-\alpha(\lambda_R)d_{R\max}}} = e^{-\alpha(\lambda_R)(d_{R\max} - d_{R\min})} \quad (3.10)$$

$$\ln\left(\frac{I_{H,R}}{I_{L,R}}\right) = -\alpha(\lambda_R)(d_{R\max} - d_{R\min}) = -\alpha(\lambda_R)\Delta d_R \quad (3.11)$$

$$\ln\left(\frac{I_{H,IR}}{I_{L,IR}}\right) = -\alpha(\lambda_{IR})(d_{IR\max} - d_{IR\min}) = -\alpha(\lambda_{IR})\Delta d_{IR} \quad (3.12)$$

The ratio R of the absorbances at the red and the infrared wavelengths is derived by dividing the last two equations. It may also be called the measuring variable.

$$R = \frac{\ln\left(\frac{I_{H,R}}{I_{L,R}}\right)}{\ln\left(\frac{I_{H,IR}}{I_{L,IR}}\right)} = \frac{\alpha(\lambda_R)\Delta d_R}{\alpha(\lambda_{IR})\Delta d_{IR}} \quad (3.13)$$

It is assumed that the optical path length of the red light is equal to the optical path length of the infrared light. Thus, the ratio R became a ratio of the absorption coefficients at the red and the infrared wavelengths, which depends only on the light absorbers that exhibit in the arterial blood.

$$R = \frac{\alpha(\lambda_R)}{\alpha(\lambda_{IR})} = \frac{\varepsilon_{RHb}(\lambda_R)C_{RHb} + \varepsilon_{O_2Hb}(\lambda_R)C_{O_2Hb}}{\varepsilon_{RHb}(\lambda_{IR})C_{RHb} + \varepsilon_{O_2Hb}(\lambda_{IR})C_{O_2Hb}} \quad (3.14)$$

Substitute C_{RHb} and C_{O_2Hb} by their functions of the functional arterial oxygen saturation by using Eq. (3.6) and Eq. (3.7) to derive R as a function of the functional S_aO_2 .

$$R = \frac{[\varepsilon_{RHb}(\lambda_R)] + [\varepsilon_{O_2Hb}(\lambda_R) - \varepsilon_{RHb}(\lambda_R)]S_aO_2}{[\varepsilon_{RHb}(\lambda_{IR})] + [\varepsilon_{O_2Hb}(\lambda_{IR}) - \varepsilon_{RHb}(\lambda_{IR})]S_aO_2} \quad (3.15)$$

Eq. (3.15) can be rewritten in a form where the functional S_aO_2 is a function of the calculated ratio R and the extinction coefficients of the RHb and O_2Hb , as follows;

$$S_aO_2 = \frac{\epsilon_{RHb}(\lambda_R) - \epsilon_{RHb}(\lambda_{IR})R}{\epsilon_{RHb}(\lambda_R) - \epsilon_{O_2Hb}(\lambda_R) + [\epsilon_{O_2Hb}(\lambda_{IR}) - \epsilon_{RHb}(\lambda_{IR})]R} \times 100\% \quad (3.16)$$

Therefore, the theoretical arterial functional oxygen saturation can be estimated by calculating the ratio R of two normalized PPG signals at red and infrared wavelengths, as described by Eq. (3.13) and by using Eq. (3.16). The relationship is plotted as the theoretical curve in Figure 3-10.

Lambert-Beer's law is based on the approximation concept that the sum of the transmitted and the absorbed light is equal to the incident light; however, incident light passing through human tissue is not only split into absorbed light and transmitted light. Some parts of the light are reflected and the others are scattered. Lambert-Beer's law does not take these physical concepts into account [Wie97].

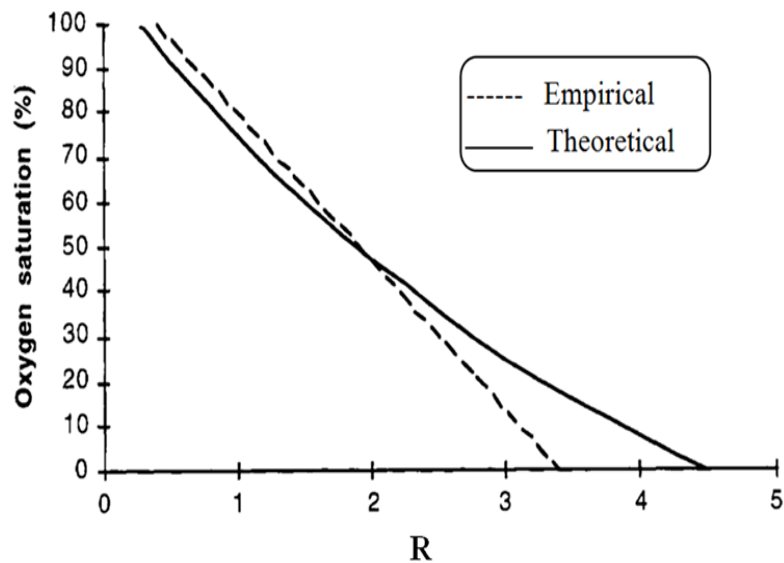


Figure 3-10: Typical calibration curves for pulse oximeters [Wie97].

Under normal circumstances, pulse oximeters can still read the functional arterial oxygen saturation accurately enough for clinical use, although light scattering highly increases the absorbance of the incident light. This is because most of the commercial pulse oximeters use a calibration curve based on empirical data (in vitro data). Figure 3-10 shows an

example for the difference between the theoretical data that is calculated using the ratio R and the empirical data. A large set of data obtained in clinical studies is collected containing information about the ratio R that is calculated by the pulse oximeter and the actual arterial oxygen saturation that is measured by an accurate invasive method “gold standard device” such as the CO-oximeter. Then, lookup tables or equations are used to find the relationship of these two variables for a pulse oximeter reading (S_pO_2) [Hor00].

3.5 Pulse oximetry limitations

Pulse Oximetry (SpO_2) is a standard monitoring device in intensive care units (ICUs). It is currently used to guide therapeutic interventions [Van01]; however, it has a number of limitations which may lead to inaccurate readings. To achieve optimum performance and precision, the following points that affect the calculation of SpO_2 should be considered [kam02] [Sev92] [Jub06] [Joh93] [Mar92] [Jub9].

3.5.1 Physiological limitations

Oxyhemoglobin dissociation curve

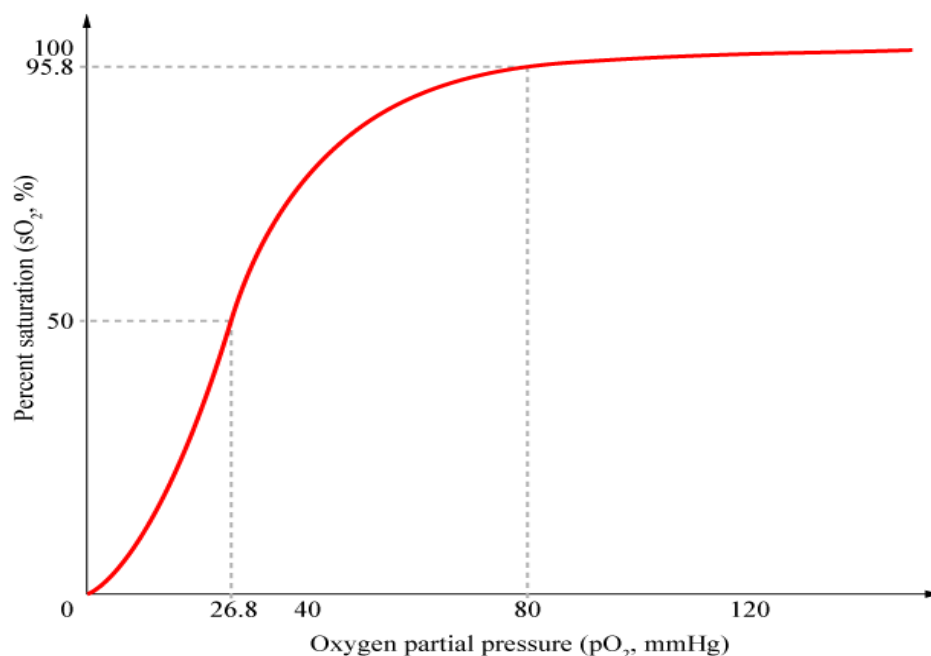


Figure 3-11: Oxyhemoglobin dissociation curve, i.e., the relationship between arterial oxygen saturation and arterial partial pressure [Wik11].

Pulse oximeters measure SaO_2 , which is physiologically related to arterial oxygen tension (PaO_2) according to the oxyhemoglobin dissociation curve, as depicted in Figure 3-11. Because the dissociation curve has a sigmoid shape, at high oxygen saturations, small changes in saturation are associated with relatively large changes in PaO_2 . Therefore, pulse oximeters have a limited ability to distinguish high but safe levels of arterial oxygen from excess oxygenation, which may be harmful, as in premature newborns, or patients with severe chronic obstructive pulmonary disease (COPD) who need the hypoxic drive to breathe [McG96] [Kam02].

3.5.2 Interference from substances

Dyshemoglobins

Pulse oximetry employs only two wavelengths of light and thus can distinguish only the two substances, (O_2Hb and RHb) to measure the functional arterial oxygen saturation. But in humans more species of hemoglobin, such as carboxyhemoglobin and methemoglobin (dyshemoglobins or dysfunctional hemoglobins) are present. These other hemoglobins absorb light as the functional hemoglobins do and hence influence the measurements. Accordingly, if the concentrations of dysfunctional hemoglobins are high, this will lead to inaccurate pulse oximetry (SpO_2) readings.

Figure 3-12 and Figure 3-13 describe the effect of carboxyhemoglobin and methemoglobin on the measured oxygen saturation by pulse oximetry (SpO_2), respectively.

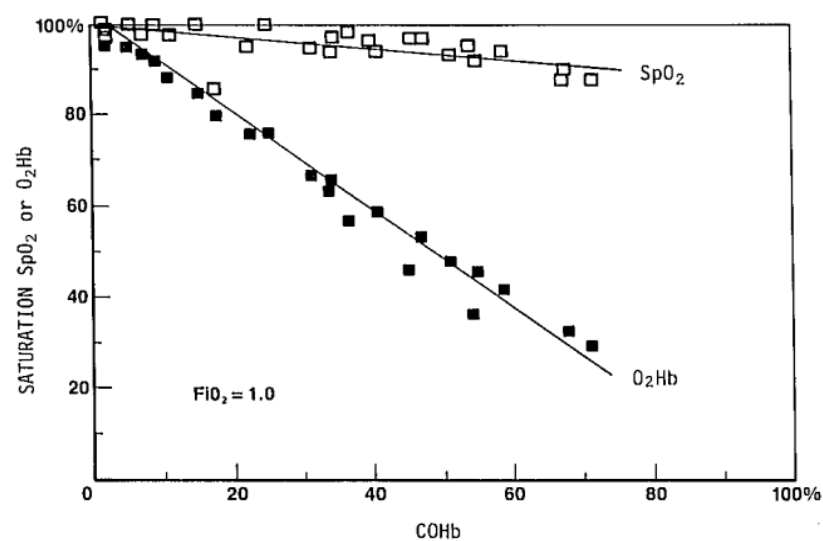


Figure 3-12: SpO_2 and O_2Hb versus carboxyhemoglobin (COHb). SpO_2 consistently overestimates saturation in the presence of COHb. At $\text{COHb}=70\%$, SpO_2 is still roughly 90%, while O_2Hb has fallen to 30% [Bar87-].

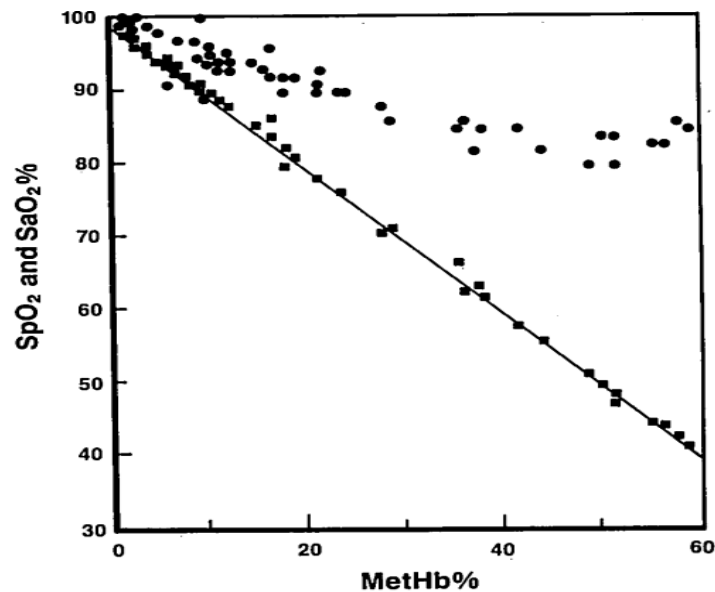


Figure 3-13: Nellcor SpO₂ readings (circles) and invasive SaO₂ (squares) versus MetHb%. Line shown is SaO₂=100-MetHb% [Bar89].

In such cases, the fractional arterial oxygen saturation should be determined which is measured according to the concentration of the total hemoglobin concentration (tHb), so that it takes the dyshemoglobins into account. Fractional SaO₂ is calculated as demonstrated by the following equation.

$$\text{Fractional } S_aO_2 = \frac{C_{O_2Hb}}{C_{tHb}} \times 100\% \quad (3.17)$$

where C_{O_2Hb} and C_{tHb} are the concentration of O₂Hb and tHb, respectively.

This point of pulse oximetry's limitation was one of the motivations of the thesis to avoid such error by measuring the fractional oxygen saturation non-invasively instead of the functional oxygen saturation.

Intravenous dyes

The use of intravenous dyes such as methylene blue (used in surgery or to treat methemoglobinaemia), indocyanine green, and indigo carmine can cause falsely low SpO₂ readings [Jub06].

Lipids and Bilirubin

High blood lipid concentrations, hyperalimentation, and hyperbilirubinemia can interfere with pulse oximeter readings. Increased concentrations of bilirubin tend to overestimate the measured oxygen saturation [Mar92].

Skin pigmentation and other pigments

Skin pigmentation and other surface light absorbers such as nail varnish might make the detected light too small to be reliably processed. Therefore, in pigmented patients, inaccurate pulse oximetry readings have been observed [Bic05] [Fei07]. In critically ill patients, a bias of more than 4% has been observed to occur more frequently in black (27%) than in white patients (11%). Acrylic nails do not interfere with readings. Nail varnish, if blue, green, or black, causes inaccurate SpO₂ readings; however, mounting the oximeter probe sideways alleviates the problem with nail varnish [Jub06]. It is better to remove nail varnish prior to measurement.

3.5.3 Limitation in the signal processing

Motion artifact

Motion artifacts contribute a significant error to readings of pulse oximetry [Nag05]. Any transient motion of the sensor relative to the skin may cause a large artifact in the transmitted light and disturb the optical measurements. An innovative technological approach, termed Masimo signal extraction technology, was introduced to extract the true signal from artifact due to noise and low perfusion. When tested in 50 postoperative patients, the pulse oximeter's alarm frequency was decreased twofold with the new system vs. a conventional oximeter. When tested under conditions of low perfusion and motion, the ability to track changes in SpO₂ and reduce nuisance alarms was improved with this technology [Gol00] [Jub06].

Low perfusion

Pulse oximetry depends on satisfactory arterial perfusion of the skin, and thus poor peripheral blood circulation that may be caused by low cardiac output, vasoconstriction, or hypothermia can make it difficult for the sensor to extract the clean photoplethysmography signal from background noise. As mentioned above, Masimo signal extraction technology has succeeded in overcoming this problem. This kind of pulse oximetry limitation will be revisited in section 4.3, as the thesis introduces a signal processing module that can extract the PPG signal under low perfusion conditions.

Delayed detection of hypoxic events

While the response time of the pulse oximeter is generally fast, there may be a significant delay between a change in alveolar oxygen tension and a change in the oximeter reading. It is possible for arterial oxygen to reach dangerous levels before the pulse oximeter alarm is activated [Bar87]

Delay in response is related to sensor location. Desaturation is detected earlier when the sensor is placed more centrally. Lag time will be increased with poor perfusion and a decrease in blood flow to the site monitored [Mar92].

Venous Pulsations

Arteriovenous anastomoses and glomuses are unusual features of the cutaneous circulation, particularly in the fingers and toes. Arterial blood is shunted into a vein, which also becomes pulsatile, causing falsely low readings [Mar92].).

Loss of accuracy at low values

Oxygen saturation values below 70% obtained by pulse oximetry are unreliable. Numerous studies have addressed the accuracy of pulse oximeters, primarily over the range of 70% to 100% saturation. Excellent correlation has been found between pulse oximetry and the “gold standard” in vitro CO-oximetry measurements [Sev92] [Tit97]. Anytime hypoxia is suspected, but not confirmed with pulse oximetry, arterial blood gases (ABGs) should be performed [Kam02].

Tolerance of the light emitting diodes

One of the most significant sources of the pulse oximetry readings' errors is the tolerance in the central wavelength of the light emitting diodes. A defect through the production stages may lead to a tolerance. LEDs also have limited temperature tolerance and falling efficiency as component temperature rises. The central wavelength of the conventional LEDs has a tolerance of +/- 15 nm. Particularly at the wavelength of 660 nm, as the absorption spectra around it is not flat enough (see Figure 3-5), any shift of the value of the wavelength will lead to changing of the extinction coefficients values and a shift in the calibration curve. This effect can be minimized by appropriate selection for the LEDs [Blo02].

Erratic performance with irregular rhythms

Irregular heart rhythms can cause erratic performance. During aortic balloon pulsation, the augmentation of diastolic pressure exceeds that of systolic pressure. This leads to a double or triple peaked arterial pressure waveform that confuses the pulse oximeter, so that it may not provide a reading. Pulse oximetry is notoriously unreliable in the presence of rapid arterial fibrillation [Kam02].

Pressure on the Sensor

Pressure on the sensor may result in inaccurate SpO₂ readings without affecting pulse rate determination.

Ambient light and optical shunting

Bright ambient light or optical shunting (light emitting diodes' light reaching to photodiode without passing through the tissue) can cause error in pulse oximetry readings. Wrapping the probe with an opaque shield can minimize this effect. Although pulse oximeters correct for ambient light, falsely low SpO₂ readings have been reported with fluorescent and xenon arc surgical lamps [Jub06].

3.5.4 Physical factors

Many physical factors should be considered when using the pulse oximeter. The following are common-sense precautions. The clinician should avoid using the grounding pad of the electrocautery near the pulse oximeter sensor. The blood pressure cuff should not be placed on the arm that is being used for the sensor. Arterial lines or sticks should not be placed or performed on extremities used for oximetry. The pulse oximeter should not be plugged into the same power source as the electrocautery unit. Finally, it must be made sure that the light-emitting diode is facing the nail bed and the photodiode is securely positioned on the opposite side of the digit [Mar92].

3.6 Current state of the art

3.6.1 The previous work towards the non-invasive determination of the fractional oxygen saturation and the total hemoglobin concentration

There are many published scientific articles and patents which present various methods for non-invasive determination of the total hemoglobin concentration and the fractional oxygen saturation. But so far these methods did not use the artificial intelligence (AI). In the following, some of them are introduced.

Selim et al. investigated to determine which digital photography could be used to calculate hemoglobin. Hemoglobin concentration in blood was determined by a cell counter. Software was developed to predict the hemoglobin value based on a formula derived using the images and known hemoglobin values from a derivation set of patients. Finally, they reported that it is possible to derive an objective method that correlates conjunctiva color with measured hemoglobin and, when applied prospectively, is able to predict hemoglobin concentration in Emergency Department (ED) patients [Sel07].

A new calculation formula including DC components of optical density was proposed by Takashi's research group. They developed an instrument to measure oxygen saturation (SpO₂), tHb, COHb, and MetHb non-invasively using multi-wavelength LEDs and used a Waseda mock circulatory system, which can simulate blood circulation in tissues and generate a pulse wave mechanically, to estimate the instrument's performance [Hir06].

Gehring's research group developed a photoplethysmography measurement device developed for the German Space Agency DLR. They used a non-invasive multi-spectral method based on the radiation of monochromatic light, emitted by laser diodes in the range 600–1400 nm, through an area of skin on the finger. After interaction with the tissue the transmitted light is detected non-invasively by photodiodes. The method makes use of the intensity fluctuations caused by the pulse wave. The ratio between the peak to peak pulse amplitudes measured at different wavelengths and its dependence on the optical absorbability characteristics of human blood yields information on the blood composition. Deferrals between the proportions of hemoglobin and water in the intravasal volume should be detected photoelectrically by signal-analytic evaluation of the signals. The computed coefficients are used for the measurement and calculation of the arterial oxygenic saturation (SaO₂) and the relative hemoglobin concentration change [Kra05].

The design and testing of a finger probe used in that optical hemoglobin monitor is presented by Yoon et al. [Yoo05]. That finger probe can have different values or settings for design parameters such as the internal color, detector area, the emission area of a light

source and the distance between the light source and detector. Design of experiment (DOE) was introduced to select the best combination of design parameters that were robust to external conditions such as finger alignment and ambient light.

In [Gan05], they developed a method that fits the non-invasive blood component concentration measurement: the dynamic spectrum (DS) method. By using this method, it was possible to eliminate the main interference of the individual discrepancy and extract some kinds of the blood component concentration by the analytic method.

Bercht et al. studied the influence of blood vessel diameter and lateral displacement of the optoacoustic probe on accuracy of total hemoglobin concentration and reported that the optoacoustic technique may provide accurate and real time non-invasive measurements of total hemoglobin concentration [Bre04].

Jeon et al. proposed a model based on the difference in optical density induced by the pulsation of the heart beat, which is developed by taking an approximation of Twersky's theory on the assumption that the variation of blood vessel size is small during arterial pulsing. A device is constructed with a five wavelength light emitting diode array as the light source. The ratio of the variations of optical density between systole and diastole at two different wavelengths is used as a variable. The research group selected several such variables that show high reproducibility among all variables. Multiple linear regression analysis is made in order to predict total hemoglobin concentration. It can be reported that they are the first group who demonstrate successfully the possibility of non-invasive hemoglobin measurement, particularly, using the wavelengths below 1000 nm [Kye02].

Timm et al. introduced a newly developed sensor system, which is able to measure the total hemoglobin concentration with just two wavelengths. Initial results for non-invasive in-vitro, and invasive in-vivo, measurement of the tHb concentration indicate the plausibility of accurately determining tHb concentration using their method [Tim10].

So far, there are no AI applications in the area of measuring the total hemoglobin concentration non-invasively according to searching AI applications in the published articles and patents of this research area [Unb09] [Wip09][Esp08].

3.6.2 Artificial intelligent applications for PPG signal

In this section, the artificial intelligent applications for the PPG signal, which have been already published in scientific articles or patents, are introduced. Some of these applications are related to the pulse oximetry area and the others are not. One of the major problems

related to the monitoring systems in general and especially for the PPG signal extraction is the motion artifact problems. The combinations of time and frequency domain analysis and fuzzy logic were developed by (Nellcor, Pleasanton, CA). These methods have been shown to have varying success on the basis of the measurement type and situations [Tak06]. In [Bel01] and [Bel02], they observed that the systolic upstroke time, the diastolic time and heart rate (HR) extracted from the PPG signal constitute features, which can be used for detecting normal and distorted PPG signal. Therefore, they developed a knowledge-based system using fuzzy logic for classifying plethysmogram pulses into two categories: valid and artifact. Alternative approaches have been suggested using artificial neural networks (ANNs) gradient methods and genetic algorithms (GAs).

The aim of the work of Siegfried Kästle, 1999 [Käs99], was to apply modern signal processing techniques such as fuzzy logic and time-frequency method to develop an algorithm, for greater security and reliability of measurement under difficult conditions of noise to process the signal of the pulse oximeter (PPG). Also, using the AI such as the fuzzy logic and the neural networks for motion artifact estimation was depicted in some of patents, such as [Mar05].

Stetson (Advanced Development Group Nellcor/Tyco Healthcare) has developed a two layer fuzzy logic system to determine the heart rate from the pulse oximeter signals subjected to strong motion artifact [Ste03]. The system finds the heart rate quickly due to its low reliance on past data. On healthy subjects, errors relative to a noise-free reference were small or negligible 77% of the time, and the average initial response time was over 7 times faster than an analogous adaptive filtering method. Also, Nellcor as a company has many patents, which reported that they use the intelligent algorithms in their inventions, which are related to pulse oximetry. But the claims of these patents have no adjusted statements including these AI or how they will use AI. Only they reported in their patents detailed description that they will use the application of programming methods techniques such as, for example, adaptive programming, fuzzy logic and genetic algorithms [Esp08] [Fre08] [Lyn07] [Lyn06].

Current monitoring systems produce frequent false alarms, but they fail to alert clinicians to significant adverse trends that might predict worsening diseases or complications. Presenting staff with continuously updated trend data is helpful in the early identification of significant physiological change and has been shown to improve the standard of care. Improvements in sensors, leads, signal extraction and artifact detection can improve the reliability of monitored data, leading to a great reduction in the number of alarms caused by artifact. Even if artifact could be excluded, monitoring information is still displayed in a raw form, with very little intelligent data integration or processing. Fuzzy logic deals with

the problem of uncertainty. Alarm settings are currently based on the principle of defining acceptable limits. A value is either normal or abnormal, and an abnormal value triggers an alarm. Fuzzy logic chips are able to deal with degrees of abnormality. When combined with neural networks, which are able to undertake complex modelling and learning, it is possible to create systems that can assimilate data from numerous sources over time and use this information to determine whether an alarm should be triggered [Bel02] [Nic04].

Photoplethysmography has been recently studied as a non-invasive indicator of circulatory and respiratory function. In [Joh03], the reflection mode photoplethysmographic (PPG) signal was studied with the aim of determining respiratory rate. The PPG signal includes respiratory synchronous components, seen as frequency modulation of the heart rate (respiratory sinus arrhythmia), amplitude modulation of the cardiac pulse and respiratory induced intensity variations (RIIVs) in the PPG baseline. PPG signals were recorded from the foreheads of 15 healthy subjects. From these signals, the systolic waveform, diastolic waveform, respiratory sinus arrhythmia, pulse amplitude and RIIVs were extracted. Using basic algorithms, the rates of false positive and false negative detection of breaths were calculated separately for each of the five components. Furthermore, a neural network was assessed in a combined pattern recognition approach. The error rates (sum of false positive and false negative breath detections) for the basic algorithms ranged from 9.7% (pulse amplitude) to 14.5% (systolic waveform). The corresponding values for the neural network analysis were 9.5-9.6%. These results suggest the use of a combined PPG system for simultaneous monitoring of respiratory rate and arterial oxygen saturation (pulse oximetry) [All07].

Many researchers used the artificial neural networks with the PPG signal as a classifier [Mas02] [Sol04] [Kno06] [kno08]. Where the artificial neural network is one such artificial intelligence method that is inspired by the way biological nervous systems, such as the brain, process information, and comprises a set of interconnected processing nodes that simulate neurons. In [Sol04], they present Artificial Neural Network (ANN) approaches that classify a PPG signal into two distinct classes. Multistage based on time-series data mining frame work for building classification models in the presence temporal high dimensional data, was suggested. First, they reduce the dimensionality by smoothing the input signal and we assume that the smoothing accuracy serve features by exploring the highly parallelised nature of multilayer feed-forward networks (MFFN). The classification results showed that multilayer perceptron neural network employing back propagation-training algorithm was effective to distinct between the two classes, based on the good selection of the training data set samples. The correct classification rate was 100% for the training data sets and 94.7% for testing data sets. The research group used for testing the algorithm 170 samples, in which 56 samples are pathologies and 114 are healthier.

The research group of Bethany Knorr-Chung recorded the photoplethysmographic (PPG) data from patients under the influence of anesthesia, but not intubated [Kno06]. Both time and frequency domain features were extracted from the PPG and used as inputs to a neural network classifier. This classifier considers inter-subject variability so that it generalizes well to a large population. This classifier provided 86.1% accuracy to classify segments as being times of ‘obstructed’ vs. ‘normal’ airways status. The same group have already improved the previous work and reported that the accuracy showed promise for use in real time monitoring situations [Kno08].

According to this review, it can be reported that the applications of the artificial intelligence for the PPG signal in general and especially for the pulse oximetry area are for Motion artifact minimization (for adaptive noise cancellations), alarms and PPG signal classifications.

3.6.3 Non-invasive tHb concentration devices in the market

Although, so far, the standard method of measuring total hemoglobin concentration is invasive, there are non-invasive measuring devices for tHb concentration in the market. Approximately, there are two devices one belongs to MPR Optical Company and the other belongs to MASIMO Company.

The device of MBR company is haemospect®. It measures tHb concentration and oxyhemoglobin and desoxyhemoglobin. The principles of operation are projecting a white light into the underlying tissue via a waveguide. Another waveguide transmits the light reflected as a result of the physical conditions back to the device. A spectrometer breaks the light down into its separate wavelengths and an electronic evaluation unit connected to the system analyses it [MBR11]. There is no available information about the accuracy of this device.

Pronto-7 is the device of MASIMO with Rainbow-4D technology for easy-to-use spot-check testing of hemoglobin (SpHb®), SpO₂, pulse rate, and perfusion index. It uses multi-wavelengths light emitting diodes sensor. This device is evaluated by testing its accuracy and compared to the accuracy of Hemocue 201⁺ as published in the technical bulletins of MASIMO [TbM11]. Also, it should be noted that hemocue 201⁺ measures the tHb concentration using only 10 µL of capillary, venous, or arterial blood. The company reported its accuracy by ±1.5% when compared to the international reference method for hemoglobin (the ICSH method) [Hem11].

According to the current state of the art, there is no a available device can measure tHb and the four hemoglobin components ratios as well. Also, using the fuzzy logic expert systems to measure these physiological variables is a new trend.

Part II
Methodology

4. Optoelectronic System Set-Up for Non-Invasive Measuring

4.1 Preliminaries

The proposed algorithms of the non-invasive measuring for the total hemoglobin concentration and the ratios of the four hemoglobin components are based on the principles of the pulse oximetry that utilizes the photoplethysmography technology to measure the functional arterial oxygen saturation. Therefore, it is very necessary to set-up an optoelectronic system that can extract the photoplethysmography (PPG) signals for further processing and calculations.

This chapter presents the developed optoelectronic system including the developed printed circuit that extracts seven PPG signals with different wavelengths, a proposed signal processing module for the cases of the low amplitude PPG signals, and collecting the seven PPG signals to be separated online in LabVIEW environment.

4.2 PPG signals extraction

The PPG signals are extracted by a developed optoelectronic circuit that is described by Figure 4-1. It is based on a Microcontroller ARM7-ADUC7020 that performs some control and interfacing functions, which are summarized as follows:

- The Microcontroller provides a synchronized illuminating for six light emitting diodes (LEDs) with different wavelengths using its timer interrupt routines and three (General Purpose Input/Output) (GPIO) to drive the three input selection pins of an eight channel Multiplexer.

- The illuminating of the 7th LED that has a wavelength of 1200 nm is controlled by the Microcontroller via digital to analog converter number two (DAC2), which is employed as an on/off control signal for the transistor circuit number two taking into account the illuminating time of the other six LEDs.
- A transimpedance amplifier circuit is used to detect the light intensity that is transmitted through the finger. This signal is received by the Microcontroller on analog to digital converter number zero (ADC0) to control it in order to be in the suitable range (1.5 volt-2.4 volt) and avoid the saturated signals via digital to analog converter number zero (DAC0) that controls the LEDs light intensity by controlling the transistor circuit number 1.
- ADC2 and DAC1 of the microcontrollers are used to develop a signal processing module in the cases of low amplitude signals. This will be demonstrated in detail in section 4.3.

The functional block diagram of ARM7-ADUC7020 of Analog Devices is depicted in Figure 4-2. Detailed information about the features of this microcontroller, such as analog I/O, clocking options, available memory and on chip-peripherals are described in its data sheet [Dat08].

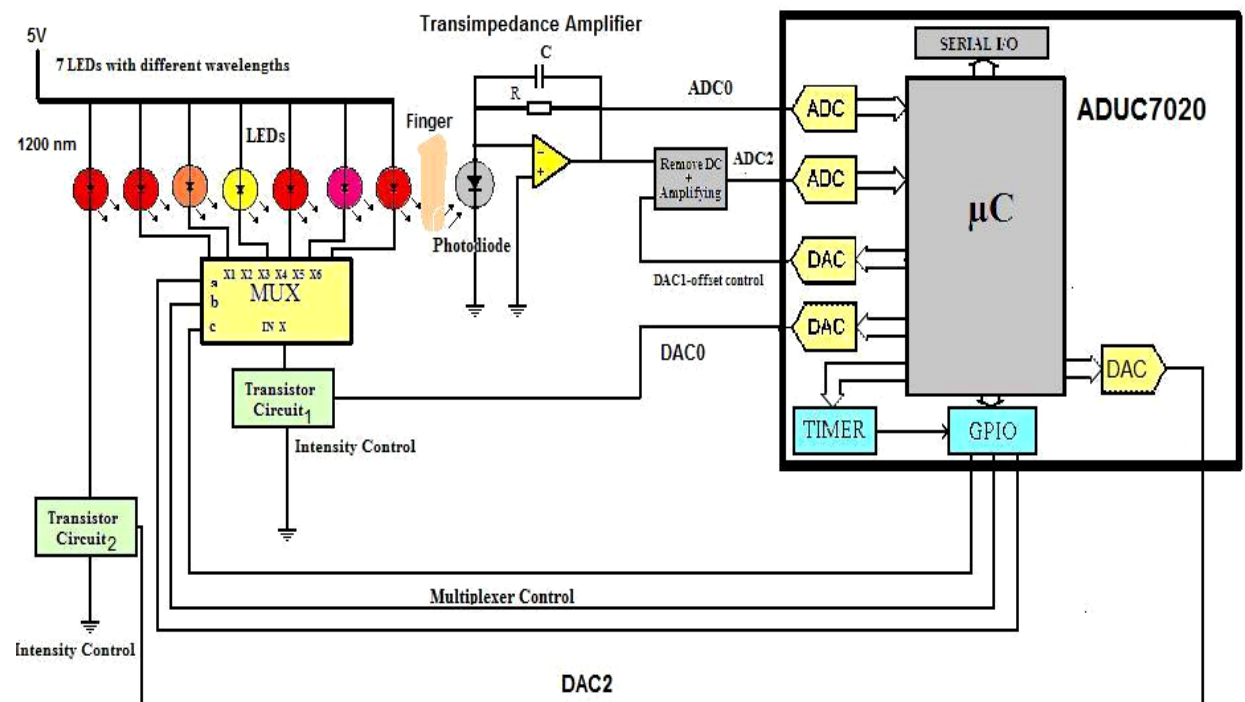


Figure 4-1: Block diagram of the developed optoelectronic circuit.

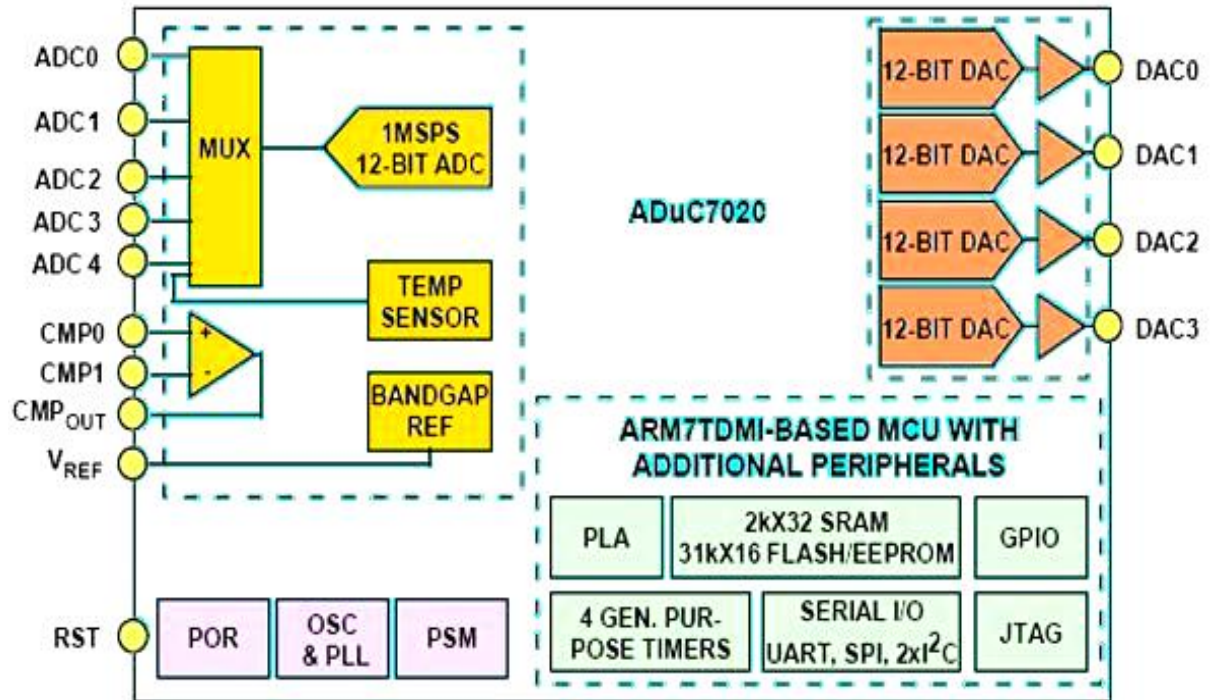


Figure 4-2: The functional block diagram of ADUC7020 (Analog Devices) [Dat08].

4.2.1 Transimpedance amplifier circuit

A simple transimpedance amplifier circuit is employed to detect the variation of the photodiode's current according to the variations of the received light intensity and convert it to voltage after amplifying it. Figure 4-3 shows the schematic diagram of the transimpedance amplifier circuit.

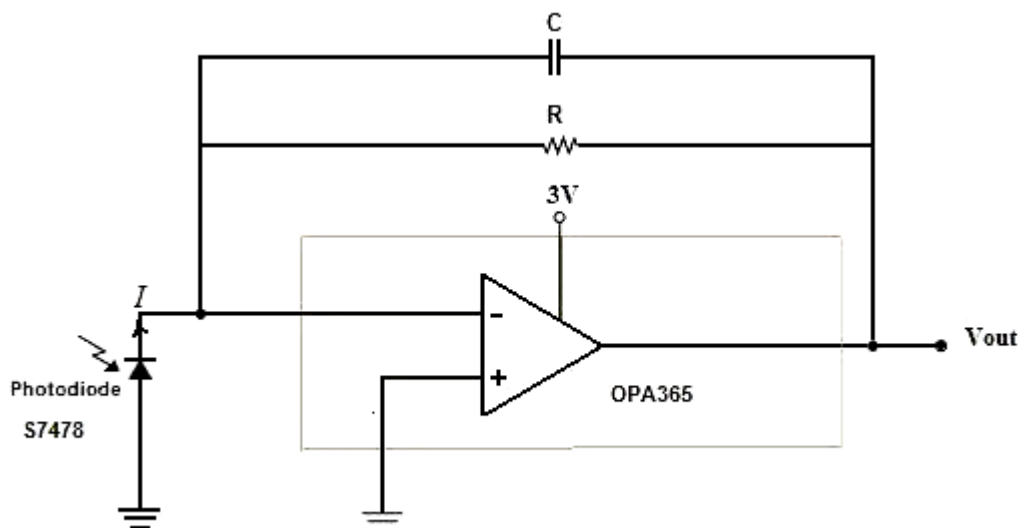


Figure 4-3: Schematic diagram of the utilized transimpedance amplifier circuit.

The transfer function of this electronic circuit can be expressed as:

$$\frac{V_{out}(s)}{I(s)} = \frac{R}{1 + RCS} \quad (4.1)$$

According to Eq. (4.1) the used transimpedance amplifier electronic circuit reacts as a first order system with a gain (R) and a time constant of (RC). As the capacitance value will be small the output response will be faster and reach the steady state value faster. That means, at the steady state, as (s) equals zero, the output will be simply equal to the input (I) multiplied by the gain (R). But by decreasing the capacitance value, the signal overshoot will appear. Therefore, the value of the capacitance was chosen according to a simulation experiment by the linear technology spice software (LTspice).

Figure 4-4 shows the output response of the circuit without a capacitance component. The simulated input current is a pulse with an on duration of 625 μ Sec for every 5 mSec. The output response is affected by high overshoot. By adding a capacitor with a capacitance of 1 pF as a negative feedback and parallel to the resistor, the overshoot is cancelled as depicted in Figure 4-5.

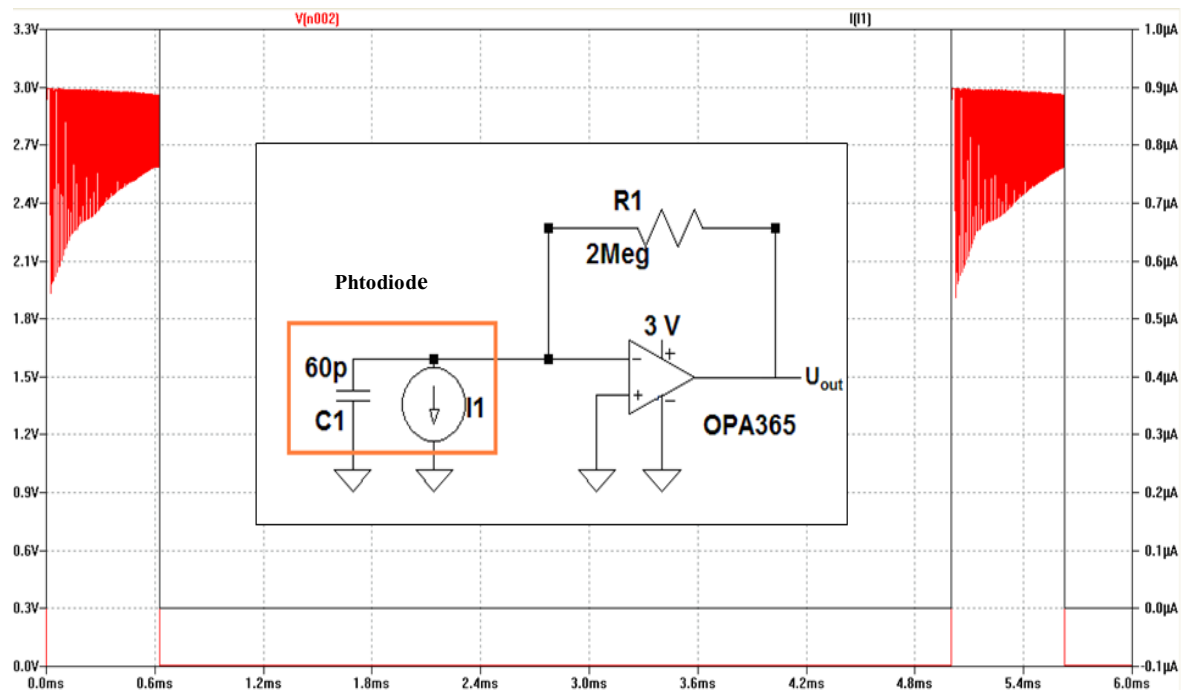


Figure 4-4: Simulation of the transimpedance amplifier circuit output before adding a negative feedback capacitor [Zab08].

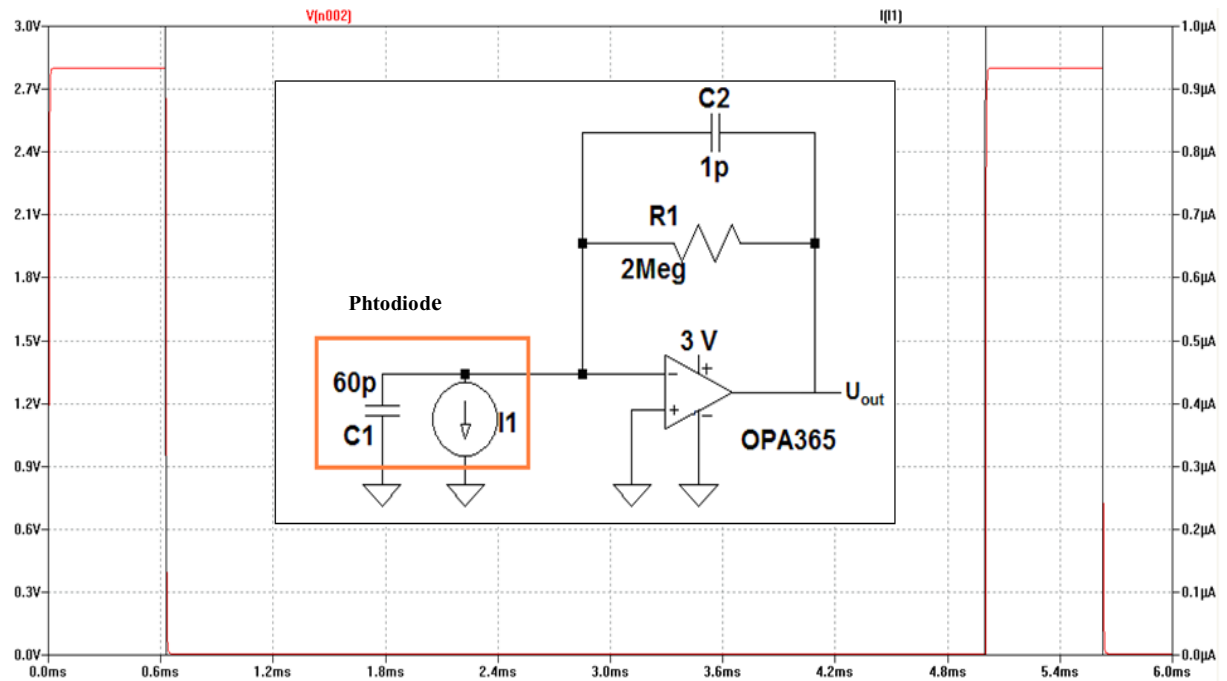


Figure 4-5: Simulation of the transimpedance amplifier circuit output after adding a negative feedback capacitor [Zab08].

4.2.2 LEDs drive circuit and control

The patients have different fingers in terms of color or dimensions and hence the absorbed light by the patient's fingers is variable, sometimes high and sometimes low according to the characteristics of the patient's finger. Thus, it is very important to control the light intensity of the light emitting diodes to prevent the transimpedance amplifier signal being saturated. If the light intensity of the LEDs is not adapted, the PPG signal can sometimes not be extracted as the AC component of the PPG signal is eliminated because of the saturation.

The functional block diagram of the LEDs drive circuit and control is depicted in Figure 4-6. Three (general purpose Input/Output) (GPIO) (P0.5, P0.6, and P0.7) are responsible for selecting a LED to be illuminated for 625μSec according to a timer interrupt routine. The number of the Multiplexer channels are eight, hence every LED is illuminated for 625μSec every 5mSec.

The 7th and 8th channels of the multiplexer are not connected to any LED. At the time interval that is related to the 7th channel, the ambient light will be detected by the transimpedance amplifier circuit to be used for further calculations. At the time interval of

the 8th channel, the LED of the wavelength of 1200 nm will be illuminated but only for 325 μ Sec not 625 μ Sec according to the signal of DAC2. The timing diagram of all light emitting diodes is illustrated by Figure 4-7.

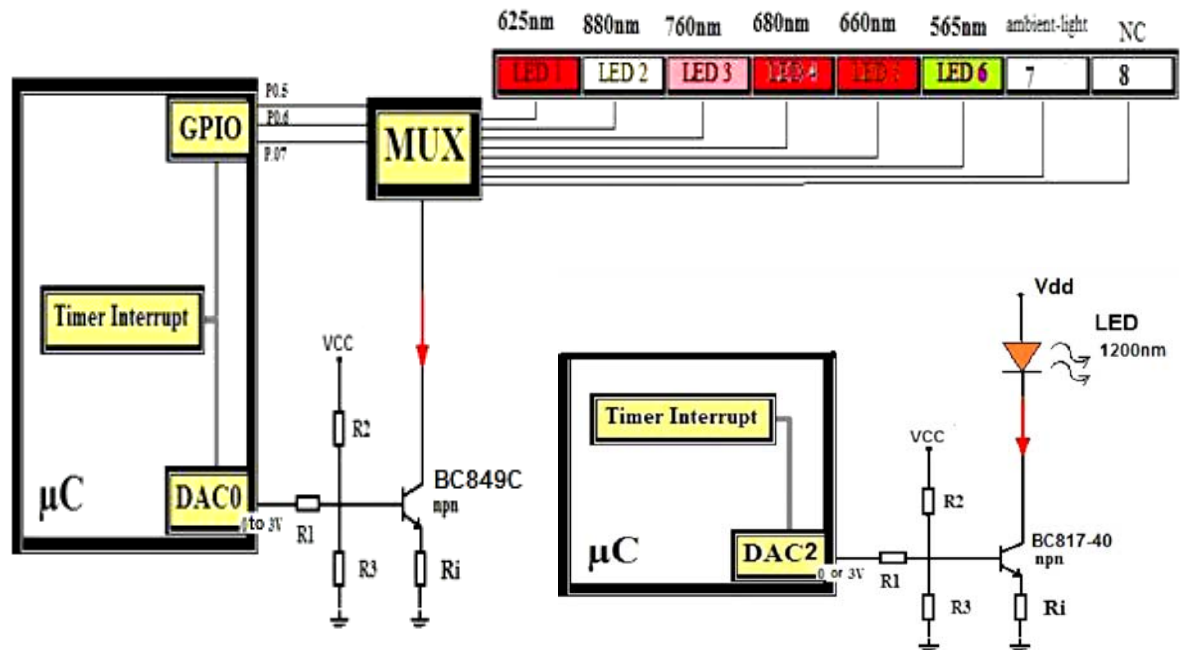


Figure 4-6: Functional block diagrams of the LEDs drive circuit and control

The LED of 1200 nm is driven by the transistor circuit number 2 because its pulse forward current is 1000 mA (as demonstrated in data sheet of (LED 1200-03) ROITHNER LASERTECHNIK) but the other LEDs have pulse forward current of approximately 120 mA, so that, it needs a special transistor and a special drive circuit, as shown in Figure 4-6.

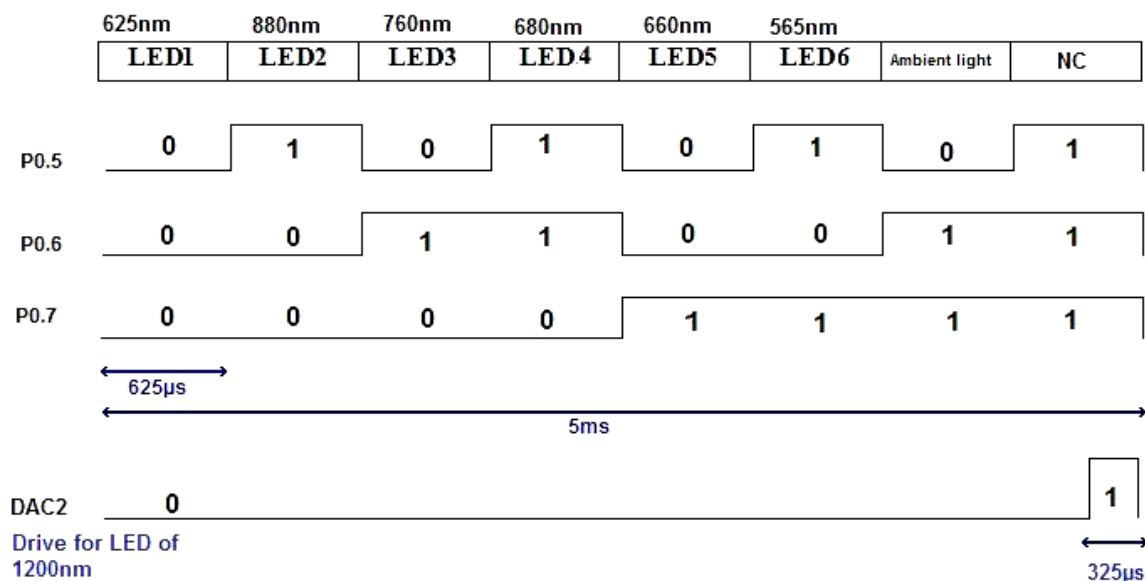


Figure 4-7: Timing diagram of the LEDs synchronized illumination.

DAC2 signal is 0 or 3V to switch off or on the npn transistor (BC817-40) of the transistor circuit number 2. DAC0 signal range is from 0 to 3V to control the collector current of the transistor (BC849C) of the transistor circuit number 1. If DAC0 is increased the base current will be increased, the collector current will be increased, and the light intensity of the LEDs will be increased and vice versa. Therefore, to control the light intensity of each LED, the signal of the transimpedance amplifier, which detects the transmitted light intensity, is transferred to ADC0. ADC0 value is read for each LED and compared to a specific range ($V_{min}=1.5$ Volt and $V_{max}=2.4$). If ADC0 value is larger than V_{max} , the DAC0 value will be decreased to be in the suitable range. If the ADC0 value is smaller than V_{min} , the DAC0 value will be increased. Figure 4-8 shows the flowchart of this light intensity control criteria.

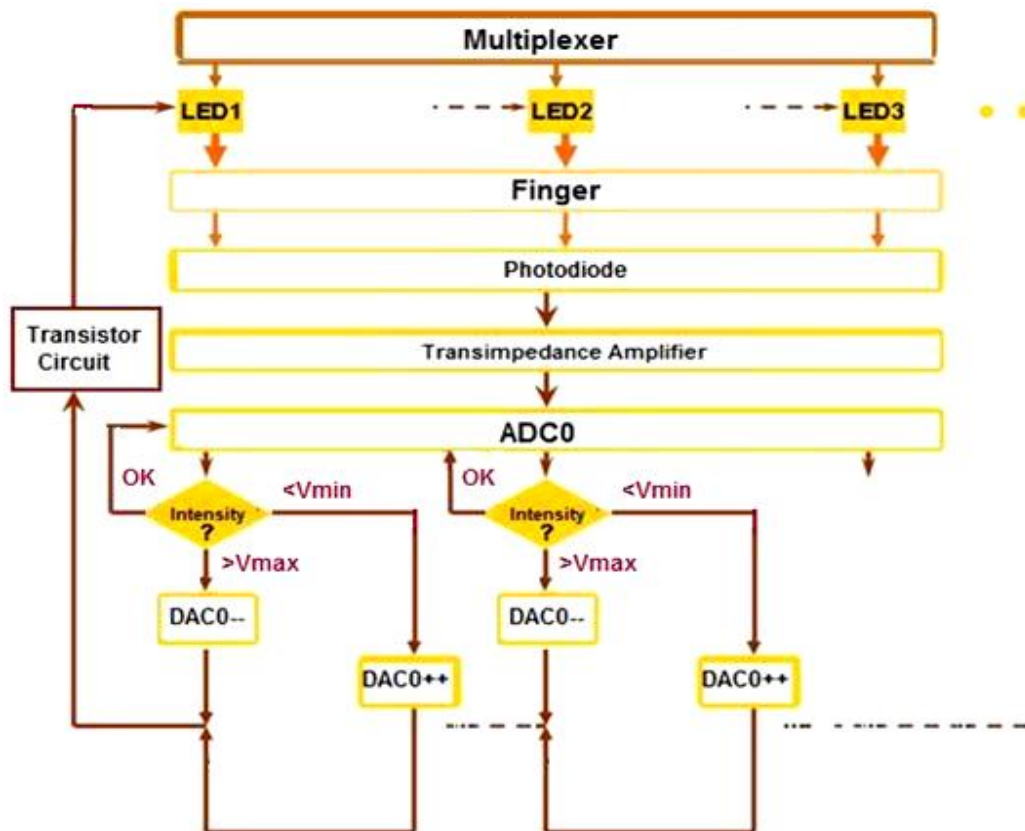


Figure 4-8: Flowchart of the LEDs intensity control loop.

4.3 Proposed low perfusion signal processing module

The PPG signal quality is very important to ensure accurate measurements. This section explores a signal processing module to improve its quality, particularly for the cases of the low signal amplitude and relatively poor signal-to-noise ratio (SNR). The proposed module consists of two stages: a differential amplifier that retains high common-mode rejection

ratio (CMRR) and a programmable gain amplifier (PGA) that utilizes a programmable potentiometer. The two stages are controlled by an ARM7 microcontroller.

A photoplethysmography signal consists of two components: DC and AC. The amplitude of the AC component may be lower than 0.1% of the DC amplitude, in cases of low perfusion. The extracted PPG signal is corrupted by noises, which are induced by ambient light changes, respiration, motion and electromagnetic disturbances. All undesired components have to be eliminated with different signal processing methods [Pil07].

When the peripheral perfusion is poor, as in states of hypothermia, vasoconstriction and low cardiac output, the amplitude of the AC component will be very low. In these circumstances, the PPG sensors fail because they are usually placed on the most peripheral parts of the body, where pulsatile flow is most affected by low perfusion [Vil99] [Him04][Web04] [Ger02].

The conventional signal processing methods overcome this problem by amplifying the PPG signal by using analog/digital amplifiers to an optimum level so that physiological parameters can be calculated. The main disadvantage of this method is that the noise, which corrupts the PPG signal, will also be amplified and lead to wrong calculations where the signal quality is relatively poor [Med11].

The proposed signal processing module limits that disadvantage by using an adaptive analog differential amplifier stage, (which has a high common mode rejection ratio (CMRR)), before the amplification stage. As each PPG signal has to be reduced by 80% of its value leading to a decrease of the DC component and the noise effect and keeping the AC component that will be amplified. The amplification stage is also adaptable using a programmable gain amplifier.

4.3.1 Functional block diagram of the proposed signal processing module

Figure 4-9 shows the functional block diagram of the proposed signal processing module. It is based on the same ARM7 microcontroller, *ADUC7020*, which receives the PPG signal from the sensor on the analog to digital converter number zero (ADC0) to be processed in order to calculate 80% of its value and transfer it by the digital to analog converter number one (DAC1) to the analog differential amplifier stage. Therefore, the original PPG signal and its ratio, which are corrupted approximately with the same noises, are the two inputs of the differential stage that was designed with unity gain. Figure 4-10 shows the circuit diagram of the differential amplifier. It is based on an operational amplifier (one channel of OPA2365, Texas Instruments).

According to the high CMRR advantage of the differential amplifiers that is based on the operational amplifiers, this stage output, which represents approximately 20% of the original PPG signal, is affected by less noise than the original PPG signal.

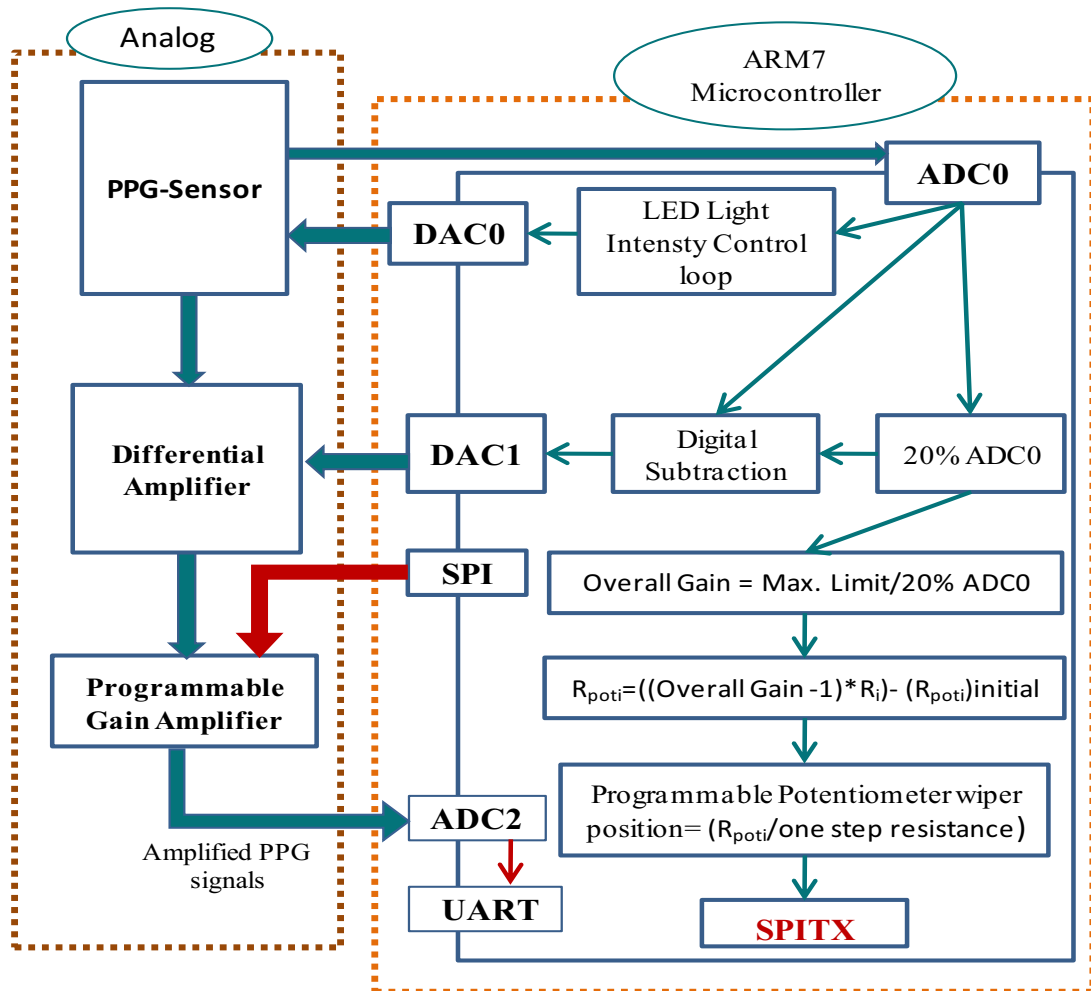


Figure 4-9: The functional block diagram of the proposed signal processing module.

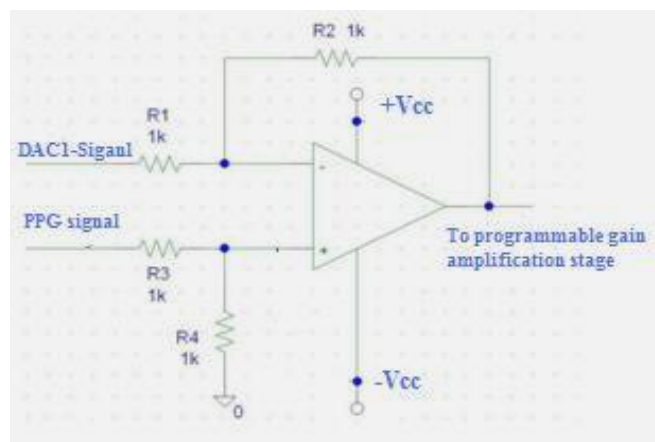


Figure 4-10: The analog differential amplifier circuit diagram.

The programmable gain amplifier is designed as a typical non-inverting amplifier circuit, as depicted in Figure 4-11. The overall gain is expressed as;

$$\text{Overall gain} = (R_{\text{poti.}}/R_i) + 1 \quad (4.2)$$

R_{poti} is the actual resistance of a programmable potentiometer (AD5231, Analog Devices) and R_i is the fixed input resistance. To define the overall gain, the R_{poti} should be chosen for each PPG signal and R_{poti} initial value should be taken into account.

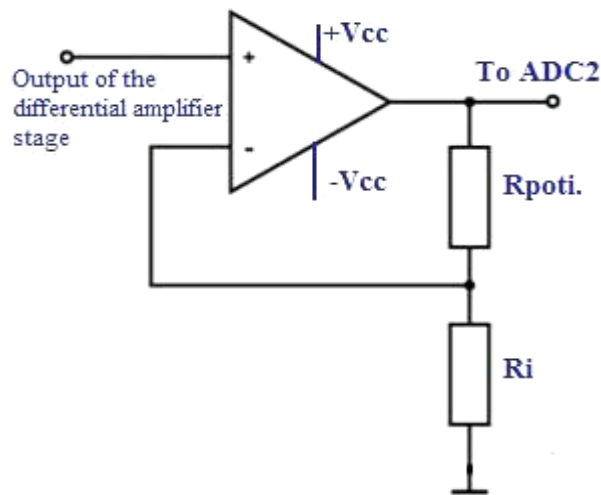


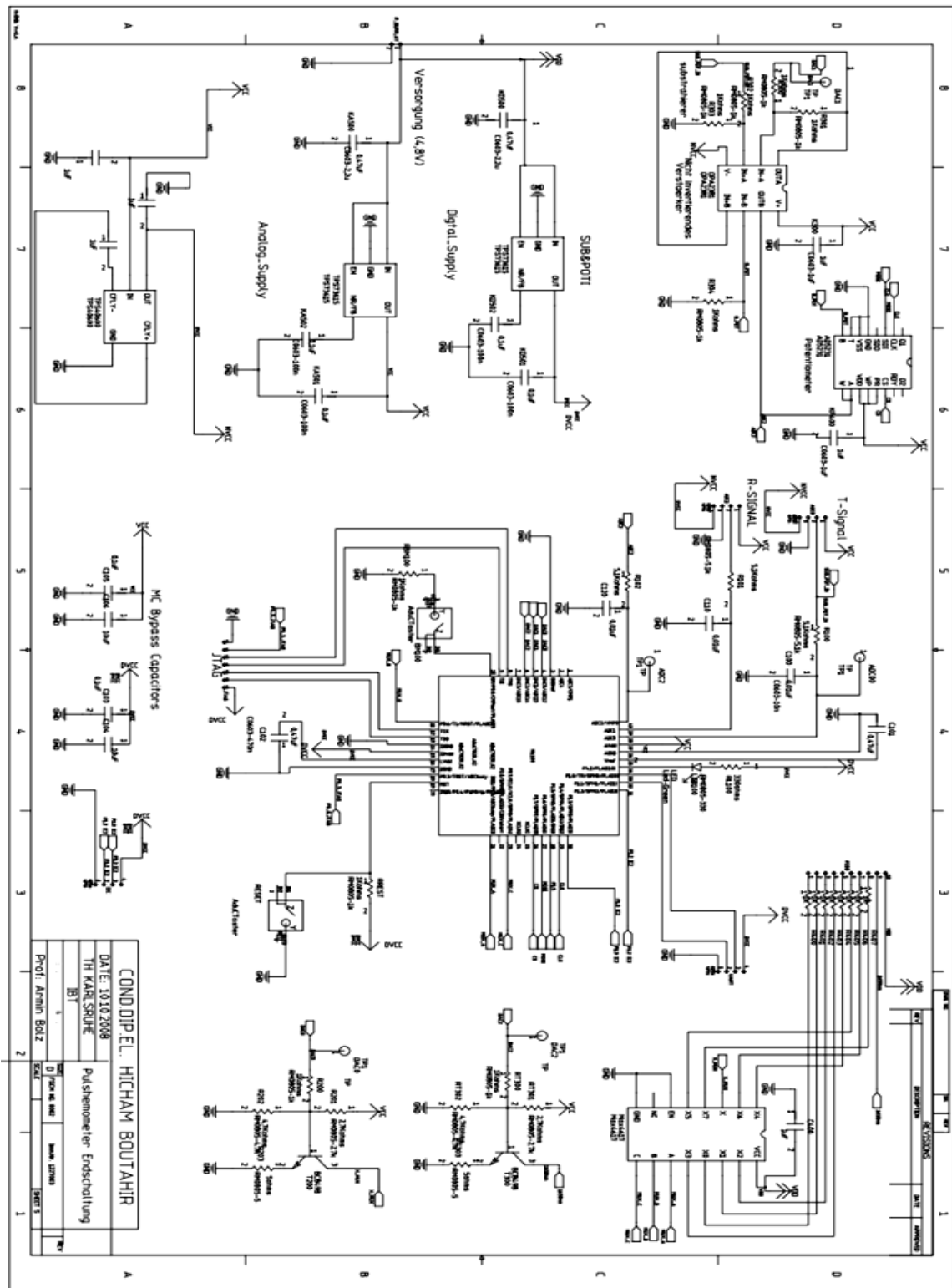
Figure 4-11: Non-inverting amplifier circuit diagram

The microcontroller performs the inverse operation by defining the desired overall gain firstly and then calculating the value of R_{poti} , taking into account its initial value as depicted in the block diagram. The overall gain is estimated by dividing the maximum value limit of the amplified PPG signal by the 20% from the original signal. According to ($R_{\text{poti.}}$) value, the wiper position of the programmable potentiometer is estimated by dividing the value of the $R_{\text{poti.}}$ by the value of the resistance that represents one step of the wiper position and so the required number of the wiper position steps is transferred to the programmable potentiometer via the Serial Peripheral Interface (SPI).

The output of this stage is the amplified PPG signals that will be received by the analog to digital converter number two (ADC2) to be transferred via the serial interface port UART to the LabVIEW environment. Also, the original PPG signal (ADC0) can be transferred via UART. The eliminated portion of the DC component as well as the overall gain values are stored by the ARM7 microcontroller for further calculations.

4.3 Proposed signal processing low perfusion module

The overall schematic diagram is shown by Figure 4-12. The layout of the developed printed circuit and the layout of the transimpedance amplifier are attached to the thesis in the appendix.



4-12: Schematic diagram of the developed optoelectronic printed circuit for the PPG signals extraction.

4.3.2 The proposed signal processing module evaluation

To evaluate the signal processing module, both the original and the amplified PPG signals are collected without using any kind of filters and are tested by calculating the signal-to-noise ratio (SNR) that was considered an index to examine the PPG signal quality [Gan06] [Sha06]. This was accomplished using the fast Fourier transform (FFT). SNR characterizes the ratio of the fundamental signal to the noise spectrum as depicted in the following equation [Str10]:

$$\text{SNR} = 20 \log ([\text{Fundamental}] / \text{SQRT}(\text{SUM} (\text{SQR}(\text{Noise})))) \quad (4.3)$$

Figure 4-13 presents an example of a PPG signal of a wavelength 970 nm, where the original and the amplified signals are shown. Their power spectrums, in different ranges of frequencies, are also depicted to illustrate the DC components, the signal fundamental harmonic and the noises harmonics. The dominant frequency of the signal is 1.29 Hz. By calculating the SNR for the two cases, the original signal has SNR of 35 dB and the amplified signal has SNR of 54 db, which means that the signal quality is relatively good even after amplification and the proposed signal processing module could overcome the disadvantage of the conventional ones, which leads to a poor signal quality by amplifying the signals, particularly in the cases of the low signal amplitude.

The involved frequencies in the power spectrum of the collected PPG signal which include the (Traube-Hering-Mayer) THM frequencies and result from the autonomic nervous system and range from 0.07 to 0.5Hz can easily be isolated by using enough resolution [Rus96].

4.3 Proposed signal processing low perfusion module

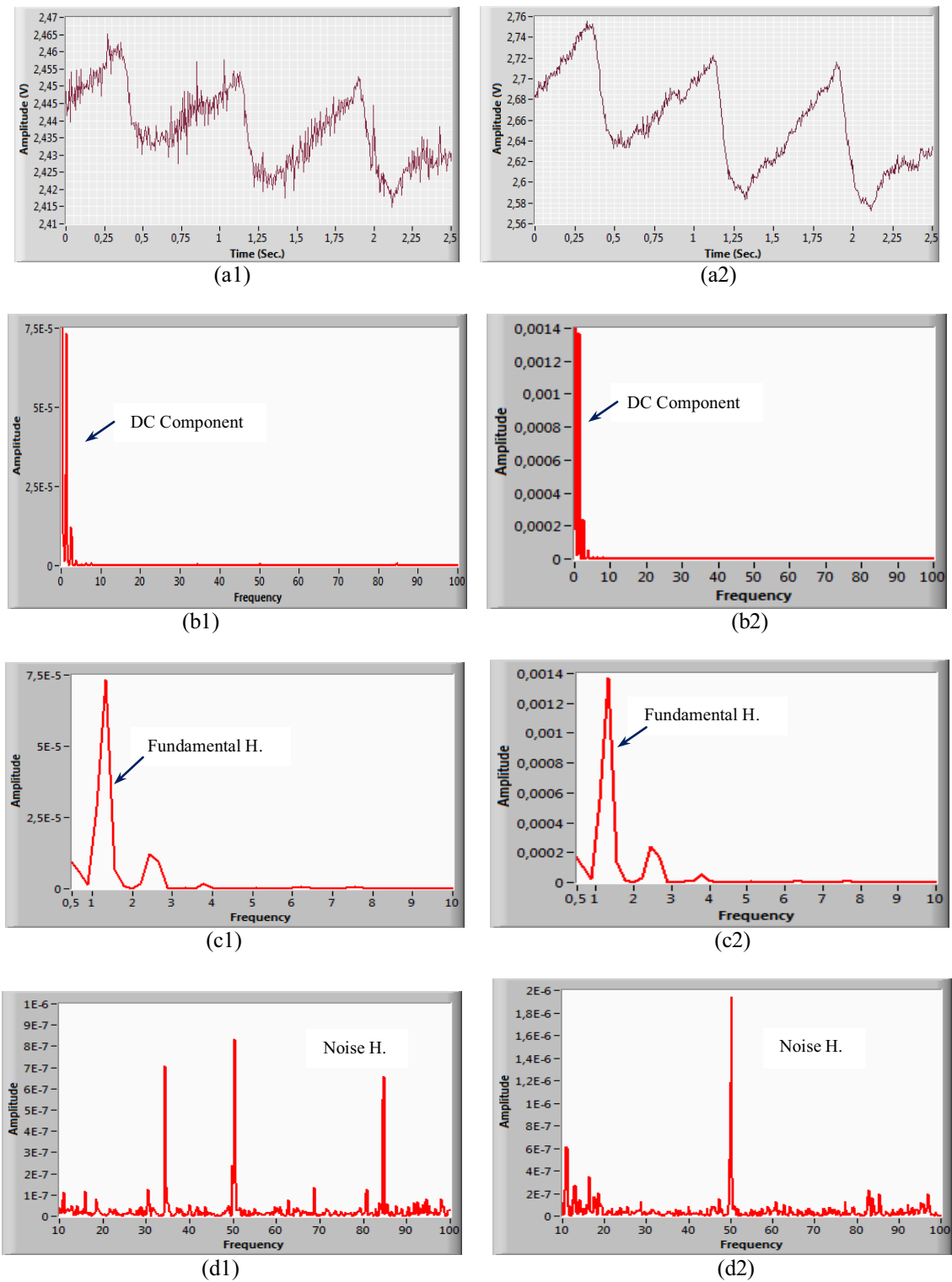


Figure 4-13: Original PPG Signal (a1), Amplified PPG One (a2), their FFT in Different Ranges of Frequencies (b, c, d).

4.4 Flow chart of the software processing outline

To summarize, the overall flow chart that shows the outline of the software processing is depicted in Figure 4-14. The main steps can be demonstrated as follows;

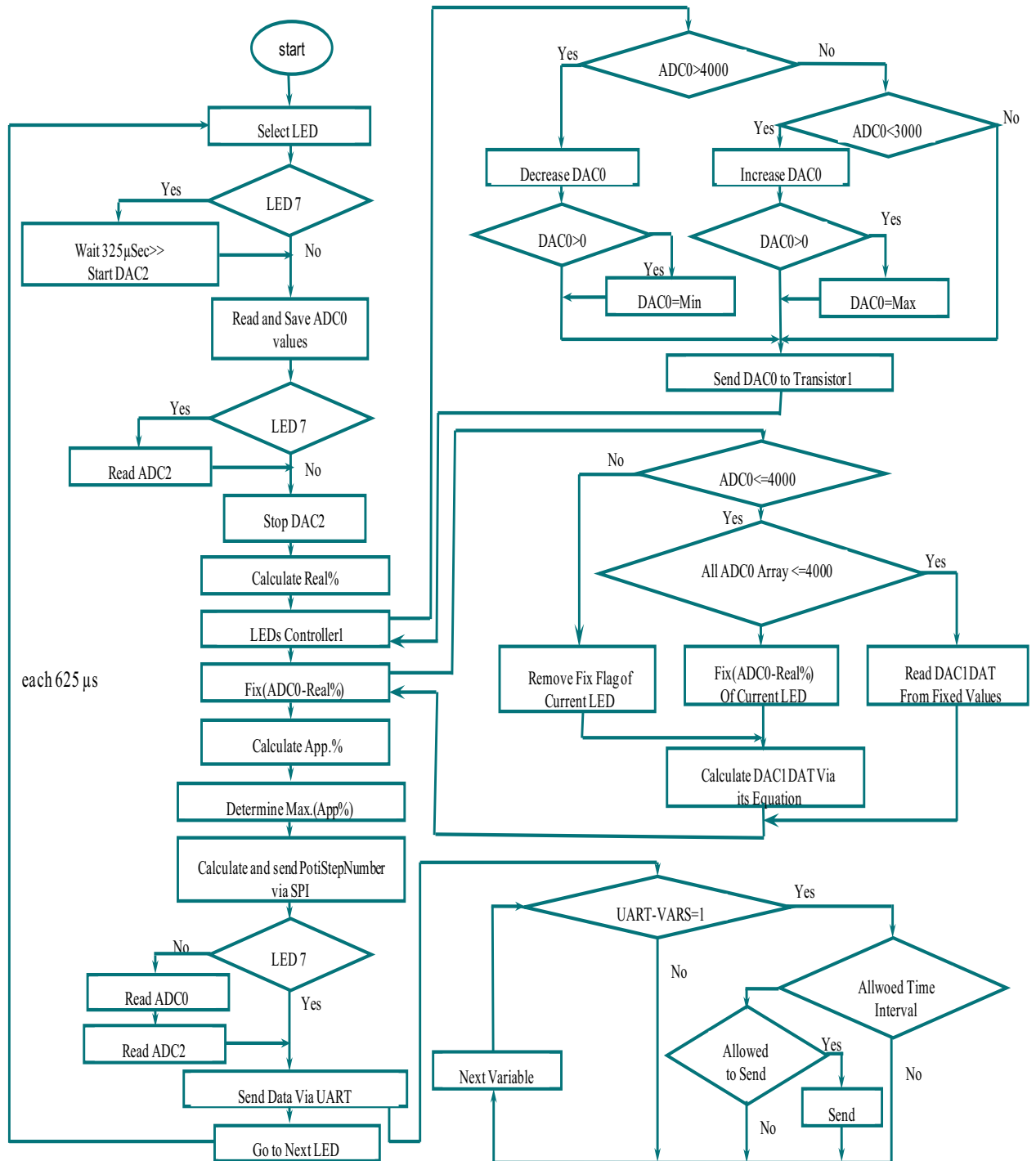


Figure 4-14: Flowchart of the software processing outline

- The main loop starts by selecting the LED number and is repeated every 625 μs according to the timer interrupt routine.
- If the LED number is seven that means this is the time interval for the LED of 1200 nm, so that, the DAC2 signal will be generated, but only after 325 μs from the beginning of the interval for 325 μs .
- ADC0 is read to be controlled by the signal of DAC0 as explained in section 3.2.2.
- The overall gain of the programmable gain amplifier stage is identified by calculating the value of the digital programmable potentiometer resistor and then sending it to the programmable gain amplifier stage via SPI.
- The output signals (7 PPG signals) transferred, as a one signal, via UART into the LabVIEW environment.

The software programs of this overall flowchart are written in CrossWorks for ARM 1.7.

4.5 Overview of the optoelectronic system output

Figure 4-15 presents a top view of the printed circuit of the optoelectronic system. It is a four-layer printed circuit and its dimensions are 40 mm \times 30 mm. The PPG signals are transferred via UART, (as a one signal), into LabVIEW environment. This signal is recorded in LabVIEW for 30 sec and then separated into seven photoplethysmography signals using a LabVIEW developed SubVI, as depicted in Figure 4-16. After this stage, the extracted seven PPG signals are ready to be processed for the demands of the calculation algorithms, which is explained in chapter five.

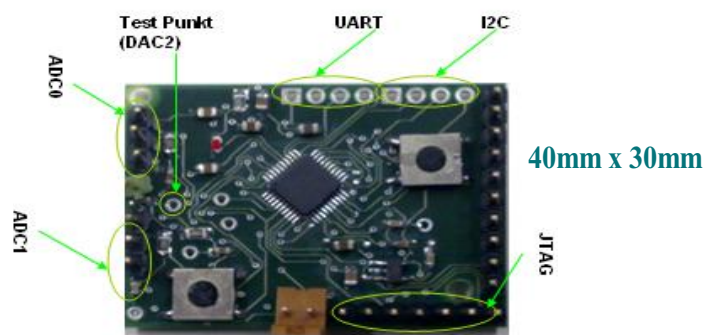


Figure 4-15: The printed circuit of the optoelectronic system.

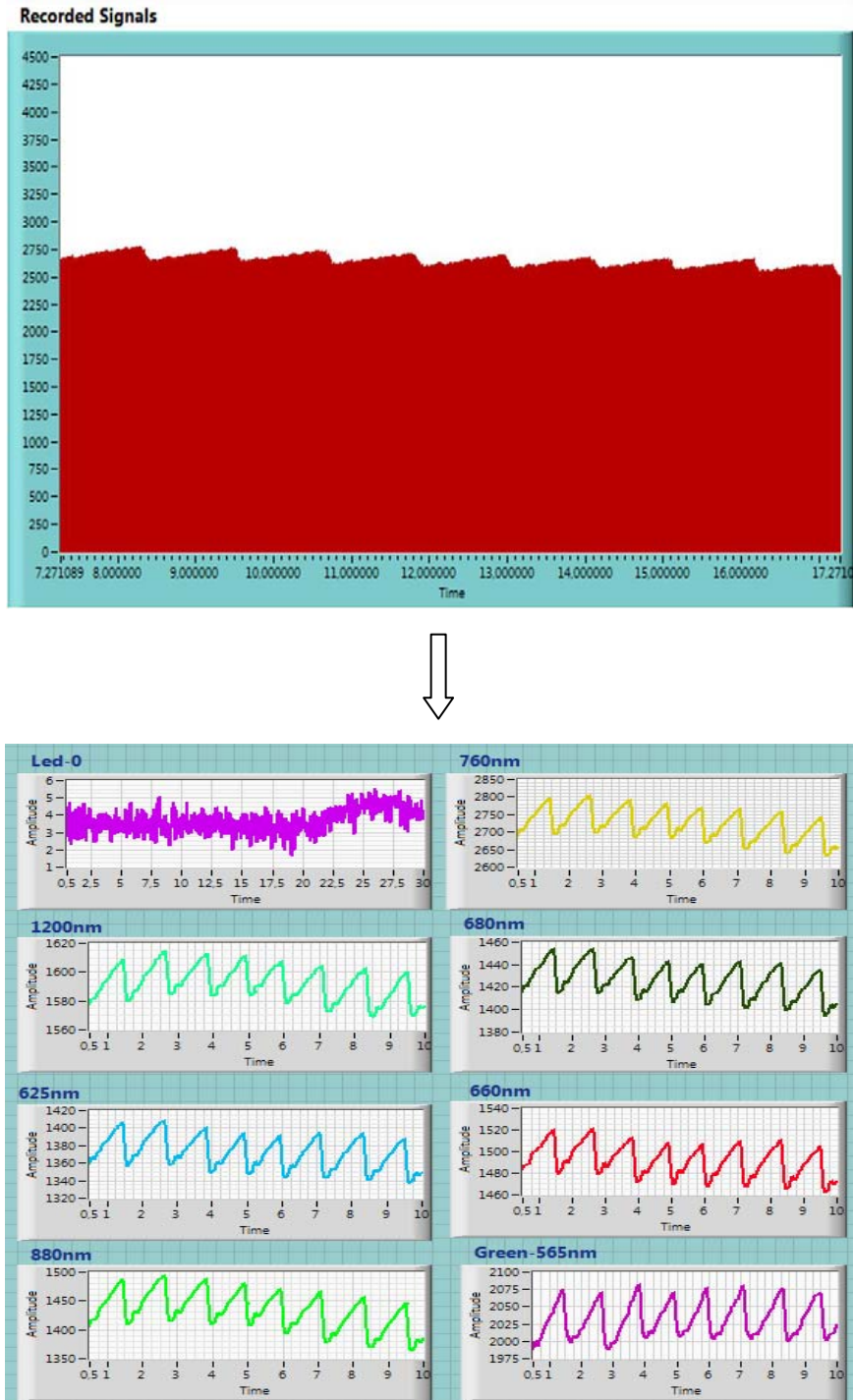


Figure 4-16: PPG signals separation in LabVIEW.

5. Proposed Estimation Approaches for Non-Invasive Measuring

5.1 Preliminaries

Non-invasive determination of total hemoglobin (tHb) concentration, oxyhemoglobin (O₂Hb) ratio, reduced hemoglobin (RHb) ratio, carboxyhemoglobin (COHb) ratio and methemoglobin (MetHb) ratio is the main objective of this thesis. Two estimation approaches are proposed in this chapter. Photoplethysmography (PPG) technology is considered the cornerstone of applying these estimation approaches, as seven PPG signals are processed and analyzed within the calculations. The most important task before applying the estimation approaches should be extracting the main features of the PPG signal, which are the values and the locations of its peaks and valleys. A robust peaks and valleys detection algorithm, which is developed in LabVIEW, is introduced in the next section of this chapter.

The first estimation approach is based on modified Lambert-Beer's law. This approach can estimate the pre-mentioned physiological variables by two methods. Each method employs a different equation, which is derived according to the principles of the modified Lambert-Beer law and pulse oximetry, as presented in section 5.3.

As a new trend, the artificial intelligent algorithms are employed in the second estimation approach to estimate those physiological variables. As demonstrated in section 5.4, a fuzzy expert system is developed to describe the operation of the measurements according to a generated fuzzy rule base and also the basis of pulse oximetry.

5.2 PPGs main distinctive features extracting

In time domain, the main distinctive features of the PPG signals are the diastolic values (peaks) and the systolic values (valleys) and their locations that are considered the cornerstone of any computerized pulse diagnosis and calculating various physiological

parameters. A lot of valuable previous research has been done to detect the peaks and valleys of the PPG signals [Sik09] [Xu08] [Cha05] [Nij07].

The further signal processing and the implementation of the estimation approaches, to measure the interesting physiological variables, are executed using LabVIEW software. Therefore, detecting of these features is required in the same software environment. Peaks/Valleys-Virtual Instrument (VI) in LabVIEW software cannot be used to detect the peaks and valleys of the PPG signal because it detects all the peaks and valleys of the signals not only the desired ones (systolic valleys and diastolic peaks), as shown in Figure 5-1. This section introduces a fast detection algorithm in LabVIEW to detect only the desired peaks and valleys reliably.

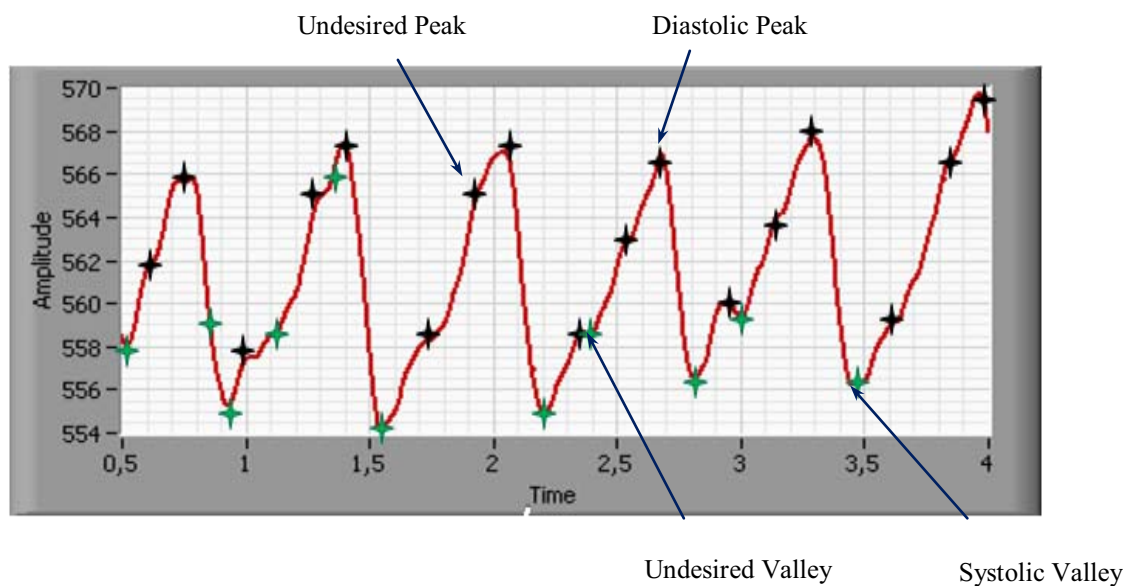


Figure 5-1: Peaks and valleys Detection by Peaks/Valleys detection VI.

The block diagram of the developed peaks and valleys detection algorithm is depicted in Figure 5-2. The steps of this algorithm can be explained as follows;

The first step is to identify the dominant frequency of the signal by means of Tone Measurements VI “LabVIEW Virtual Instrument” then the signal is filtered by a low pass filter that has a cut off frequency lower than its dominant frequency. At the right of Figure 5-2, the PPG signal and the filtered one are depicted. The filtered signal has a number of peaks that are exactly equal to the number of the desired peaks but with little shift to the right direction.

Hence, the second step is to extract all peaks of the filtered signal using Peaks VI. Then, the original signal is cut at the location of every peak, which belongs to the filtered signal, and so the Peaks VI is applied on this part with a threshold equal to the filtered peak value. The desired peak of the original PPG signal is chosen as the peak that has a maximum location.

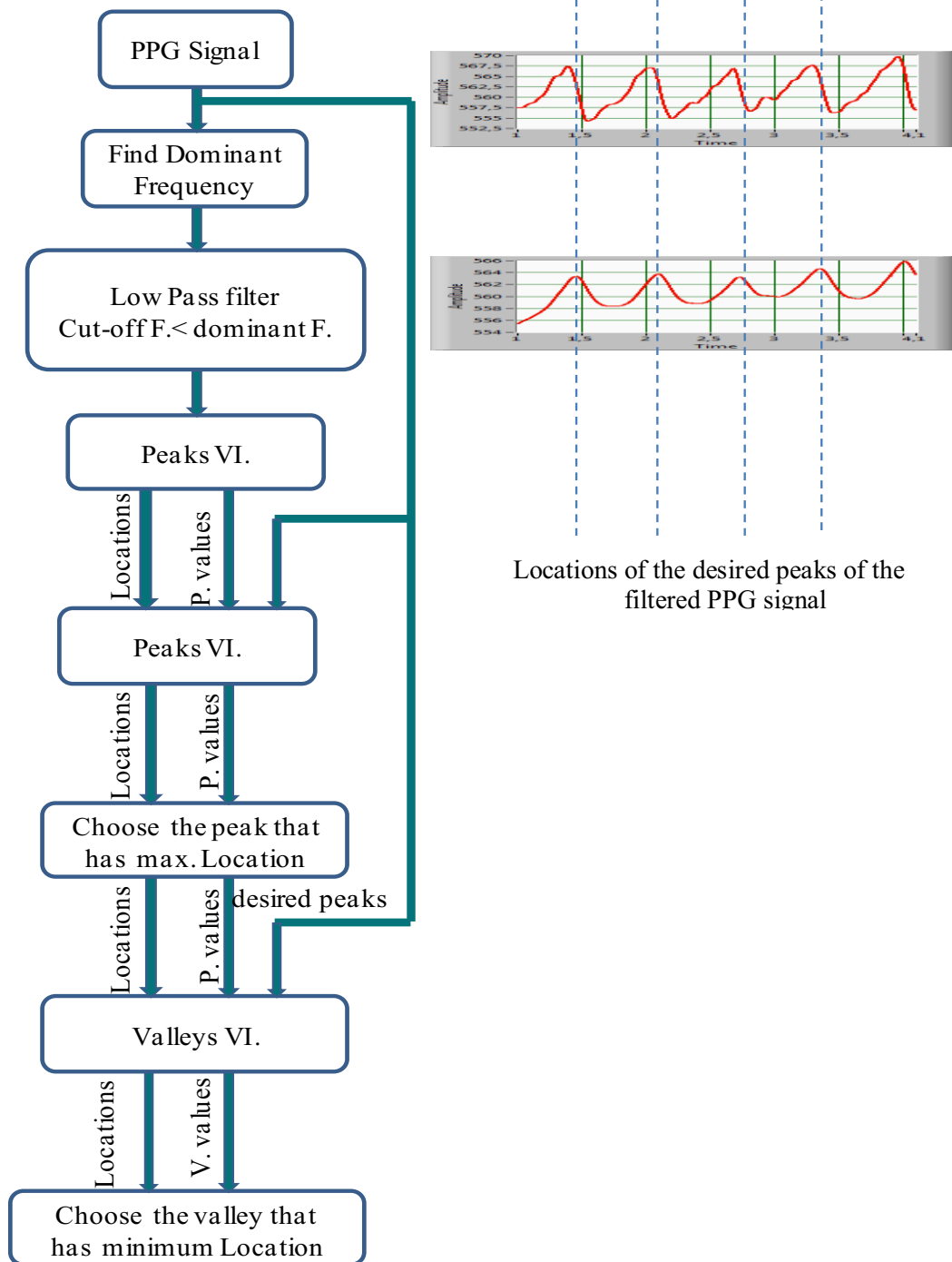


Figure 5-2: Block diagram of the developed peaks and valleys detection algorithm in LabVIEW.

The third step is to detect the corresponding valley of each extracted desired peak. At the location of each desired peak, the original signal is cut and Valleys VI is applied. Then the valley that has the minimum location next to the desired peak will be chosen as the desired valley of the original PPG signal.

As demonstrated in Figure 5-3, the explored peaks and valleys detection algorithm could extract the desired ones effectively unlike the Peaks/Valleys VI, which detects all the available peaks and valleys. The developed algorithm is fast and reliable, as it was tested using more than 1000 PPG signals.

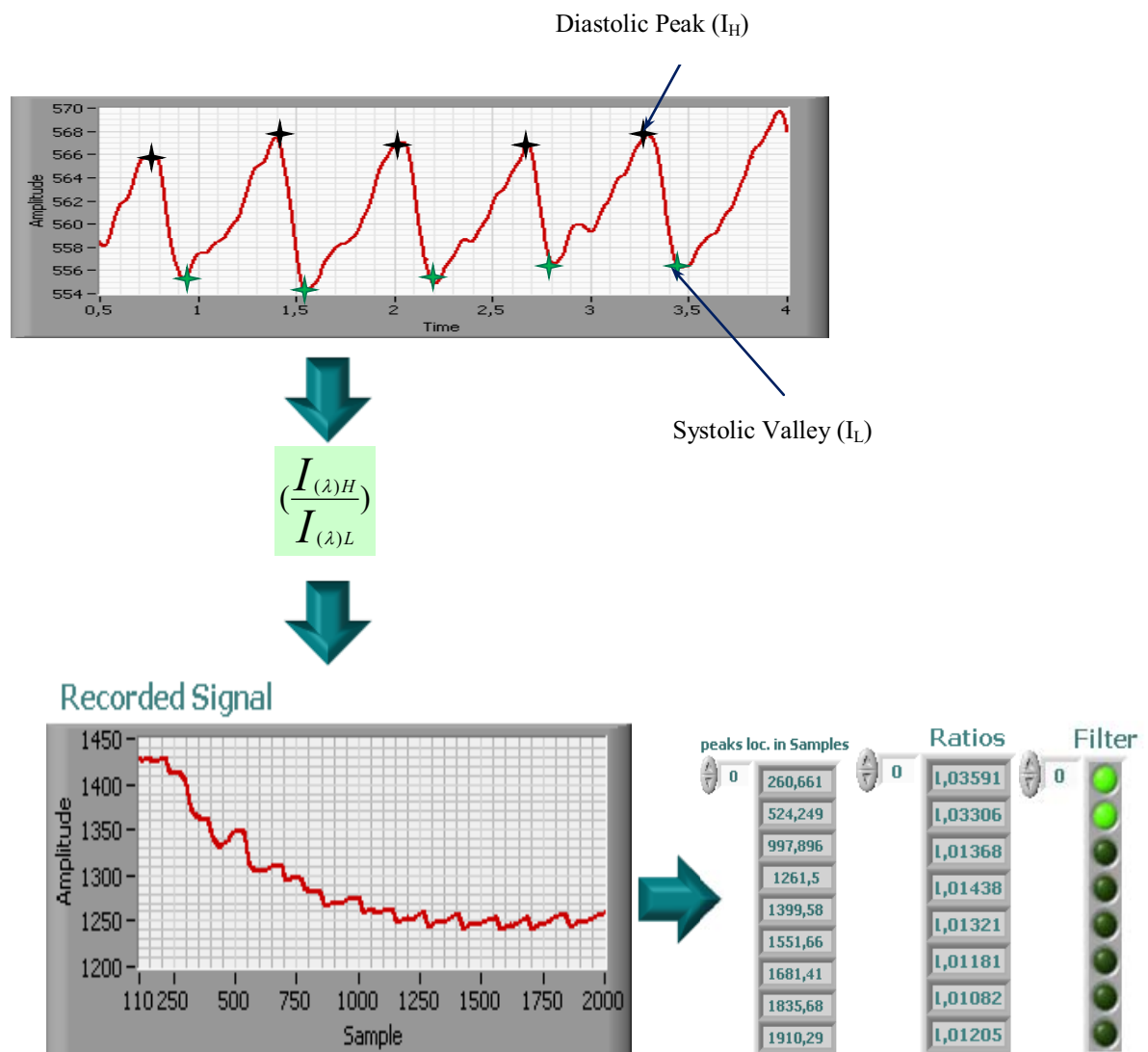


Figure 5-3: Desired peaks and valleys detection by the improved algorithm the ratios filter.

The highly noised pulses of PPG signals should be neglected. The ratios of (I_H) by (I_L) are measured for every pulse of the recorded PPG signal and then calculating the standard deviation of these ratios in order to delete the ratios that has a large deviation than the mean value. Therefore, the highly corrupted pulses of the PPG signals will not be taken into account during the calculations. As shown in Figure 5-3, the filter detected that the first two pulses of the recorded signal should be neglected for any further calculations, as the standard deviation of these two ratios are large.

5.3 Proposed algorithm based on modified Lambert-Beer law

The proposed estimation approach of tHb concentration, the ratios of O₂Hb, RHb, COHb, and MetHb using the principles of Lambert-Beer law is introduced in the following.

5.3.1 Modified Lambert-Beer law

The simple Lambert-Beer's law derivation of pulse oximetry does not take some physical concepts such as light scattering into account [Wie97]. It assumes that the optical path length of the two employed wavelengths, which pass through the tissue, is equal and can be cancelled out by each other (see Eq. (3.13)).

Visible and near IR light, however, are strongly scattered by human tissue; the detected light is more accurately described as an ensemble of independent photon paths. Some of the detected photons travel shorter routes without migrating far from the direct line between the emitter (light source such as LED) and detector (photodetector), and some scatter farther from this line without being absorbed or lost at a boundary (photons that are absorbed or lost cannot contribute to the photocurrent). Therefore, scattering effects may cause elongation of the optical path length. Paul D. Mannheim illustrates this graphically using the results of a random walk model for photons scattering through a simulated homogenous tissue, as depicted in Figure 5-4 [Man07]. Regions travelled most commonly by the migrating photons that reach the detector are shown as dark blue, progressing through green, tan, and gray, each indicating decreasing visitation. Photons that are absorbed or reach the top or bottom surface other than at the detector are considered to be lost (not detected); their routes accordingly do not contribute.

Although the calculations will be complicated, it is very important to employ the modified Lambert-Beer law that considers the effect of the photon scattering that is dependent on the wavelength as described in the following equation.

$$I = I_0 e^{-(\alpha(\lambda)dA_\lambda)+G_\lambda} \quad (5.1)$$

$$\alpha(\lambda) = \varepsilon(\lambda)c \quad (5.2)$$

where,

I_0 : intensity of irradiated light.

I : intensity of transmitted light.

α : absorption coefficient.

C : the concentration of the probe.

ε : molar extinction coefficient.

d : thickness of the irradiated probe.

A_λ : Multiplication factor to consider the optical path length elongation of the photons due to scattering of the medium (It depends on the wavelength.).

G_λ : a factor considering the geometry of the probe and the loss of photons due to scattering.

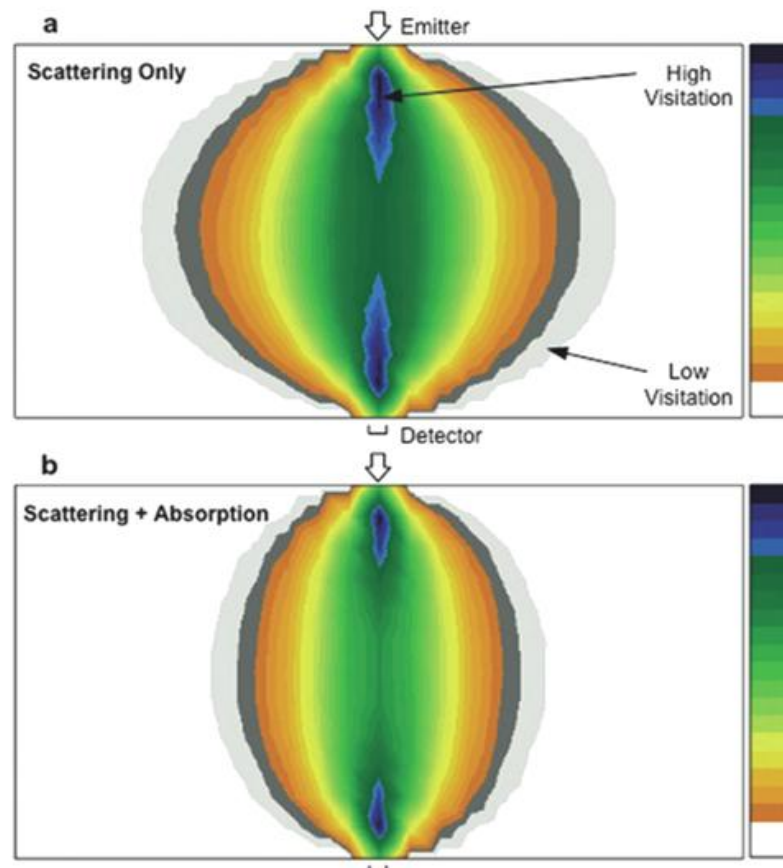


Figure 5-4: Relative visitation probabilities based on a Monte-Carlo random walk of photons are shown for red light transmitted through a simulated homogeneous tissue in (a) the absence of absorption and (b) with absorption consistent with human tissues [Man07].

5.3.2 Modified Lambert-Beer law revisited for PPG signals

In the following, the modified Lambert-Beer's law, which is demonstrated by Eq. (5.1), is employed according to the principles of pulse oximetry technology, as explained in section 3.4.2.

For a significant wavelength λ , Eq. (5.1) can be rewritten in the cases of the systole and the diastole of the arterial to express the transmitted light, which is detected by the photodetector and presented by the PPG signal, as shown in Figure 5-5.

In the case of systole, the optical path length is increased by Δd as the arterial diameter is increased.

$$(I_{sys})_{\lambda} = (I_0)_{\lambda} e^{-(\alpha(\lambda)(\Delta d+d)A_{\lambda})+G_{\lambda}} \quad (5.3)$$

In the case of diastole, the optical path length is considered d .

$$(I_{dia})_{\lambda} = (I_0)_{\lambda} e^{-(\alpha(\lambda)dA_{\lambda})+G_{\lambda}} \quad (5.4)$$

By dividing Eq. (5.3) by Eq. (5.4), some terms of the numerator are cancelled by the equalled terms of the denominator to get Eq. (5.6).

$$\left(\frac{I_{sys}}{I_{dia}}\right)_{\lambda} = \frac{e^{-(\alpha(\lambda)(d+\Delta d)A_{\lambda})+G_{\lambda}}}{e^{-(\alpha(\lambda)dA_{\lambda})+G_{\lambda}}} \quad (5.5)$$

$$\left(\frac{I_{sys}}{I_{dia}}\right)_{\lambda} = e^{-\alpha(\lambda)\Delta dA_{\lambda}} \quad (5.6)$$

The natural logarithm (ln) is applied to both sides of Eq. (5.6) to derive Eq. (5.8).

$$\ln\left(\frac{I_{sys}}{I_{dia}}\right)_{\lambda} = -\alpha(\lambda)\Delta dA_{\lambda} \quad (5.7)$$

$$\ln\left(\frac{I_{dia}}{I_{sys}}\right)_{\lambda} = \alpha(\lambda)\Delta dA_{\lambda} \quad (5.8)$$

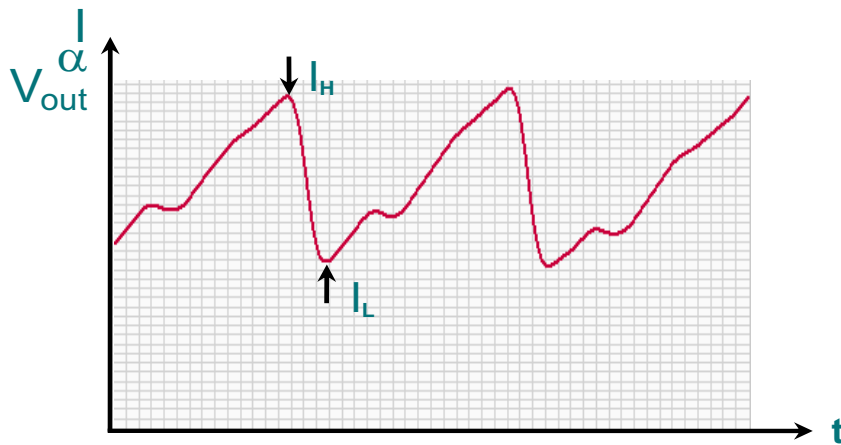


Figure 5-5: PPG signal (transmitted light).

According to Figure 5-5, I_{sys} is substituted by I_L and I_{dia} is substituted by I_H to get Eq. (5.9) from Eq. (5.8) as follows;

$$\ln\left(\frac{I_H}{I_L}\right)_\lambda = \Delta d A_\lambda \alpha(\lambda) \quad (5.9)$$

Pulse oximetry considers the approximation concept of the arterial blood containing only the functional hemoglobin components (O_2Hb and RHb) to measure the functional arterial oxygen saturation, as it uses only two wavelengths to distinguish between O_2Hb and RHb . To estimate the tHb concentration, all the hemoglobin components or at least the four hemoglobin components (O_2Hb , RHb , $COHb$, $MetHb$) should be taken into consideration, as the tHb concentration is the summation of the concentrations of these four hemoglobin components. Therefore, in this case, the absorption coefficient is expressed as the summation of the concentrations of the four hemoglobin components multiplied by their extinction coefficients, as described in the following equation;

$$\alpha(\lambda) = [\varepsilon_{COHb_\lambda} COHb(c) + \varepsilon_{C_2HB_\lambda} O_2Hb(c) + \varepsilon_{MetHb_\lambda} MetHb(c) + \varepsilon_{RHb_\lambda} RHb(c)] \quad (5.10)$$

Substitute from Eq. (5.10) into Eq. (5.9) to get Eq. (5.11). It is one of the two equations, which will be used in the further calculations to estimate the interesting physiological parameters.

$$\ln\left(\frac{I_H}{I_L}\right)_\lambda = \Delta d A_\lambda [\varepsilon_{COHb_\lambda} COHb(c) + \varepsilon_{C_2HB_\lambda} O_2Hb(c) + \varepsilon_{MetHb_\lambda} MetHb(c) + \varepsilon_{RHb_\lambda} RHb(c)] \quad (5.11)$$

In the following, this section introduces a derivation of the second equation that is also special for the PPG signal and is according to modified Lambert-Beer law and pulse oximetry principles.

By differentiating Eq. (5.1) in the discrete time between t_1 and t_2 (see Figure 5-6) to get Eq. (5.12).

$$\frac{\partial I}{\partial t} = I_0 e^{-\alpha A d + G} \left(-\alpha A \frac{\partial d}{\partial t} \right) \quad (5.12)$$

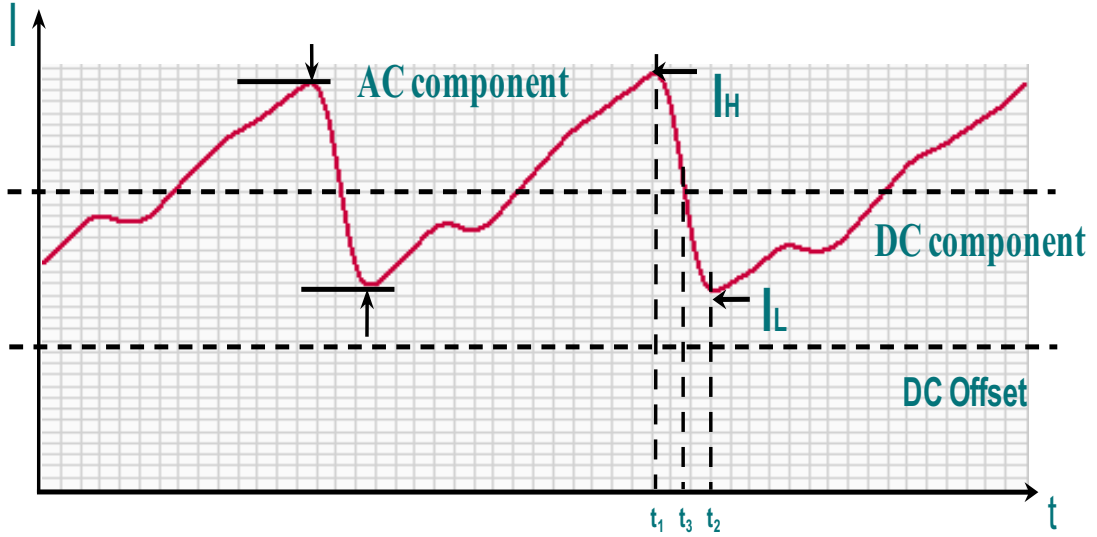


Figure 5-6: AC component and DC component of PPG signal (transmitted light).

Partial I by partial t and partial d by partial t are calculated by Eq. (5.13) and Eq. (5.14), respectively. The AC component and the DC component are shown in Figure 5-6, as the AC component is the difference between the diastolic peak and the systolic valley.

$$\frac{\partial I}{\partial t} = \frac{I(t_2) - I(t_1)}{t_2 - t_1} = \frac{I_L - I_H}{t_2 - t_1} = \frac{-AC_{component}}{t_2 - t_1} \quad (5.13)$$

$$\frac{\partial d}{\partial t} = \frac{d(t_2) - d(t_1)}{t_2 - t_1} = \frac{d_L - d_H}{t_2 - t_1} = \frac{\Delta d}{t_2 - t_1} \quad (5.14)$$

Substitute of Partial I by partial t and partial d by partial t by their equations (Eq. (5.13) and Eq. (5.14)) into Eq. (5.12) and divide the result by I (consider I at t_3 , which is equal to the DC component) to derive Eq. (5.18).

$$\frac{\partial I}{\partial t} = \frac{-AC_{component}}{t_2 - t_1} = I_0 e^{-\alpha A d + G} \left(-\alpha A \frac{\Delta d}{t_2 - t_1} \right) \quad (5.15)$$

$$\frac{-AC_{component}}{I} = (-\alpha A \Delta d) \quad (5.16)$$

$$\frac{AC_{component}}{I_{t_3}} = (\alpha A \Delta d) \quad (5.17)$$

$$\frac{AC_{component}}{DC_{component}} = (\alpha A \Delta d) = \Delta d A [\varepsilon_{COHb_{21}} COHb(c) + \varepsilon_{C2HB_{21}} O_2Hb(c) + \varepsilon_{MetHb_{21}} MetHb(c) + \varepsilon_{RHb_{21}} RHb(c)] \quad (5.18)$$

Eq. (5.18) is the second equation, which is used to estimate the interesting physiological variables.

Six photoplethysmography signals with different wavelengths are employed to find a solution for the concentrations of the four hemoglobin components, as the summation of their concentrations is considered the tHb concentration. Five PPG signals with different wavelengths (625 nm, 880 nm, 760 nm, 680 nm, 660 nm, 1200 nm) are used to build a system of equations that is according to the two derived equations (Eq. (5.11) and Eq. (5.18)). The sixth wavelength (1200 nm) is used to indicate the change of the arterial diameter during the systole. All the unknown parameters of Eq. (5.11) and Eq. (5.18) should be calculated to solve a system of equations for the concentrations of COHb, O₂Hb, MetHb and RHb concentrations.

In the following, the unknown parameters are calculated. These parameters are the extinction coefficients of the four hemoglobin components, A_λ and Δd .

5.3.3 Extinction coefficients of the four hemoglobin components

The determination of the extinction coefficients of COHb, O₂Hb, MetHb and RHb is performed by the help of the published biochemistry valuable papers and books [Kue94] [Zij00] and also the graph, which is depicted in Figure 5-7.

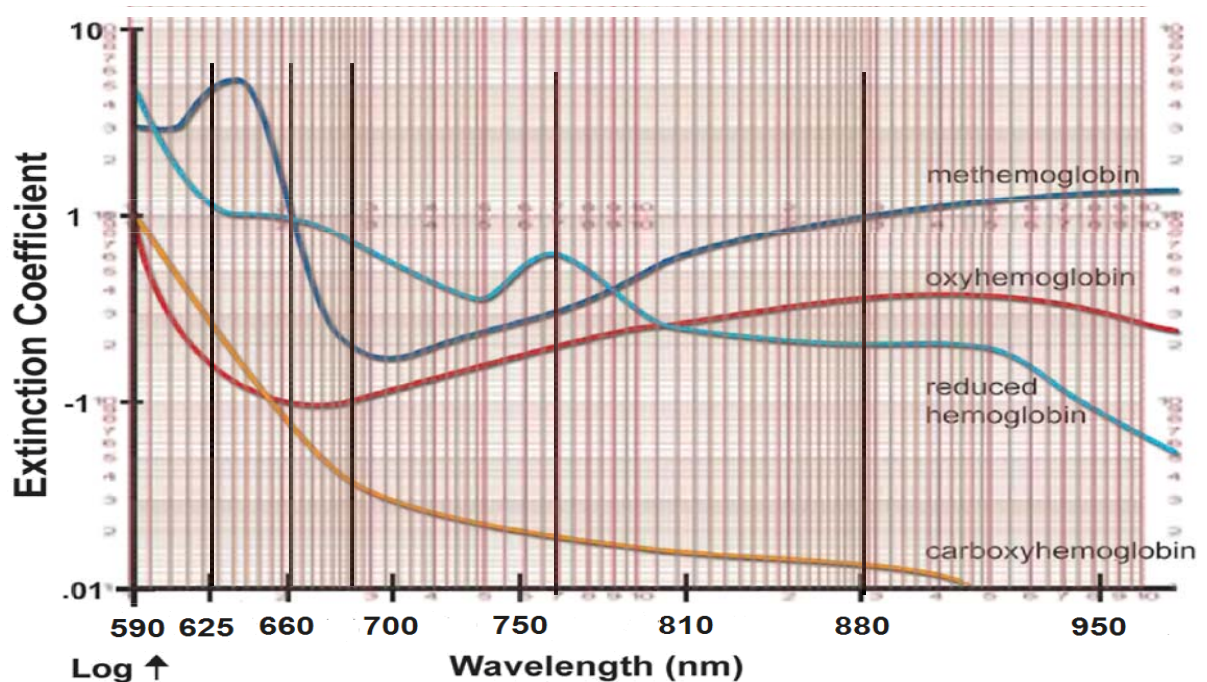


Figure 5-7: The extinction coefficients of the four hemoglobin components [Web98].

After the comparison between the mentioned published biochemistry, the extinction coefficients of the four hemoglobin components could be determined and considered as demonstrated in Table 5-1.

Table 5-1: Extinction coefficients of the four hemoglobin components at the employed wavelengths.

Wavelength(nm)	ϵ_{COHb}	$\epsilon_{\text{O}_2\text{Hb}}$	ϵ_{MetHb}	ϵ_{RHb}	L/(mmol*cm)
625	0.2495	0.172	3.7805	1.1445	
880	0.005	0.284	0.611	0.2	
760	0.012	0.145	0.27	0.38	
680	0.033	0.085	0.258	0.61	
660	0.061	0.08	0.819	0.814	

5.3.4 Proposed indication for Δd applying

The PPG signal could not be extracted at the wavelength of 1650 nm where the water absorption coefficient is equal to the hemoglobin absorption coefficients because the absorption coefficient, at this wavelength, is quite large.

Therefore, by searching for the same conditions but with a low absorption coefficient, the PPG signal could be extracted at the wavelength of 1200 nm.

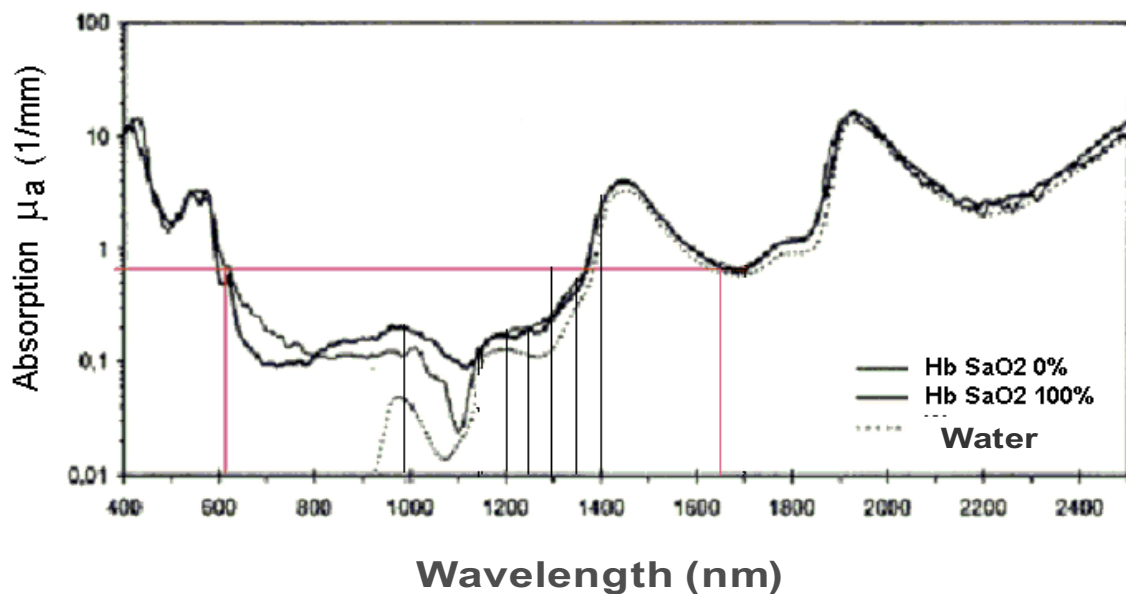


Figure 5-8: Absorption coefficients of the hemoglobin versus water.

Eq. (5.11) and Eq. (5.18) is rewritten for the wavelength of 1200 nm, as demonstrated in Eq. (5.19) and Eq. (5.21), respectively.

At this wavelength, the absorption coefficient α_{1200nm} consists of the absorption coefficient of hemoglobin and the absorption coefficient of water. The two absorption coefficients are approximately equal (see Figure 5-8). Thus, it cannot in anyway indicate hemoglobin concentration, as the increase of water concentration or hemoglobin concentration will affect the whole absorption coefficients α_{1200} in the same manner. Therefore, α_{1200nm} can be assumed as a parameter that is related only to the wavelength 1200 nm and can be combined with the parameter A_{1200nm} to be one parameter that is named K_{1200nm} .

Thus, according to Eq. (5.19) and Eq. (5.21), Δd can be represented by Eq. (5.20) and Eq. (5.22), respectively.

$$\left(\frac{AC}{DC}\right)_{1200nm} = \alpha A \Delta d \quad (5.19)$$

$$\Delta d = \frac{\left(\frac{AC}{DC}\right)_{1200nm}}{A_{1200nm} \alpha_{1200nm}} = K_{1200nm} \left(\frac{AC}{DC}\right)_{1200nm} \quad (5.20)$$

$$\ln\left(\frac{I_H}{I_L}\right)_{1200nm} = \alpha A \Delta d \quad (5.21)$$

$$\Delta d = \frac{\ln\left(\frac{I_H}{I_L}\right)_{1200nm}}{A_{1200nm} \alpha_{1200nm}} = K_{1200nm} \ln\left(\frac{I_H}{I_L}\right)_{1200nm} \quad (5.22)$$

Substitute for Δd from Eq. (5.20) and Eq. (5.22) into Eq. (5.11) and Eq. (5.18), respectively.

$$\begin{aligned} \ln\left(\frac{I_H}{I_L}\right)_\lambda &= \alpha_\lambda A_\lambda K_{1200nm} \ln\left(\frac{I_H}{I_L}\right)_{1200nm} \\ &= A_\lambda K_{1200nm} \ln\left(\frac{I_H}{I_L}\right)_{1200nm} [\varepsilon_{COHb} C_{COHb} + \varepsilon_{O_2Hb} C_{O_2Hb} + \varepsilon_{MetHb} C_{MetHb} + \varepsilon_{RHb} C_{RHb}]_\lambda \end{aligned} \quad (5.23)$$

$$\begin{aligned} \left(\frac{AC}{DC}\right)_\lambda &= a_\lambda A_\lambda K_{1200nm} \left(\frac{AC}{DC}\right)_{1200nm} \\ &= A_\lambda K_{1200nm} \left(\frac{AC}{DC}\right)_{1200nm} [\varepsilon_{COHb} C_{COHb} + \varepsilon_{O_2Hb} C_{O_2Hb} + \varepsilon_{MetHb} C_{MetHb} + \varepsilon_{RHb} C_{RHb}]_\lambda \end{aligned} \quad (5.24)$$

In order to combine the two factors (A_λ) and (K_{1200nm}), substitute for ($A_\lambda K_{1200nm}$) by (K_λ) into the two above equations to derive Eq. (5.25) and Eq. (5.26).

$$\ln\left(\frac{I_H}{I_L}\right)_\lambda = K_\lambda \ln\left(\frac{I_H}{I_L}\right)_{1200nm} [\epsilon_{COHb}C_{COHb} + \epsilon_{O2Hb}C_{O2Hb} + \epsilon_{MetHb}C_{MetHb} + \epsilon_{RHb}C_{RHb}]_\lambda \quad (5.25)$$

$$\left(\frac{AC}{DC}\right)_\lambda = K_\lambda \left(\frac{AC}{DC}\right)_{1200nm} [\epsilon_{COHb}C_{COHb} + \epsilon_{O2Hb}C_{O2Hb} + \epsilon_{MetHb}C_{MetHb} + \epsilon_{RHb}C_{RHb}]_\lambda \quad (5.26)$$

To check the balance of units for Eq. (5.25) and Eq. (5.26):

1. $\ln\left(\frac{I_H}{I_L}\right)_\lambda$ and $\left(\frac{AC}{DC}\right)_\lambda$ are unitless.
2. $\ln\left(\frac{I_H}{I_L}\right)_{1200nm}$ and $\left(\frac{AC}{DC}\right)_{1200nm}$ are unitless.
3. ϵ $L.mmol^{-1}.cm^{-1}$
4. C $mmol/L$ or g/dl ($1 g/dl = 0.6206 mmol/L$ [Unc11]))
5. K_λ cm

The multiplication of ϵ , C and K_λ is unitless. Therefore, both sides of the equations are balanced. It should be noted that, if the concentration is considered by the units of g/dl , K_λ will involve the factor (0.6206) of the two units conversions.

5.3.5 Recommended strategy of estimation based on modified Lambert-Beer law

Some strategies of using modified Lambert-Beer law were tested to estimate tHb and the ratios of COHb, O₂Hb, MetHb and RHb through the research stage. In the following, the recommended strategy is introduced. The estimation process will be performed twice, in exactly the same manner, the first one being based on Eq. (5.25) and the second on Eq. (5.26).

According to Eq. (5.26), the steps of the method are explained below in detail.

1. A system of equations is built, as an equation for a significant wavelength.

$$\begin{pmatrix} \left(\frac{AC}{DC}\right)_{\lambda_1} \\ \left(\frac{AC}{DC}\right)_{\lambda_2} \\ \left(\frac{AC}{DC}\right)_{\lambda_3} \\ \left(\frac{AC}{DC}\right)_{\lambda_4} \end{pmatrix} = \left(\frac{AC}{DC}\right)_{1200nm} \times \begin{bmatrix} K_{\lambda_1}\epsilon_{COHb\lambda_1} & K_{\lambda_1}\epsilon_{O2Hb\lambda_1} & K_{\lambda_1}\epsilon_{MetHb\lambda_1} & K_{\lambda_1}\epsilon_{RHb\lambda_1} \\ K_{\lambda_2}\epsilon_{COHb\lambda_2} & K_{\lambda_2}\epsilon_{O2Hb\lambda_2} & K_{\lambda_2}\epsilon_{MetHb\lambda_2} & K_{\lambda_2}\epsilon_{RHb\lambda_2} \\ K_{\lambda_3}\epsilon_{COHb\lambda_3} & K_{\lambda_3}\epsilon_{O2Hb\lambda_3} & K_{\lambda_3}\epsilon_{MetHb\lambda_3} & K_{\lambda_3}\epsilon_{RHb\lambda_3} \\ K_{\lambda_4}\epsilon_{COHb\lambda_4} & K_{\lambda_4}\epsilon_{O2Hb\lambda_4} & K_{\lambda_4}\epsilon_{MetHb\lambda_4} & K_{\lambda_4}\epsilon_{RHb\lambda_4} \end{bmatrix} \times \begin{pmatrix} C_{COHb} \\ C_{O2Hb} \\ C_{MetHb} \\ C_{RHb} \end{pmatrix} \quad (5.27)$$

Solve for the vector of the four hemoglobin components concentration;

$$\begin{pmatrix} C_{COHb} \\ C_{O_2Hb} \\ C_{MetHb} \\ C_{RHb} \end{pmatrix} = \frac{1}{\left(\frac{AC}{DC}\right)_{1200nm}} \times \begin{bmatrix} K_{\lambda_1} \epsilon_{COHb\lambda_1} & K_{\lambda_1} \epsilon_{O_2Hb\lambda_1} & K_{\lambda_1} \epsilon_{MetHb\lambda_1} & K_{\lambda_1} \epsilon_{RHb\lambda_1} \\ K_{\lambda_2} \epsilon_{COHb\lambda_2} & K_{\lambda_2} \epsilon_{O_2Hb\lambda_2} & K_{\lambda_2} \epsilon_{MetHb\lambda_2} & K_{\lambda_2} \epsilon_{RHb\lambda_2} \\ K_{\lambda_3} \epsilon_{COHb\lambda_3} & K_{\lambda_3} \epsilon_{O_2Hb\lambda_3} & K_{\lambda_3} \epsilon_{MetHb\lambda_3} & K_{\lambda_3} \epsilon_{RHb\lambda_3} \\ K_{\lambda_4} \epsilon_{COHb\lambda_4} & K_{\lambda_4} \epsilon_{O_2Hb\lambda_4} & K_{\lambda_4} \epsilon_{MetHb\lambda_4} & K_{\lambda_4} \epsilon_{RHb\lambda_4} \end{bmatrix}^{-1} \times \begin{pmatrix} \left(\frac{AC}{DC}\right)_{\lambda_1} \\ \left(\frac{AC}{DC}\right)_{\lambda_2} \\ \left(\frac{AC}{DC}\right)_{\lambda_3} \\ \left(\frac{AC}{DC}\right)_{\lambda_4} \end{pmatrix} \quad (5.28)$$

Using the PPG signals, which are extracted by the developed electronic system (see Figure 5-9), $\left(\frac{AC}{DC}\right)_\lambda$ can be calculated for each PPG and also for the PPG of the wavelength of 1200 nm. The extinction coefficients of the four hemoglobin components at each wavelength are demonstrated in Table 5-1. So far, K_λ for each wavelength is the only unknown variable. It should be calculated to find a solution for the four hemoglobin components using Eq. (5.28).

2. Some invasive measurements are required to solve the inverse problem for K_λ . Ten invasive measurements are performed and at the same time, the developed optoelectronic system collects the PPG signals. The range of tHb is 12.6 g/dl to 16.5 g/dl, as depicted in Table 5-2.

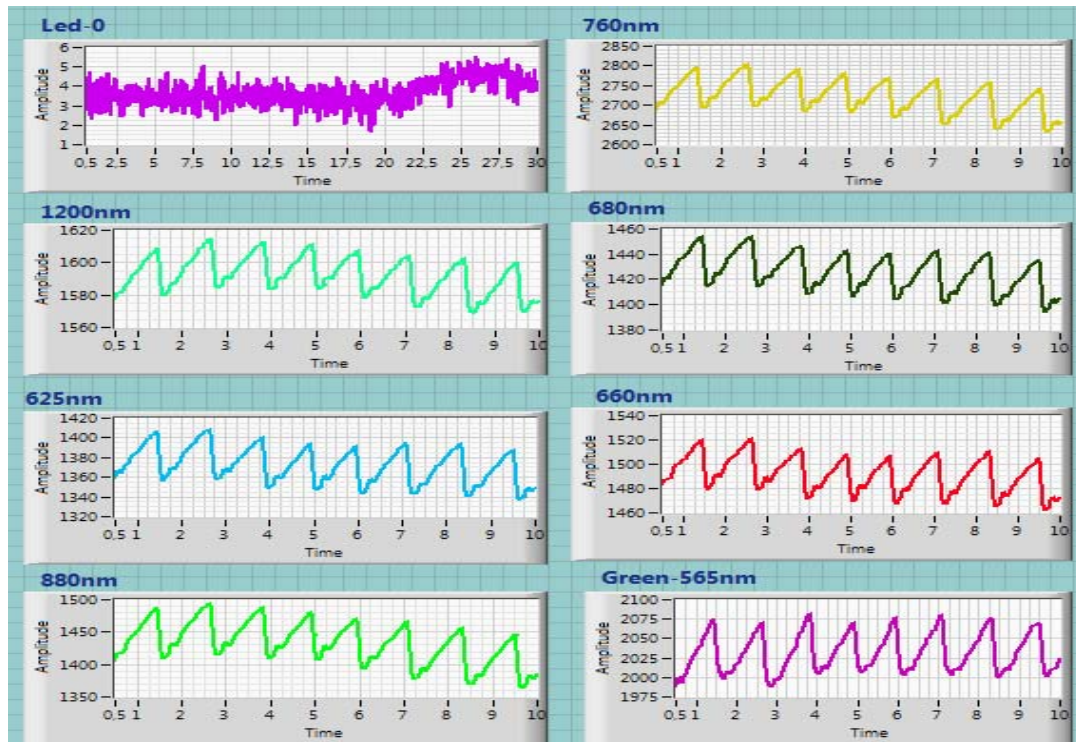


Figure 5-9: Seven extracted PPG signals using the developed optoelectronic system.

Table 5-2: Reference laboratory invasive measurements.

tHb(g/dl)	COHb(g/dl)	O ₂ Hb(g/dl)	MetHb(g/dl)	RHb(g/dl)
13	0.13	12.685	0.056	0.127
13.9	0.278	13.4382	0.0473	0.135
16.5	0.165	16.02	0.152	0.162
14.4	0.144	13.804	0.0245	0.426
14.3	0.086	13.842	0.079	0.282
13.1	0.131	12.427	0.024	0.517
14.6	0.292	14.111	0.054	0.142
12.9	0.077	12.388	0.050	0.383
12.6	0.076	12.2238	0.052	0.248
14.8	0.444	14.016	0.052	0.286

3. Develop a cubic Hermite interpolation for K_λ in the all range of tHb invasive measurements (from 12.5 g/dl to 16.5 g/dl) and not only for the ten discrete invasive measurements [Nat11]. Therefore, the value of K_λ can be read for any case.
4. So far, the system of equations (Eq. (5.28)) has no unknown variables and can be solved for the four hemoglobin components to calculate the tHb concentration, as described in the functional block diagram of Figure 5-10.

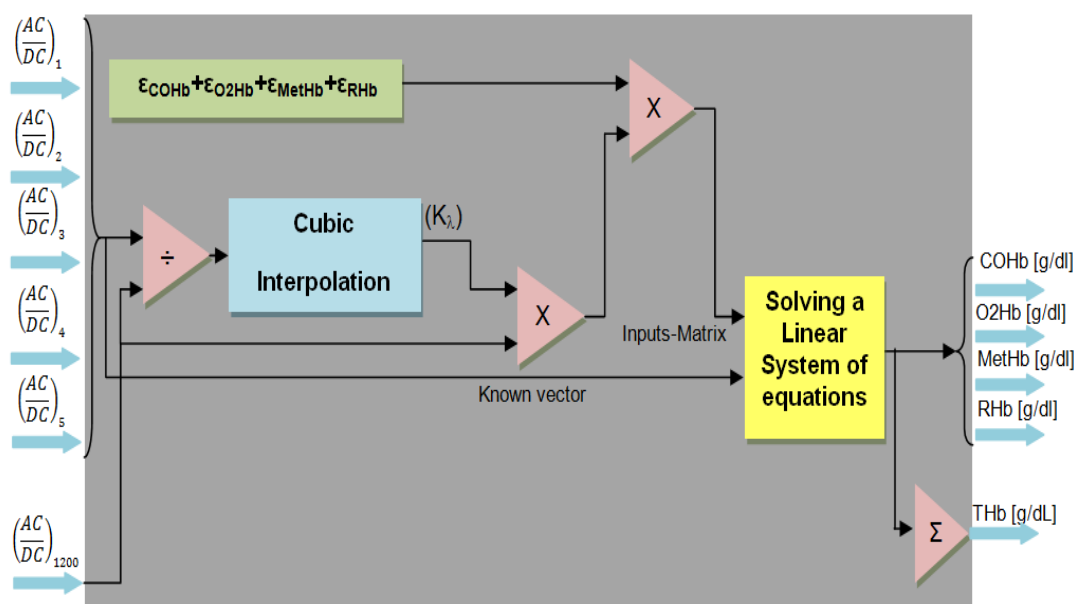


Figure 5-10: Functional block diagram of estimating tHb concentration process.

5. Eq. (5.25) and Eq. (5.26) can be rewritten considering the ratios of four hemoglobin components as follows;

$$\ln\left(\frac{I_H}{I_L}\right)_\lambda = K_\lambda(\text{ratio}) \ln\left(\frac{I_H}{I_L}\right)_{1200nm} [\varepsilon_{COHb}COHb\% + \varepsilon_{O_2Hb}O_2Hb\% + \varepsilon_{MetHb}MetHb\% + \varepsilon_{RHb}RHb\%]_\lambda \quad (5.29)$$

$$\left(\frac{AC}{DC}\right)_\lambda = K_\lambda(\text{ratio}) \left(\frac{AC}{DC}\right)_{1200nm} [\varepsilon_{COHb}COHb\% + \varepsilon_{O_2Hb}O_2Hb\% + \varepsilon_{MetHb}MetHb\% + \varepsilon_{RHb}RHb\%]_\lambda \quad (5.30)$$

As the unit of $K_\lambda(\text{ratio})$ (briefly $K_{\lambda R}$) is cm divided by the unit of the tHb, Eq. (5.29) and Eq. (5.30) are balanced. In this case, the system of equation can be rewritten for Eq. (5.30) as given below;

$$\begin{pmatrix} COHb\% \\ O_2Hb\% \\ MetHb\% \\ RHb\% \end{pmatrix} = \frac{1}{\left(\frac{AC}{DC}\right)_{1200nm}} \times \begin{bmatrix} K_{\lambda R_1} \varepsilon_{COHb\lambda_1} & K_{\lambda R_1} \varepsilon_{O_2Hb\lambda_1} & K_{\lambda R_1} \varepsilon_{MetHb\lambda_1} & K_{\lambda R_1} \varepsilon_{RHb\lambda_1} \\ K_{\lambda R_2} \varepsilon_{COHb\lambda_2} & K_{\lambda R_2} \varepsilon_{O_2Hb\lambda_2} & K_{\lambda R_2} \varepsilon_{MetHb\lambda_2} & K_{\lambda R_2} \varepsilon_{RHb\lambda_2} \\ K_{\lambda R_3} \varepsilon_{COHb\lambda_3} & K_{\lambda R_3} \varepsilon_{O_2Hb\lambda_3} & K_{\lambda R_3} \varepsilon_{MetHb\lambda_3} & K_{\lambda R_3} \varepsilon_{RHb\lambda_3} \\ K_{\lambda R_4} \varepsilon_{COHb\lambda_4} & K_{\lambda R_4} \varepsilon_{O_2Hb\lambda_4} & K_{\lambda R_4} \varepsilon_{MetHb\lambda_4} & K_{\lambda R_4} \varepsilon_{RHb\lambda_4} \end{bmatrix}^{-1} \times \begin{pmatrix} \left(\frac{AC}{DC}\right)_{\lambda_1} \\ \left(\frac{AC}{DC}\right)_{\lambda_2} \\ \left(\frac{AC}{DC}\right)_{\lambda_3} \\ \left(\frac{AC}{DC}\right)_{\lambda_4} \end{pmatrix} \quad (5.31)$$

In the same manner, a cubic Hermite interpolation is performed for $K_{\lambda R}$ using the invasive measurements that are depicted in Table 5-2 and the AC/DC components are calculated using the extracted PPG signals which are shown by Figure 5-9. Thus, the system of equations (Eq. (5.30)) has no unknown variables and could be used to find a solution for (COHb%, O₂Hb%, MetHb%, and RHb%), as described in the functional block diagram in Figure (5-11).

An advantage of using this equation of the hemoglobin components ratios is that the summation of the four ratios is already known exactly as 100%, so that this will cancel any ill-posed problem in solving the system of the equations for the ratios.

If Eq. (5.25) and Eq. (5.29) are employed to find the solution for the tHb concentration and the ratios of COHb, MetHb, O₂Hb, and RHb, the method is named by Method-1-part1. And If Eq. (5.26) and Eq. (5.30) are employed; the method is named by Method-1-part2, as depicted in chapter 7.

Table 5-3: Reference laboratory invasive measurements (four Hb components ratios)

tHb(g/dl)	COHb%	O ₂ Hb%	MetHb%	RHb%
13	1	97.58	0.43	0.98
13.9	2	96.68	0.34	0.97
16.5	1	97.09	0.92	0.98
14.4	1	95.86	0.17	2.96
14.3	0.6	96.8	0,55	1.97
13.1	1	94.86	0.18	3.95
14.6	2	96.65	0.37	0.97
12.9	0.6	96.03	0.39	2.97
12.6	0.6	97.01	0.41	1.97
14.8	3	94.7	0.35	1.93

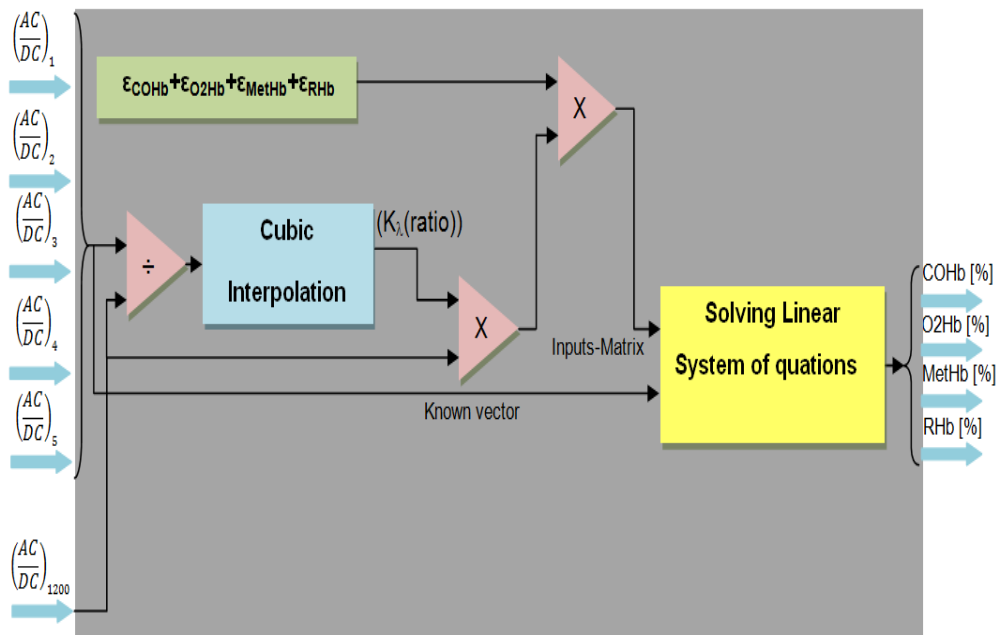


Figure 5-11: Functional block diagram of estimation the four hemoglobin ratios process.

5.4 Proposed algorithm based on fuzzy logic systems

5.4.1 Introduction to fuzzy logic

Fuzzy logic systems, neural networks, evolutionary computing, and probabilistic models are the main constituents of the soft computing (Artificial Intelligent (AI)) discipline that combines these technologies to solve the complex problems in many technical areas. This is because they can deal with difficulties arising from uncertainty and complexity.

Fuzzy logic was introduced by Zadeh in the 1960s, as a method in which the objects of computation are words and propositions drawn from the natural language. Fuzzy logic systems have the ability to deal with system uncertainty using their logically oriented reasoning techniques. The fuzzy inference system is a popular computing framework based on the concepts of fuzzy set theory, fuzzy if-then rules and fuzzy reasoning. It has been successfully applied in fields such as automatic control, data classification, decision analysis, and expert systems.

Nowadays, fuzzy logic plays an important role in medicine, where fuzzy set theory is a suitable formalism to deal with the imprecision intrinsic to many biomedical and bioinformatics complex problems. It is a method to render precise what is imprecise in the world of medicine [Tor06] [Phu01].

5.4.3.1 Architecture of fuzzy logic systems

The fuzzy expert system is an expert system that incorporated fuzzy logic into its reasoning process and knowledge representation scheme. Figure 5-12 describes the basic configuration of a fuzzy system which is depicted as the follows [Har02];

The fuzzifier:

Fuzzification can be defined as the operation that maps a crisp object to a fuzzy set, i.e., to a membership function. That is:

$$y = \text{Fuzz}(x) \quad (5.32)$$

where x is a crisp input value, y is a fuzzy set and $\text{Fuzz}(\cdot)$ stands for a fuzzy operator. The fuzzification interface generally performs the following functions:

- Scaling the range of the input and output data into corresponding universes of discourse,
- Fuzzifying the scaled data.

A knowledge base:

It contains definitions of fuzzy sets and the fuzzy operators. The database includes three operations namely quantization of universes of discourse, fuzzy partitioning and definition of fuzzy sets.

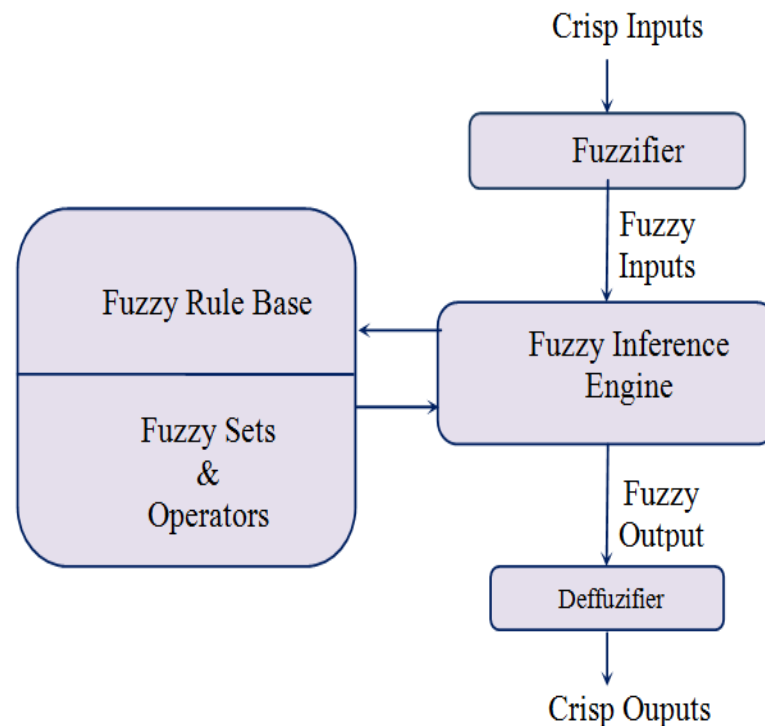


Figure 5-12: Basic components of a fuzzy logic system

The quantization process is for discretising continuous universes. Partitioning of a universe of discourse is carried out to determine the initial number of fuzzy subsets required to represent that universe. Fuzzy sets are usually selected to cover the whole universe of discourse. These fuzzy sets can either be represented as a vector of numbers or in function forms such as triangle-shaped, bell-shaped and trapezoidal-shaped membership functions. There is no systematic method to decide either the shape and/or number of the fuzzy sets or their degree of overlap. These parameters strongly depend upon the designer's experience.

Defining the fuzzy rule base includes the choice of the input and the output variables of the controlled process and a set of fuzzy rules that describe the control policy in the domain of expertise. Fuzzy rules normally describe process behaviour in a fuzzy

logic system. Derivation methods for these fuzzy rules are the cornerstone in a fuzzy logic system.

Fuzzy inference engine:

It is a method for inferring a fuzzy output based on employing a fuzzy inference (fuzzy reasoning) scheme. There are many employed fuzzy inference schemes, such as Takagi-Sugeno model and Mamdani model. For example, the reasoning algorithm based on the Takagi-Sugeno model can be described, as defined in Eq. (5.33) [Tak85].

$$R_i : \text{IF } x_1 \text{ is } \dots \text{ and } x_2 \text{ is } \dots \text{ and } x_3 \text{ is } \dots \text{ THEN } y = f_i(x_1, x_2, x_3) \quad (5.33)$$

where $f_i(\cdot)$ is a linear function of the process state variables x_1, x_2 and x_3 , which are defined in the input subspace and y , is a variable of the consequent whose value is inferred. Mamdani inferring model will be described in the following in detail, as it is employed for the developed fuzzy expert system.

The defuzzifier:

A defuzzification function basically maps fuzzy inference results from the fuzzy domain into crisp outputs in a crisp domain. These crisp outputs should represent the output of the modeled operation. A defuzzifier for this mapping can be expressed as:

$$z = \text{Defuzz}(Y) \quad (5.34)$$

where z is the crisp operation output, Y is the fuzzy set that represents the distribution of the operation output and $\text{Defuzz}(\cdot)$ stands for the defuzzification operator. There are many defuzzification methods. The center of area method is employed as will be described below.

5.4.2 Reasons behind using fuzzy logic system

There are two major imperatives for computing with words. First, computing with words is a necessity when the available information is too imprecise to justify the use of numbers; and second, when there is a tolerance for imprecision which can be exploited to achieve tractability, robustness, low solution cost and better rapport with reality [Zad02].

As described in section 5.3, by applying the modified Lambert-Beer law, the parameters of ϵ , A , and Δd have to be defined accurately in order to find a solution for the tHb

concentration and the ratios of COHb, O₂Hb, MetHb, and RHb. That is the most difficult task of this calculation method, which depends on a conventional optical equation, as these parameters will still have imprecise values. Fuzzy logic systems provide a simple way to draw definite conclusions from imprecise information. Also, reasoning with fuzzy logic is possible without the need for much data because the backbone of that logic is expressed as if-then rules. Therefore, this thesis employs fuzzy logic to solve the problem of estimating the pre-mentioned vital physiological variable optically regardless of solving any complex optical equations, as a new trend. Where, fuzzy logic expert systems can deal with the imprecise information.

5.4.3 Building the fuzzy logic expert system

5.4.3.1 Defining the crisp inputs and outputs of the fuzzy system

It is clear that the outputs of the fuzzy expert system should be the tHb concentration and the ratios of COHb, O₂Hb, RHb, and MetHb, as it is built to find a solution for these physiological variables. The most difficult task is to define the crisp inputs of this fuzzy expert system. The problem is how to find the inputs which will not be changed as the outputs are not changed. The information about the available inputs is accomplished by the features of the extracted photoplethysmography PPG signals, which are extracted by the developed non-invasive optoelectronic system.

In order to define the inputs of this expert system, many experiments are conducted. The PPG signals (with different wavelengths) are extracted from the same case (person) many times by the optoelectronic system, then some features are calculated, such as the ratio of I_H and I_L, the natural logarithm of the ratio of I_H and I_L, and the ratio of the AC component and the DC component. Empirically, the inputs are chosen as follows: R1, R2, R3, and R4

$$\left[\begin{array}{c} \left(\frac{AC_{comp.}}{DC_{comp.}} \right)_{\lambda=625nm} \\ \left(\frac{AC_{comp.}}{DC_{comp.}} \right)_{\lambda=880nm} \end{array} \right] = R1, \left[\begin{array}{c} \left(\frac{AC_{comp.}}{DC_{comp.}} \right)_{\lambda=660nm} \\ \left(\frac{AC_{comp.}}{DC_{comp.}} \right)_{\lambda=880nm} \end{array} \right] = R2,$$

$$\left[\begin{array}{c} \left(\frac{AC_{comp.}}{DC_{comp.}} \right)_{\lambda=680nm} \\ \left(\frac{AC_{comp.}}{DC_{comp.}} \right)_{\lambda=880nm} \end{array} \right] = R3, \text{ and } \left[\begin{array}{c} \left(\frac{AC_{comp.}}{DC_{comp.}} \right)_{\lambda=760nm} \\ \left(\frac{AC_{comp.}}{DC_{comp.}} \right)_{\lambda=880nm} \end{array} \right] = R4.$$

The employed wavelengths for this purpose are: 880 nm, 625 nm, 660 nm, 680 nm, and 760 nm. According to the extinction coefficients of the four hemoglobin components that are shown by Figure 5-7, the largest extinction coefficient of the oxyhemoglobin, which is considered the largest component of hemoglobin, is at the wavelength of 880 nm, that is the largest wavelength amongst the employed wavelengths. Therefore, it is chosen to be the reference value for all the other employed wavelengths.

The input values combination will be changed as the concentration of the tHb and its four components changes. Therefore, these values can indicate the pre-mentioned interesting physiological variables.

5.4.3.2 Employing the fuzzy inference scheme

Mamdani's fuzzy inference scheme was applied to infer the fuzzy output as it was graphically illustrated for a multi inputs (four inputs) single output system, for an example, by Figure 5-13, The fuzzy output can be inferred by applying the intersection compositional operator to the input fuzzy sets (from A_1 to D_1 and from A_2 to D_2) and the union operator to the output fuzzy sets (M_1 and M_2). That will be illustrated in detail in as follows:

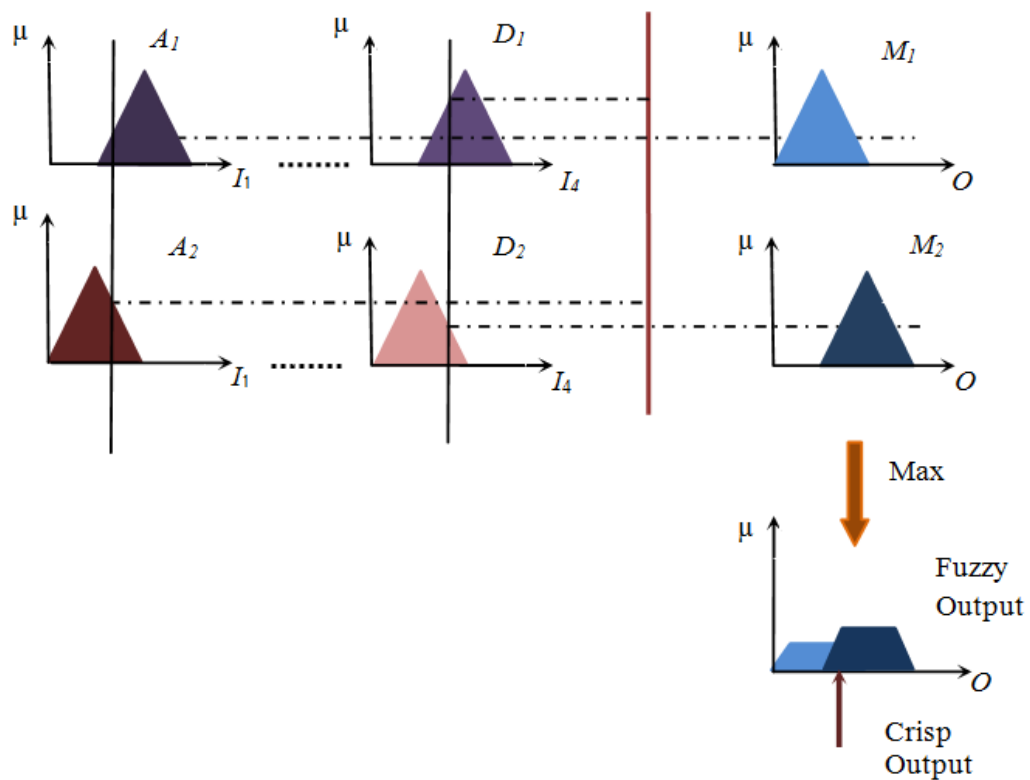


Figure 5-13: Mamdani's fuzzy inference scheme graphical interpretation for multi-inputs single-output system, as an example.

The system in question has four inputs and five outputs that represent the vital interesting physiological parameters. Therefore, the kth fuzzy rules can be expressed based on Mandani's model as follows:

IF i_1 is A_k and i_2 is B_k and i_3 is C_k and i_4 is D_k THEN o_1 is M_k and o_2 is P_k and o_3 is Q_k and o_4 is R_k and o_5 is S_k

where, $i_1, i_2, i_3, i_4, o_1, o_2, o_3, o_4,$ and o_5 are the linguistic variables that represent the multi inputs multi outputs model. $A_k, B_k, C_k, D_k, M_k, P_k, Q_k, R_k$ and S_k are the fuzzy sets of those variables in the universes of discourse $I_1, I_2, I_3, I_4, O_1, O_2, O_3, O_4,$ and $O_5,$ respectively.

Based on the compositional operators, the fuzzy output of each vital physiological parameter can be inferred as the result of the following steps.

Step 1: Normalize the crisp inputs and then fuzzify them to calculate the value of the membership function of each input's fuzzy set, $\mu_{\text{Fuzzy/set}}$. The membership function is a curve that defines the distribution of the truth variables around values which vary in the interval $[0, 1]$ by agreement. Eleven membership functions were defined as overlapped triangular functions.

Step 2: Based on the compositional operator, the intersection operator (\cap) is used, which means to get the minimum; the kth fuzzy rule can be inferred as follows:

$$R_k: \mu_{A_k} \cap \mu_{B_k} \cap \mu_{C_k} \cap \mu_{D_k} \cap \mu_{E_k} \cap \mu_{F_k}$$

Step 3: Repeat the second step to infer the other fuzzy rules in the rule base.

Step 4: Using the union operator (U), means getting the maximum. The fuzzy output will be:

$$O_{\text{Fuzzy}} = U (R_k, k = 1, 2, \dots, n) \quad (5.35)$$

where n is the total number of the fuzzy rules.

Center of area (COA) criteria was applied for the defuzzification stage to extract the crisp output (O_{crisp}) from the fuzzy output (O_{fuzzy}). COA generates the centre of gravity O_{crisp} of the possibility distribution of the expected outputs as demonstrated by the following equation:

$$O_{\text{Crisp}} = \frac{\sum_{k=1}^m \mu(w_k) * W_k}{\sum_{k=1}^m \mu(w_k)} \quad (5.36)$$

where m is the number of quantization levels of the universe O and W_k is the point in the k th quantization level in the universe O at which μ achieves its maximum value $\mu(w_k)$. The crisp outputs are considered the final results of the fuzzy system after the denormalization stage.

In the denormalization stage, the crisp outputs are converted from the normalized range $[0,1]$ into its normal range.

5.4.3.3 Fuzzy rule base generation

The fuzzy rules have been generated based on Wang-Mendel method, which has been widely used to produce relatively small rule bases with good classification rates and no conflicting or redundant rules [Wan03] [Cin08]. To apply this method, real input-output data pairs should be measured. The outputs are the values of the total hemoglobin concentration and the ratios of the four hemoglobin components (RHb%, COHb%, O2Hb% and MetHb%), which are measured invasively by the aid of a reference laboratory, as depicted in Table 5-3. The inputs are R1, R2, R3, and R4 of the corresponding PPG signals, which are extracted by the non-invasive optoelectronic system at the same time of conducting the invasive measurements

The method can be conducted easily by five steps, which can be introduced briefly as follows [Wan92]:

Step 1: Divide the input and output spaces of the given numerical data into a number of fuzzy sets.

Step 2: Generate fuzzy rules from the given data. First, determine the degrees of the given data in different fuzzy sets. Second, assign it to the set with a maximum degree. Finally, obtain one rule from one pair of the input-output data pairs.

Step 3: Assign a degree for each generated rule for the purpose of resolving conflicts among the generated rules, if there are conflicting rules.

Step 4: Eliminate conflicting rules. If two or more rules of the remaining set have equal antecedents, discard the rule with the smallest importance degree.

Step 5: Compose the final rule base using the remaining rules.

Therefore, the number of the fuzzy rules can be increased by increasing the number of the input-output data pairs that means, the expert system will take more possible cases into its consideration, and so, a large fuzzy rule base can be built.

5.4.3.4 Data flow of the proposed fuzzy expert system

Figure 5-14 describes the data flow through the developed fuzzy expert system. As, the developed non-invasive electronic system extract the seven PPG signals. Five of them that have the wavelengths of (880 nm, 625 nm, 660 nm, 680 nm, 760 nm) are employed in order to calculate the four ratios R1, R2, R3, and R4, as demonstrated in section 5.4.3.1. These ratios are the crisp inputs of the expert system, which are normalized into the range [0,1], as the first step. The normalized values are fuzzified into eleven fuzzy sets. Then the fuzzy rule based will be fired in order to infer the fuzzy output. Then, the fuzzy outputs are defuzzified by the center of area method to get the crisp outputs after the denormalization stage. The crisp outputs are the tHb concentration and the ratios of RHb, COHb, O2Hb and MetHb.

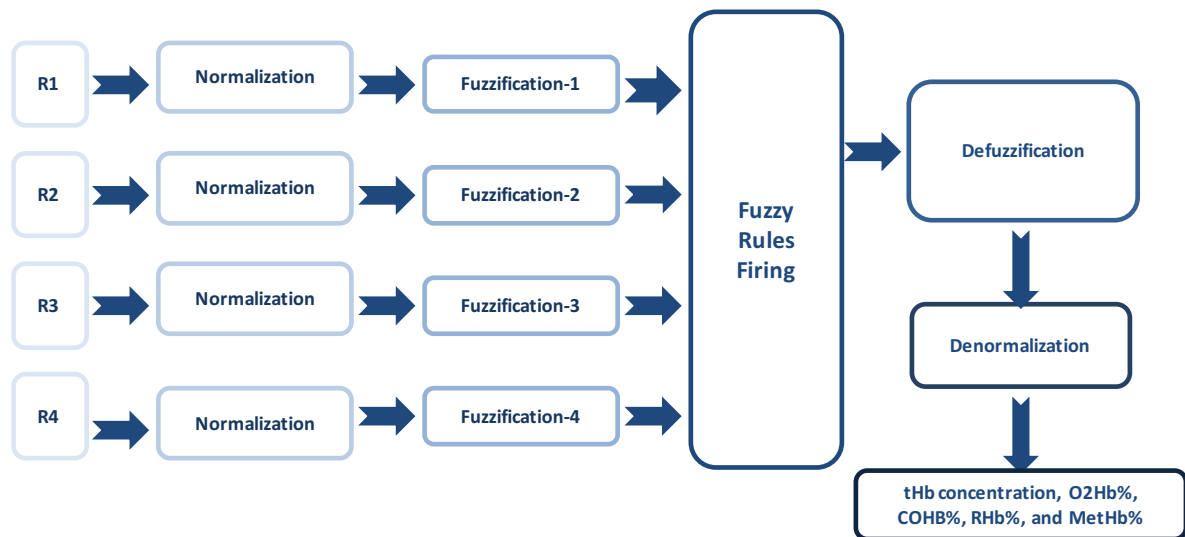


Figure 5-14: Data flow block diagram of the developed fuzzy expert system.

6. Proposed Estimation Algorithm for Invasive Measuring

6.1 Preliminaries

The conventional laboratory invasive methods to determine the total hemoglobin concentration (tHb) and the four hemoglobin components ratios (carboxyhemoglobin (COHb%), oxyhemoglobin (O₂Hb%), reduced hemoglobin (RHb%), and methemoglobin (MetHb%)) dissipate time and blood. Using a few drops of blood, a compact hemoglobin components analyzer can measure these physiological variables fast. Developing new calculation algorithms for these kinds of hemoglobin analyzer is one of the thesis objectives. This chapter introduces a fast robust estimation approach, which considered the essential ingredient of the analyzer. It does not depend directly on the optical equations such as Lambert Beer's law. Because using these optical equations includes defining some of unknown parameters that is considered the most difficult task. As a new trend and according to the general concept of the optical equations without defining any of their unknown parameters, the proposed approach is based on a unification of two fuzzy expert systems. One provides high interpretability and the other provides high accuracy. The principles of the fuzzy expert system are explained in detail in section 5.4. Therefore, this chapter describes briefly the building of this fuzzy experts system and its own features.

6.2 Building the fuzzy expert system

6.2.1 Defining the crisp inputs and outputs of the fuzzy expert system

The hemoglobin analyzer works according to the spectrophotometry principles. It employed six light emitting diodes with different wavelengths between 600 nm and 950 nm. The outputs of the fuzzy expert system are defined as the tHb concentration and the ratios of COHb, O₂Hb, MetHb, and RHb.

According to the general concept of the optical equations, the measured light intensity is related to the absorption coefficient for the transmitted light and the scattering coefficient of radiation transfer at a certain wavelength [Fen90] [Mig02]. The absorption coefficient depends on the extinction coefficient and the concentration of the medium substance. Where the scattering coefficient describes a medium containing many scattering particles at a concentration described as a volume density and so the scattering coefficient is essentially the cross-sectional area per unit volume of the medium.

If the medium substance is a few drops of blood in a very small size cuvette, the geometry of the medium will be fixed. And, if a number of light sources with different wavelengths are used, the extinction coefficients of the blood components and also the scattering coefficient will be changed according to each wavelength. Figure 6-1 presents the relation between the wavelength of the light source and the related extinction coefficients for the four hemoglobin derivatives. At a certain wavelength, different components of hemoglobin are absorbed to a larger or lesser extent, as illustrated in the figure below.

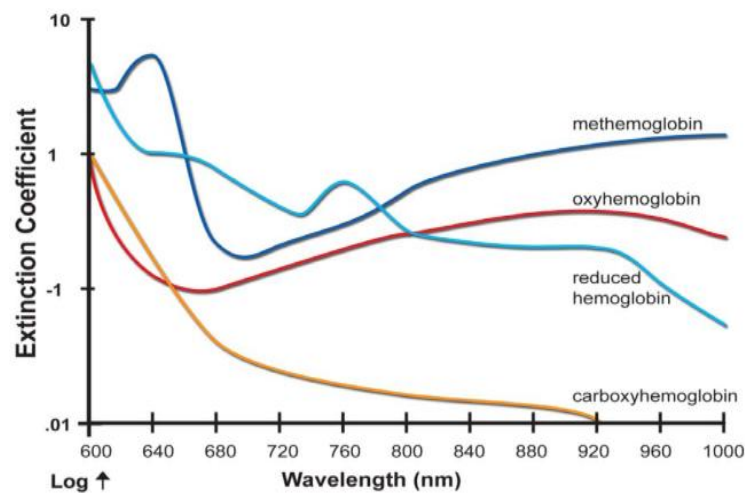


Figure 6-1: Extinction coefficients: ϵ_{O_2Hb} , ϵ_{RHb} , ϵ_{COHb} , and ϵ_{Met-Hb} at wavelengths between 600 nm and 1000 nm [Web98].

Therefore, the concentration of the blood hemoglobin components mainly depends on a combination of a number of measured light intensities with different wavelengths. Six different wavelengths are chosen between 600nm and 950nm. At these wavelengths, different extinction coefficients combinations of the four hemoglobin components can be detected in order to distinguish their ratios and also to estimate the total hemoglobin concentration.

Thus, that system can be modelled where its inputs and outputs are known and the reactions inside the system can be described regardless of solving any complex optical equation. The inputs are a number of light intensity with different wavelengths. And the outputs are the

total hemoglobin concentration and the ratios of the four hemoglobin components (RHb%, COHb%, O₂Hb% and MetHb%).

6.2.2 Employing the fuzzy inference scheme

The fuzzy expert system has six inputs and five outputs that represent the vital physiological parameters. Therefore, the k th fuzzy rules can be expressed based on Mandani's model as follows;

IF i_1 is A_k and i_2 is B_k and i_3 is C_k and i_4 is D_k and i_5 is E_k and i_6 is F_k THEN O_1 is M_k and o_2 is P_k and o_3 is Q_k and o_4 is R_k and o_5 is S_k

where $i_1, i_2, i_3, i_4, i_5, i_6, o_1, o_2, o_3, o_4,$ and o_5 are the linguistic variables that represent the multi inputs multi outputs model. $A_k, B_k, C_k, D_k, E_k, F_k, M_k, P_k, Q_k, R_k$ and S_k are the fuzzy sets of those variables in the universes of discourse $I_1, I_2, I_3, I_4, I_5, I_6, O_1, O_2, O_3, O_4,$ and $O_5,$ respectively.

Based on the compositional operators, the fuzzy output of each vital physiological parameter can be inferred as the result of some steps, as explained in section 5.4.3.2.

6.2.3 Fuzzy rule base generation

The fuzzy rule base is generated by applying Wang-Mendel method. This method requires real input-output data pairs. The inputs are six values of the light intensity with different wavelengths that were measured by the optical stage of the hemoglobin compact analyzer. And the outputs are the values of the total hemoglobin concentration and the ratios of the four hemoglobin components (RHb%, COHb%, O₂Hb% and MetHb%), which were measured with the aid of a reference laboratory. The real input-output data patches are measured by OPTI Medical Company research team. This rule generation method is conducted easily by five steps, which were introduced before in section 5.4.3.3.

6.3 The whole fuzzy expert system

Any fuzzy model faces two challenges to assess its quality [Cas03]:

- Interpretability; it refers to the capability of the fuzzy model to express the behaviour of the system in an understandable way. This is a subjective property that depends on several factors, mainly the model structure, the number of input variables, the number of linguistic terms, the number of fuzzy rules and the shape of the fuzzy sets.

- Accuracy; it refers to the capability of the fuzzy model to faithfully represent the modelled system. It is regards as closeness, we understand the similarity between the response of the real system and the fuzzy model.

To gain the two advantages of the interpretability and the accuracy, two fuzzy models were designed for the whole fuzzy expert system. One provides high interpretability and the other provides high accuracy.

The fuzzy model, which has high accuracy, uses twenty two fuzzy sets to fuzzify all the input variables and eleven fuzzy sets to fuzzify all the outputs. It applies Wang & Mendel (W&M) method to generate the fuzzy rule base.

On the other hand, to increase the interpretability, the other fuzzy model uses 11 fuzzy sets only to fuzzify all the inputs and all the outputs. It applies a new proposed modified version of (W&M) method to generate the fuzzy rule base. This modified one is the same as the original one with the exception of the second step. The second step can be demonstrated as follows:

Step 2: Generate fuzzy rules from the given data. First, determine the degrees of the given data in the different fuzzy sets. Second, obtain two rules from one pair of the input-output data pairs.

The combination of the two models is conducted as follows:

The inputs (six light intensities) are always given firstly to the fuzzy model which has high accuracy,

- If the physiological variables are already calculated, the program will be ended and its results will be considered as the final result of the whole fuzzy expert system.
- If the physiological variables could not be calculated, the program will forward the inputs (six light intensities) to the other fuzzy model which has high interpretability. Therefore, its results will be considered as the final result of the whole fuzzy expert system.

Part III
Results and Conclusions

7. Results and Discussion

7.1 Preliminaries

Non-invasive measuring of total hemoglobin (tHb) concentration and the ratios of oxyhemoglobin (O₂Hb), reduced hemoglobin (RHb), carboxyhemoglobin (COHb), and methemoglobin (MetHb) is the main objective of this thesis. Thus, an optoelectronic measuring system is developed to measure these physiological variables. Two proposed methods are applied for the estimation. The results of the two methods are demonstrated in section 7.2.

Using a few drops of blood, invasive measuring of the same physiological variables is also one of the thesis objectives. A new calculation method is developed which is based on two fuzzy expert systems and according to the general concept of the optical equations for a compact hemoglobin components analyzer. The results are very promising, as depicted in section 7.3.

The final part of this chapter introduces a discussion of the invasive and the non-invasive results.

7.2 Results: non-invasive measuring

The non-invasive measuring system consists of two parts. The first part is the developed optoelectronic printed circuit, which is responsible for extracting the photoplethysmography signals and transferring them as one signal into LabVIEW environment. The second part is responsible for separating the seven PPG signals, processing the signals and extracting their main features, and applying the estimation methods. Two estimation methods are explored for calculating the tHb concentration and

the ratios of COHb, O₂Hb, RHb, and MetHb, as explained in detail in chapter 5. The second part is implemented in LabVIEW in order to calculate these physiological variables online.

The steps of performing an online measurement using the developed non-invasive optoelectronic measuring system are described as follows:

- The finger is put inside the fingertip probe which has seven light emitting diodes (LEDs) with different wavelengths. Seven synchronized photoplethysmography (PPG) signals are generated and transferred into LabVIEW environment via UART of ARM7-ADUC7020 Microcontroller as one signal containing seven PPG signals.
- That transferred signal is recorded for 30 sec. Then, it is separated into the detecting signal of the ambient light and 7 PPG signals with the following wavelengths: 1200 nm, 625 nm, 880 nm, 760 nm, 680 nm, 660 nm, and 565 nm, as shown in the front panel of the LabVIEW online program of the measuring system.
- The effect of the ambient light on the measurements is limited, as its detected signal is taken into account before calculating the terms of AC component, the DC components, I(High) and I(Low), which are extracted by processing the separated PPG signals.
- Then, the two calculation methods are applied, as their inputs are already extracted from the separated PPG signals. The method that is based on the modified Lambert-Beer law is applied using two different equations. One considers the ratio of the AC component and the DC component and the other considers the natural logarithm (ln) of the ratio of I(High) and I(Low). Therefore, the developed non-invasive measuring system calculates tHb concentration and the ratios of COHb, O₂Hb, RHb, and MetHb three times and generates three estimation values for each physiological variable.
- Each online measurement is executed in approximately 50 seconds: 30 seconds for recording the transferred signal and 20 seconds for the separation, signal processing, applying the developed algorithms and generating the results.

The LabVIEW front panel of the program of the non-invasive measuring system is shown by Figure 7-1. The recorded signal that contains the seven PPG signals, marked in red lies to the left of the figure. The separated seven PPG signals are shown on the right side of the same figure. (Result (1)) and (Result (2)) are related to the calculation method that is based on Lambert-Beer law and Fuzzy Test is the results of the method that depends on fuzzy expert systems.

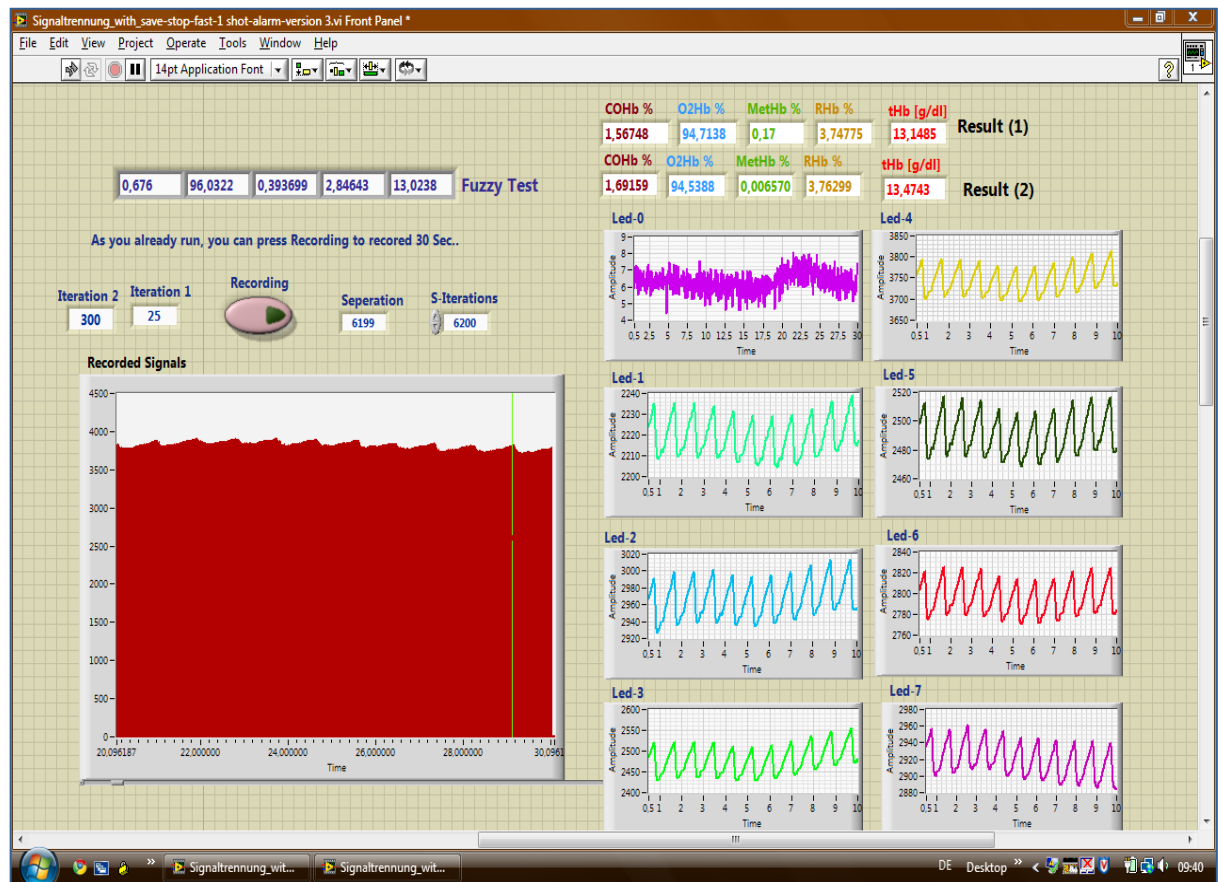


Figure 7-1: The LabVIEW front panel of the non-invasive measuring system.

7.2.1 Results of the method that is based on modified Lambert-Beer law

In chapter 5, two equations are derived according to the modified Lambert-Beer law and the principles of the pulse oximetry. These equations are Eq. (5.25) and Eq. (5.26) and are rewritten considering the ratios of the four hemoglobin components in Eq. (5.29) and Eq. (5.30), respectively.

$$\ln\left(\frac{I_H}{I_L}\right)_\lambda = K_\lambda \ln\left(\frac{I_H}{I_L}\right)_{1200nm} [\varepsilon_{COHb}C_{COHb} + \varepsilon_{O2Hb}C_{O2Hb} + \varepsilon_{MetHb}C_{MetHb} + \varepsilon_{RHb}C_{RHb}]_\lambda \quad (5.25)$$

$$\left(\frac{AC}{DC}\right)_\lambda = K_\lambda \left(\frac{AC}{DC}\right)_{1200nm} [\varepsilon_{COHb} C_{COHb} + \varepsilon_{O_2Hb} C_{O_2Hb} + \varepsilon_{MetHb} C_{MetHb} + \varepsilon_{RHb} C_{RHb}]_\lambda \quad (5.26)$$

$$\ln\left(\frac{I_H}{I_L}\right)_\lambda = K_\lambda(ratio) \ln\left(\frac{I_H}{I_L}\right)_{1200nm} [\varepsilon_{COHb} COHb\% + \varepsilon_{O_2Hb} O_2Hb\% + \varepsilon_{MetHb} MetHb\% + \varepsilon_{RHb} RHb\%]_\lambda \quad (5.29)$$

$$\left(\frac{AC}{DC}\right)_\lambda = K_\lambda(ratio) \left(\frac{AC}{DC}\right)_{1200nm} [\varepsilon_{COHb} COHb\% + \varepsilon_{O_2Hb} O_2Hb\% + \varepsilon_{MetHb} MetHb\% + \varepsilon_{RHb} RHb\%]_\lambda \quad (5.30)$$

Applying Method-1-part1:

By solving two systems of equations using Eq. (5.25) and Eq. (5.29), the tHb concentration and the ratios of COHb, O₂Hb, RHb, and MetHb are calculated after performing cubic Hermite interpolation for K_λ and $K_\lambda(ratio)$. The interpolation of these parameters is executed with the aid of ten invasive measurements and the extracted PPG signals by the optoelectronic system, as explained in detail in section 5.3.5.

Applying Method-1-part2:

By solving two systems of equations using Eq. (5.26) and Eq. (5.30), the tHb concentration and the ratios of COHb, O₂Hb, RHb, and MetHb are calculated after performing cubic Hermite interpolation for K_λ and $K_\lambda(ratio)$, as described in Figure 5-10 and Figure 5-11.

Table 7-1 shows the root mean square errors (RMS) of the results during the offline training stage of applying the Method-1-part1 and the Method-1-part2. At the training stage, the PPG signals that are extracted at the same time of performing the invasive measurements at the reference laboratory (in the range of 12.6 g/dl to 16.5 g/dl) are employed in order to find a solution for the interesting pre-mentioned physiological variables.

Table 7-1: Root Mean Square error (RMS) of the results of the offline training stage (Method-1).

Method	Applied Equations	COHb% [RMS]	O₂Hb% [RMS]	MetHb% [RMS]	RHb% [RMS]	tHb g/dl [RMS]
Method-1-part1	Eq. (5.25) and Eq. (5.29)	0.83	0.898	0.062	0.133	0.31
Method-1-part2	Eq. (5.26) and Eq. (5.30)	0.637	0.645	0.067	0.157	0.23

Table 7-2 presents the root mean square errors (RMS) of the results during the online test stage of applying the Method-1-part1 and the Method-1-part2. At the online test stage, the online measurements were conducted two weeks after the offline training stage, in the same range of the training stage (12.6 g/dl to 16.5 g/dl) and most of the volunteers of the invasive measurements.

Table 7-2: Root Mean Square error (RMS) of the online test results (Method-1).

Method	Applied Equations	COHb% [RMS]	O ₂ Hb% [RMS]	MetHb% [RMS]	RHb% [RMS]	tHb g/dl [RMS]
Method-1-part1	Eq. (5.25) and Eq. (5.29)	0.569	1.371	0.181	0.961	0.75
Method-1-part2	Eq. (5.26) and Eq. (5.30)	0.611	0.499	0.239	0.954	0.63

According to Method-1-part1, Tables 7-3, 7-4, 7-5, 7-6, and 7-7 demonstrate the values of the reference laboratory and their online test non-invasive estimated values for COHb%, O₂Hb%, MetHb%, RHb%, and tHb (g/dl) respectively.

Table 7-3: Reference laboratory COHb% and its non-invasive value (Method-1-part1).

RL COHb%	Estimated COHb%
0.6	1.339
0.6	0.495
1	0.600
1	1.628
2	3.236
0.6	0.600
1	0.557
2	2.283
1	0.995

Table 7-4: Reference laboratory O₂Hb% and its non-invasive value (Method-1-part1).

RL O ₂ Hb%	Estimated O ₂ Hb%
97.010	95.744
96.040	97.057
97.584	99.138
94.867	95.178
96.683	94.484

96.873	97.889
95.865	97.910
96.654	95.361
97.099	96.854

Table 7-5: Reference laboratory MetHb% and its non-invasive value (Method-1-part1).

RL MetHb%	Estimated MetHb%
0.41	0.049
0.39	0.521
0.43	0.507
0.18	0.132
0.34	0.347
0.55	0.464
0.17	0.368
0.37	0.299
0.92	0.623

Table 7-6: Reference laboratory RHb% and its non-invasive value (Method-1-part1).

RL RHb%	Estimated RHb%
1.980	2.867
2.970	1.926
0.986	0.866
3.953	3.062
0.977	1.933
1.977	1.897
2.965	1.166
0.976	2.056
0.981	1.528

Table 7-7: Reference laboratory tHb (g/dl) and its non-invasive value (Method-1-part1).

RL tHb	Estimated tHb [g/dl]
12.6	14.001
12.9	13.104
13	13.339
13.1	13.369
13.9	14.118
14.3	13.12
14.4	13.929
14.6	14.235
16.5	15.55

According to Method-1-part1, Figure 7-2 shows the plot of the reference laboratory measurements of tHb concentration versus the estimated online non-invasive measurements.

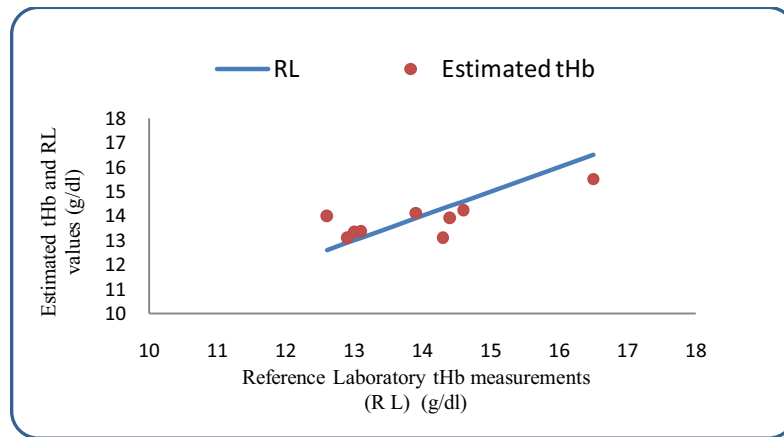


Figure 7-2: Plot of tHb (g/dl) estimated vs. reference laboratory (RL) tHb (g/dl) measurements (Method-1-part1).

According to Method-1-part2, Tables 7-8, 7-9, 7-10, 7-11, and 7-12 demonstrate the values of the reference laboratory and their online non-invasive estimated values for COHb%, O₂Hb%, MetHb%, RHb%, and tHb (g/dl) respectively.

Table 7-8: Reference laboratory COHb% and its non-invasive value (Method-1-part2).

RL COHb%	Estimated COHb%
0.6	0.582
0.6	1.027
1	0.871
1	1.956
2	2.282
0.6	0.192
1	1.967
2	1.680
1	1.982

Table 7-9: Reference laboratory O₂Hb% and its non-invasive value (Method-1-part2).

RL O ₂ Hb%	Estimated O ₂ Hb%
97.010	96.985
96.040	96.359
97.584	97.841
94.867	95.000
96.683	96.077
96.873	97.257

95.865	96.521
96.654	95.814
97.099	96.461

Table 7-9: Reference laboratory MetHb% and its non-invasive value (Method-1-part2).

RL MetHb%	Estimated MetHb%
0.41	0.235
0.39	0.538
0.43	0.363
0.18	0.170
0.34	0.209
0.55	0.459
0.17	0.817
0.37	0.297
0.92	0.834

Table 7-10: Reference laboratory RHb% and its non-invasive value (Method-1-part2).

RL RHb%	Estimated RHb%
1.980	2.198
2.970	2.076
0.986	0.925
3.953	3.328
0.977	1.432
1.977	2.092
2.965	0.694
0.976	2.209
0.981	0.724

Table 7-11: Reference laboratory tHb (g/dl) and its non-invasive value (Method-1-part2).

RL tHb [g/dl]	Estimated tHb [g/dl]
12.6	13.395
12.9	13.491
13	13.634
13.1	13.361
13.9	14.189
14.3	13.527
14.4	14.384
14.6	15.271
16.5	15.5

According to Method-1-part2, Figure 7-3 shows the plot of the reference laboratory measurements of tHb concentration versus the estimated online non-invasive measurements.

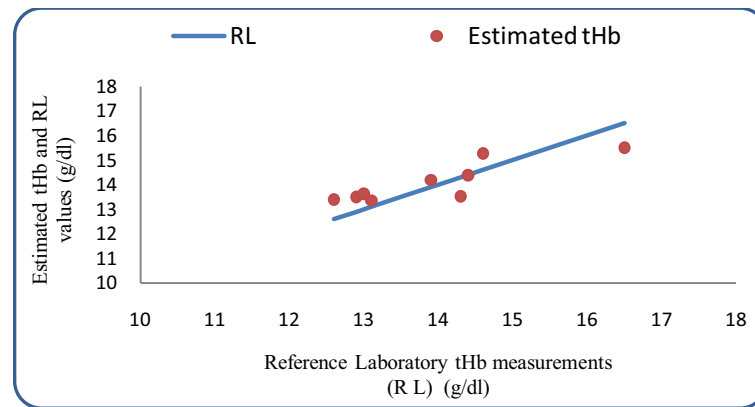


Figure 7-3: Plot of tHb (g/dl) estimated vs. reference laboratory (RL) tHb (g/dl) measurements (Method-1-part2).

Reproducibility test of Method-1:

The reproducibility of the proposed non-invasive measuring system was tested using the calculation method of Method-1-part2. According to the reference laboratory measurement, the tHb concentration of the volunteer is 13 g/dl. Five online non-invasive measurements were executed by the developed optoelectronic measuring system for the same volunteer and by employing different hand-fingers. The non-invasive measuring trials are depicted in Table 7-12. The mean-value of the non-invasive measurements trials is 13.267 g/dl, the variance is 0.305 g/dl, and the standard deviation is 0.552 g/dl.

Table 7-12: Reproducibility test of (Method-1).

Trial No.	Estimated tHb [g/dl]
1	12.57
2	12.9
3	13.6
4	13.3
5	13.965
Mean-value	13.267
St. Dev.	0.552
Variance	0.305

7.2.2 Results of fuzzy expert system algorithm

As explained in detail in section 5.4, a fuzzy expert system is developed to measure the tHb concentration and COHb%, O₂Hb%, RHb%, MetHb%. The fuzzy rule base is generated based on ten invasive measurements of a reference laboratory (see Table 5-3) according to Wang-Mendel method. At the same time of the invasive measurements, the corresponding PPG signals are extracted using the developed optoelectronic system. The extracted features of these PPG signals are used to build the fuzzy rule base as well as the reference laboratory invasive measurements through the offline training stage. Table 7-13 shows the RMS error between the reference laboratory invasive measurements and the results of the offline training stage.

Table 7-13: Root mean square error (RMS) of the results of the offline training stage (method-2).

	RMS error
tHb	0.056 g/dl
MetHb%	0.0095%
O₂Hb%	0.035%
COHb%	0.055%
RHb%	0.043%

Table 7-14 demonstrates the RMS of the results during the online test stage of applying Method-2. At the online test stage, the online measurements were conducted two weeks after the offline training stage, in the same range of the training stage (12.6 g/dl to 16.5 g/dl) and for most of the volunteers of the invasive measurements.

Table 7-14: Correlation (R) and root mean square (RMS) error of the online test results (Method-2).

	RMS error	R
tHb	0.103 g/dl,	0.996
MetHb%	0.015%,	0.997
O₂Hb%	0.075%,	0.995
COHb%	0.055%,	0.995

RHb%	0.15%,	0.991
-------------	--------	-------

According to Method-2, Tables 7-15, 7-16, 7-17, 7-18, and 7-19 demonstrate the values of the reference laboratory and their online test non-invasive estimated values for COHb%, O₂Hb%, MetHb%, RHb%, and tHb (g/dl) respectively.

Table 7-15: Reference laboratory COHb% and its non-invasive value (Method-2).

RL COHb%	Estimated COHb%
0.6	0.640
0.6	0.624
1	0.962
1	0.96
2	2.04
0.6	0.655
1	0.965
2	1.878
1	0.96

Table 7-16: Reference laboratory O₂Hb% and its non-invasive value (Method-2).

RL O₂Hb%	Estimated O₂Hb%
97.01	97.011
96.04	96.007
97.58	97.55
94.87	94.860
96.68	96.724
96.87	96.867
95.87	95.864
96.65	96.445
97.01	97.154

Table 7-17: Reference laboratory MetHb% and its non-invasive value (Method-2).

RL MetHb%	Estimated MetHb%
0.41	0.395
0.39	0.395
0.43	0.433
0.18	0.185
0.34	0.358
0.55	0.545

0.17	0.178
0.37	0.332
0.92	0.913

Table 7-18: Reference laboratory RHb% and its non-invasive value (Method-2).

RL RHb%	Estimated RHb%
1.98	2.018
2.97	2.911
0.986	1.012
3.953	3.892
0.977	1.021
1.977	2.018
2.965	2.911
0.976	1.433
0.981	1.005

Table 7-19: Reference laboratory tHb (g/dl) and its non-invasive value (Method-2).

RL tHb	Estimated tHb [g/dl]
12.6	12.665
12.9	12.99
13	12.99
13.1	13.185
13.9	13.965
14.3	14.355
14.4	14.355
14.6	14.345
16.5	16.462

According to Method-2, Figure 7-4 shows the plot of the reference laboratory measurements of tHb concentration versus the estimated online non-invasive measurements.

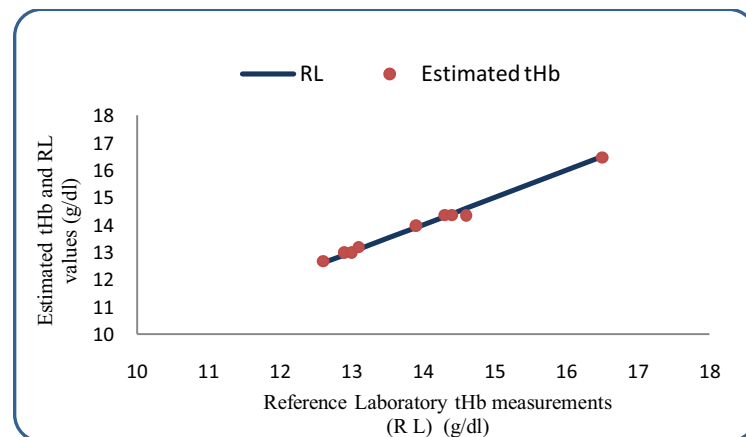


Figure 7-4: Plot of tHb (g/dl) estimated vs. reference laboratory (RL) tHb (g/dl) measurements (Method-2).

Reproducibility test of (Method-2):

The reproducibility of the proposed non-invasive measuring system was tested using the calculation method of Method-2. According to the reference laboratory measurement, the tHb concentration of the volunteer is 12.9 g/dl. Five online non-invasive measurements are executed by the developed optoelectronic measuring system for the same volunteer. The non-invasive measuring trials are depicted in Table 7-22. The mean-value of the non-invasive measurements trials is 12.912 g/dl, the variance is 0.024 g/dl and the standard deviation is 0.155 g/dl.

Table 7-20: Reproducibility test of (Method-2).

Trial No.	Estimated tHb [g/dl]
1	12.99
2	12.64
3	13.01
4	12.93
5	12.99
Mean-value	12.912
St. Dev.	0.155
Variance	0.024

7.3 Results: invasive measuring

The optoelectronic invasive measuring system of the compact hemoglobin analyzer belongs to OPTI Medical Company and all the data patches are extracted by the company research team. It uses a few drops of blood in a small tube and six LEDs with different wavelengths. Six light intensity ratios are the inputs of the whole fuzzy expert system, which consists of two combined fuzzy expert systems, as explained in detail in chapter 6. The outputs of the whole expert system are tHb concentration and the ratios of COHb, O₂Hb, MetHb, and RHb and the inputs are the six light intensity ratios.

The first data patch (D-Patch-1):

The first data patch is 300 measurements. Each measurement comprises six light intensity ratios and the invasive measuring values of a reference laboratory of tHb concentration and the ratios of COHb, O₂Hb, MetHb, and RHb. These measurements are used to build the fuzzy rule base according to Wang-Mendel method as well as the proposed modified Wang-Mendel method.

After building the whole fuzzy expert system, it is tested by hundred and sixty different cases, in the same range of the training data. The accuracy of the proposed approach was tested by means of root mean square error (RMS) and correlation (R) values, as depicted in Table 7-21.

Table 7-21: Correlation and Root Mean Square error (RMS) of (D-Patch-1).

	RMS error	R
tHb(g/dl)	All over the range =0.82 g/dl, below than 14 g/dl= 0.79 g/dl, higher than 14 g/dl= 0.87 g/dl.	0.98
MetHb%	All over the range=3.37%, below than 50%= 2.75%, higher than 50%= 5.8%.	0.99
O₂Hb%	2.99%, All over the range.	0.99
COHb%	2.58%, All over the range.	0.99
RHb%	1.85%, All over the range.	0.98

Scatter plots of the estimated tHb concentrations, RHb%, O₂Hb%, COHb%, and MetHb% versus the corresponding measurements of the reference laboratory are shown by Figures 7-5, 7-6, 7-7, 7-8, and 7-9 respectively.

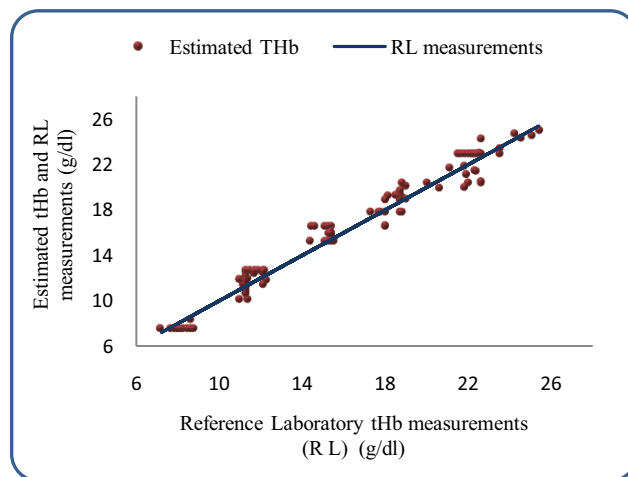


Figure 7-5: Plot of tHb (g/dl) estimated vs. Reference laboratory (RL) tHb (g/dl) measurements (D-Patch-1).

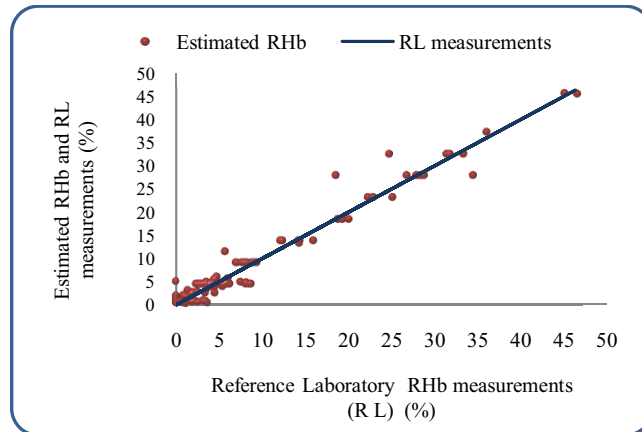


Figure 7-6: Plot of RHB% estimated vs. Reference laboratory (RL) RHB% measurements (D-Patch-1).

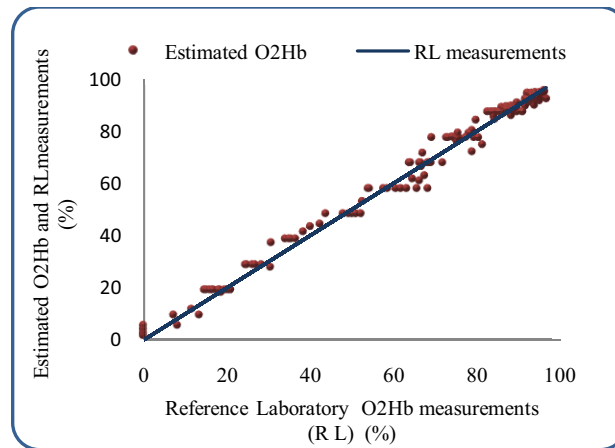


Figure 7-7: Plot of O₂Hb% estimated vs. Reference laboratory (RL) O₂Hb% measurements (D-Patch-1).

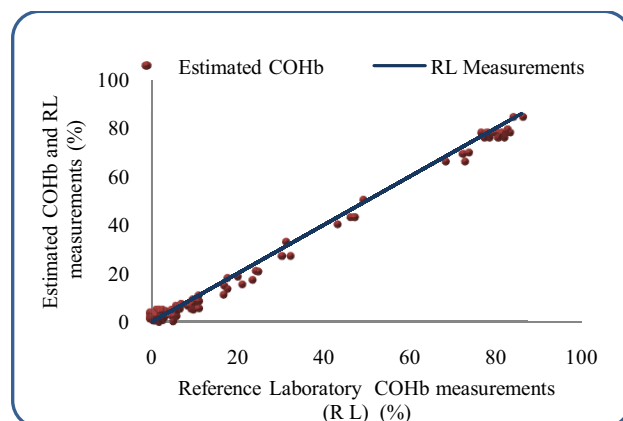


Figure 7-8: Plot of COHb% estimated vs. Reference laboratory (RL) COHb% measurements (D-Patch-1).

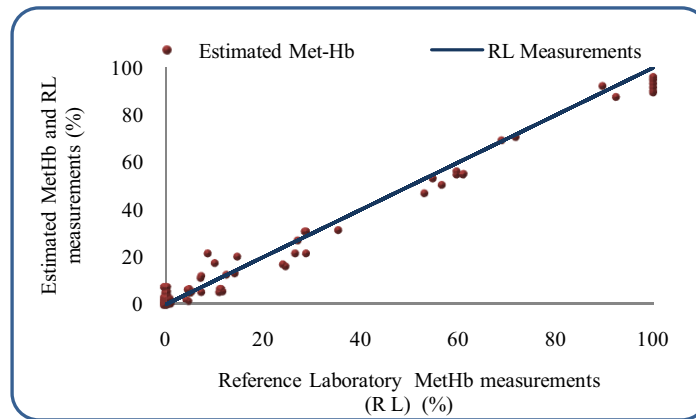


Figure 7-9: Plot of MetHb% estimated vs. Reference laboratory (RL) MetHb% measurements (D-Patch-1).

The second data patch (D-Patch-2):

The OPTI Medical performed some technical changes to its optoelectronic measuring system. Therefore, the algorithms should be redeveloped according to these changes. The second data patch is extracted for 373 measurements. Each measurement comprises six light intensity ratios and the invasive measuring values of a reference laboratory of tHb concentration and the ratios of COHb, O₂Hb, MetHb, and RHb. These measurements are used to build the fuzzy rule base of the two developed fuzzy expert systems according to Wang-Mendel method as well as the proposed modified Wang-Mendel method.

The accuracy of the proposed approach is tested by means of Root Mean Square error (RMS) and Correlation (R) values for the results of the training stage (372 measurements), as depicted in Table 7-21.

Table 7-22: Correlation and Root Mean Square error values of the training stage (D-Patch-2).

	RMS error	R
tHb(g/dl)	0.36 g/dl	0.98
MetHb%	0.8%	0.99
O₂Hb%	1.26%	0.99
COHb%	1.23%	0.99
RHb%	1.28%	0.98

Scatter plots of the estimated tHb concentrations, O₂Hb%, RHb%, COHb%, and MetHb% of the results of the training stage versus the corresponding measurements of the reference laboratory are shown by Figures 7-10, 7-11, 7-12, 7-13, and 7-14 respectively.

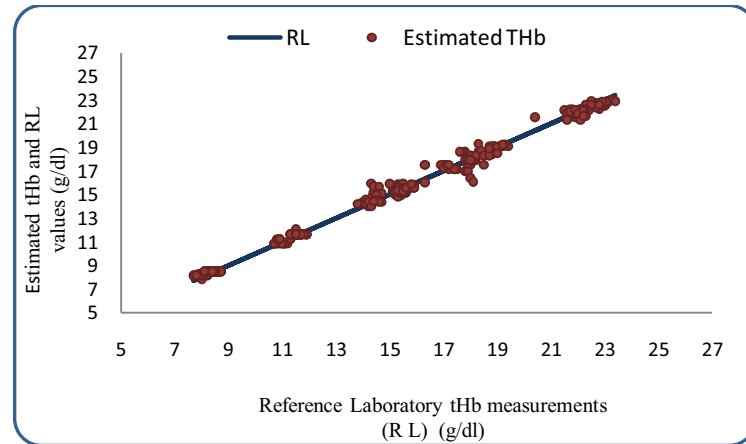


Figure 7-10: Plot of tHb (g/dl) estimated vs. reference laboratory (RL) tHb (g/dl) measurements of the training stage (D-Patch-2).

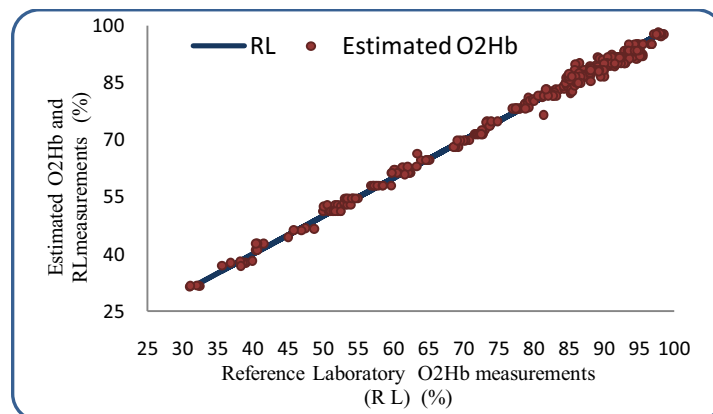


Figure 7-11: Plot of O₂Hb% estimated vs. reference laboratory (RL) O₂Hb% measurements of the training stage (D-Patch-2).

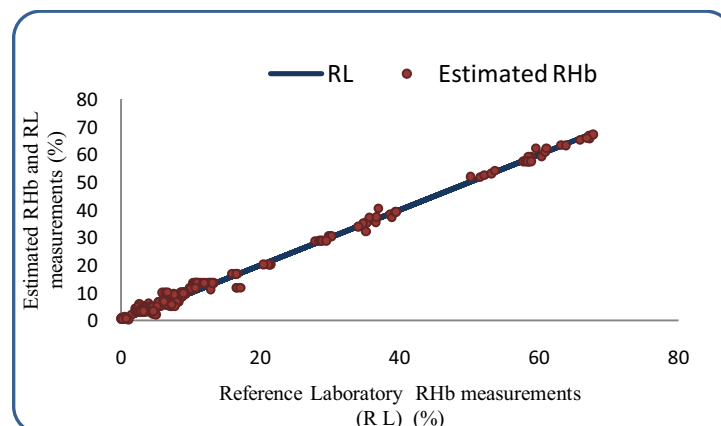


Figure 7-12: Plot of RHb% estimated vs. reference laboratory (RL) RHb% measurements of the training stage (D-Patch-2).

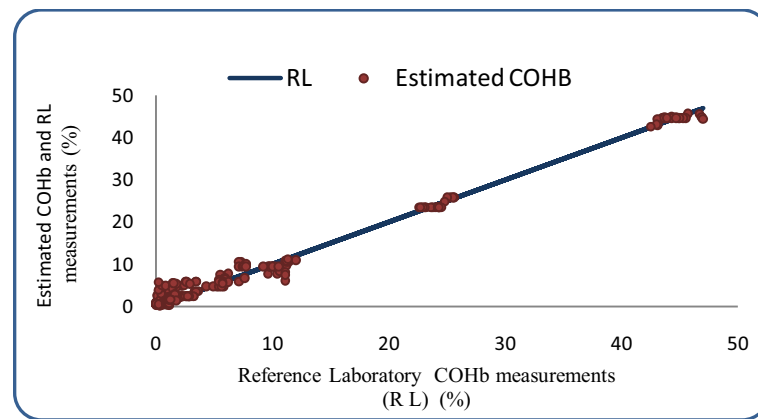


Figure 7-13: Plot of COHb% estimated vs. reference laboratory (RL) COHb% measurements of the training stage (D-Patch-2).

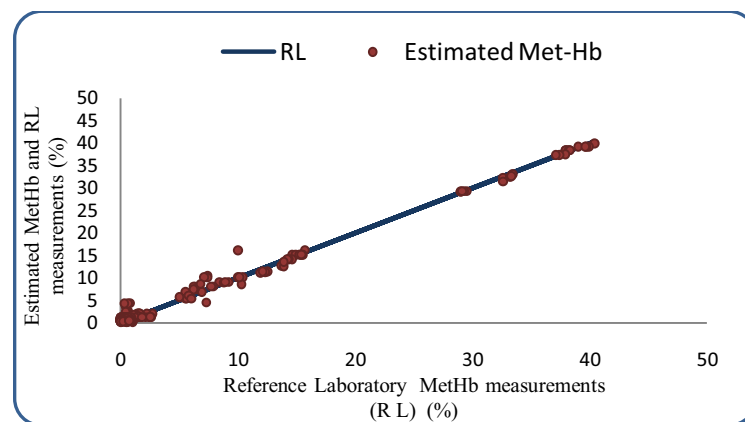


Figure 7-14: Plot of MetHb% estimated vs. reference laboratory (RL) MetHb% measurements of the training stage (D-Patch-2).

The test stage of the second data patch algorithm (Test-D-Patch-2):

This test is performed by OPTI Medical research team after building the algorithm of the whole fuzzy expert system according to the second data patch. For instance, the algorithm is tested by tHb concentration measurements that are not involved absolutely in the second data patch in order to test the ability, effectiveness and reliability of the developed algorithm. As an example, in the second data patch, tHb concentrations steps are (8, 11, 15, 18, 22) g/dl. The tested steps of tHb concentration are (10, 13, 17, 20) g/dl.

Scatter plots of the estimated tHb concentrations of the test stage versus the corresponding measurements of the reference laboratory are shown by Figure 7-15. The accuracy is tested by means of root mean square (RMS) error and the correlation (R), as RMS value is equal to 1.79 g/dl and R is equal to 0.92.

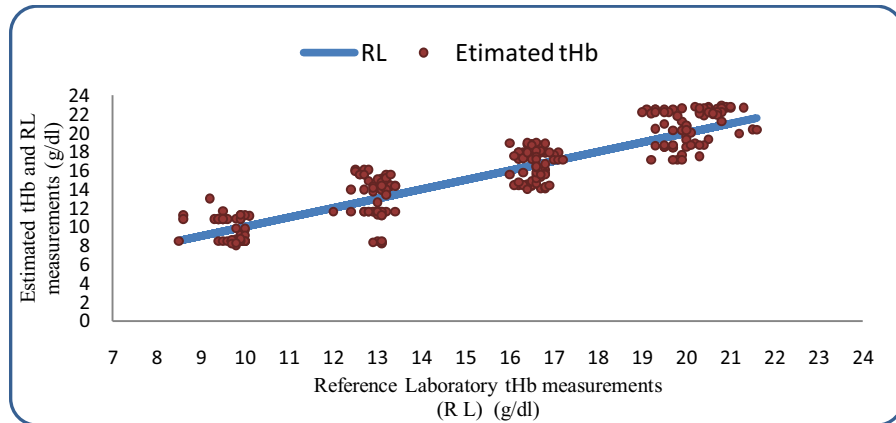


Figure 7-15: Plot of tHb (g/dl) estimated vs. reference laboratory (RL) tHb (g/dl) measurements (Test-D-Patch-2).

7.4 Discussion of the results

7.4.1 Non-invasive measuring results

Method-1:

Method-1 includes two parts, Method-1-part1 and Method-1-part2. Each part employs different equations which are derived according to the principles of pulse oximetry and the modified Lambert-Beer law.

Table 7-1 shows the root mean square (RMS) error between the reference laboratory invasive measurements and the estimated values by Method-1-part1 and Method-1-part2 through the training stage for tHb concentration and the ratios of COHb, O₂Hb, MetHb, and RHb. The RMS error of the applied Method-1-part2 is smaller than the RMS error of applying Method-1-part1 for all the concerned physiological variables except for MetHb%. The difference between the RMS error of Method-1-part1 and the RMS of Method-1-part2 is not large and is acceptable. For instance, it is 0.07 g/dl for the tHb concentration.

Table 7-2 introduces the RMS error between the online test measurements of the developed non-invasive optoelectronic measuring system and the corresponding reference laboratory measurements for the same physiological variables of interest. In this stage, the RMS error of applying Method-1-part2 is also smaller than the RMS error of applying Method-1-part1 for tHb concentration, COHb%, O₂Hb%, and RHb%. For MetHb%, the RMS error of applying Method-1-part1 is smaller than the RMS error of applying Method-1-part2, as in the training stage. The difference between the RMS error of Method-1-part1 and the RMS of Method-1-part2 is acceptable. For the case of O₂Hb%, it is 0.87% and is 0.12 g/dl for the case of tHb concentration. The correlation value (R) is calculated for the results of tHb

concentration by applying Method-1-part1 and Method-1-part2. The non-invasive measurements by applying Method-1-part2 are more correlated to the reference laboratory invasive measurements than the non-invasive measurements by applying Method-1-part1, as R is equal to 0.87 and 0.78 in the case of Method-1-part2 and Method-1-part1 respectively.

In any case, the accuracy of the offline training measurements is higher than the accuracy of the online measurements either for Method-1-part1 or Method-1-part2.

The developed non-invasive optoelectronic measuring system could calculate the tHb concentration within the range of 12.6 g/dl to 16.5 g/dl using Method-1. If the extracted PPG signals could not be processed because of the motion artifact, for example, the developed alarm system will indicate that there are no results. In order to increase the range of the measured tHb concentration, further invasive measurements with the aid of a reference laboratory should be conducted and the algorithms should be redeveloped.

Table 7-2 demonstrates the reproducibility of Method-1 by applying Method-1-part2 that has better results than Method-1-part1. The reference laboratory measurement is 13 g/dl. Five non-invasive online measurements are performed by the developed non-invasive optoelectronic measuring system for the same case. The measuring system is reproducible, as the mean-value of the five trial measurements is 13.267 g/dl and the variance and the standard deviation values are acceptable.

Method-2:

This method is based on a fuzzy expert system, which has four inputs and five outputs. The inputs are extracted features of five PPG signals with different wavelengths and the outputs are tHb concentration and the ratios of COHb, O₂Hb, MetHb, and RHb.

Table 7-13 shows the root mean square (RMS) error between the reference laboratory invasive measurements and the estimated values by Method-2 through the training stage for tHb concentration and the ratios of COHb, O₂Hb, MetHb, and RHb. The RMS error is approximately zero.

The correlation values and RMS error between the online test measurements of the developed non-invasive optoelectronic measuring system and the corresponding reference laboratory measurements for the same interesting physiological variables is introduced by Table 7-14. The estimated values are highly correlated to the reference laboratory measurements, as R values are larger than 0.99. The RMS error values are promising when

compared to the RMS error values of Method-1. Method-2 still needs a large number of invasive reference laboratory measurements to increase the fuzzy rule base in order to build a reliable fuzzy expert system that can interpret the measuring operation of tHb concentration and the ratios of COHb, O₂Hb, MetHb, and RHb with high accuracy.

The reproducibility of the non-invasive measuring system by applying Method-2 is tested as demonstrated in Table 7-20. The reference laboratory measurement is 12.9 g/dl. Five non-invasive online measurements are performed by the developed non-invasive optoelectronic measuring system for the same case. The measuring system is reproducible, as the mean-value of the five trial measurements is 12.912 g/dl. For this method, the variance and the standard deviation values are smaller than their corresponding values for Method-2.

7.4.2 Invasive measuring results

The first data patch (D-Patch-1):

The range of the tHb concentration of this data patch is from 7.2 g/dl to 25.4 g/dl. The fuzzy expert system is built with the aid of three hundred invasive measurements and takes the accuracy and the interpretability into account. The RMS error and the correlation R values are depicted in Table 7-21. The estimated values by the expert system are highly correlated to the reference laboratory measurements, as R values are larger than 0.9. The root mean square error for the tHb concentration is 0.82 g/dl for all over the range.

So far, the OPTI Medical company research team has reported that this new idea (as a new trend) is promising and that the feasibility study has been completed successfully.

The second data patch (D-Patch-2):

After some technical changes for the optoelectronic system, a new data patch is extracted. The range of the tHb concentration is from 7.7 g/dl to 23.4 g/dl. The results of the training stage are promising, as demonstrated in Table 7-22. The root mean square error of the tHb concentration is 0.36 g/dl. The estimated physiological variables are highly correlated to the reference laboratory measurements, as the R values are larger than 0.9.

The test stage of the second data patch algorithm (Test-D-Patch-2):

The algorithm is tested by 300 measurements. The estimated tHb concentration values by the developed algorithm are highly correlated to the reference laboratory, as the correlation

value is larger than 0.9. The root mean square error is 1.79 g/dl. It is considered large for an invasive method even when it uses a few drops of blood. Therefore, the improvement is already being continued, till the time this thesis was being written. The test results are promising and the cause of this large RMS value is being analyzed. It may be because of technical defects or because the algorithm needs some sort of membership function tuning.

8. Conclusions and Future Work

8.1 Preliminaries

In general, the invasive measuring of the physiological variables has many disadvantages, such as blood loss, time consumption, lack of continuous measurements, risk of infection and suffering from pain for some patients. The main objective of this work was to measure tHb concentration and the ratios of COHb, O₂Hb, MetHb, and RHb non-invasively. By measuring tHb concentration and the concentration of O₂Hb, the fractional oxygen saturation can be calculated according to Eq. (3.17).

Also, developing new algorithms for a compact hemoglobin analyzer in order to measure the same physiological variables, using a few drops of blood, was one of the thesis objectives. This chapter summarises the conclusions of the work and proposes topics for future work.

8.2 Contributions and conclusions

8.2.1 Non-invasive measuring

The developed optoelectronic non-invasive measuring system:

The present thesis introduces an optoelectronic non-invasive system, which is based on ARM7-Microcontroller ADUC7020, in order to measure the pre-mentioned physiological variables. It could control the light intensity of seven light emitting diodes in order to overcome the saturated signals. This system extracts seven photoplethysmography (PPG) signals with different wavelengths successfully and transfers them as one signal into LabVIEW environment to be separated and processed. It also gives an indication for the ambient light in order to take it into account during the calculation process.

The signal processing for the extracted PPG signals:

A signal processing module for the case of low-amplitude PPG signals was explored which is based on a unity gain difference amplifier stage and a programmable amplification stage. The quality of PPG signals, which are extracted after the programmable amplification stage, is tested by calculating the signal-to-noise ratio (SNR) values. The PPG signals exhibit good quality, as the SNR values are larger than 40 db.

Using LabVIEW software, a reliable algorithm was developed in order to detect the values and the locations of the peaks and the valleys of the PPG signals. These main distinctive features are considered the cornerstone of any further computations to calculate various physiological variables.

The results of the developed non-invasive measuring system are sensitive to motion artifacts, although the highly corrupted pulses of the PPG signals are neglected for further calculations during the PPG signal processing.

From a more practical standpoint, it should be noted that placing the finger improperly inside the sensor leads to incorrect results, as the results are very sensitive to the position of the finger.

The proposed calculation methods for the non-invasive measuring:

The concentration of tHb and the ratios of COHb, O₂Hb, MetHb, and RHb could be estimated by two proposed methods non-invasively. Therefore, the fractional arterial oxygen saturation can be measured according to Eq. (3.17), as the tHb concentration and the concentration of O₂Hb are calculated by employing Eq. (5.25) or Eq. (2.26). Also, the ratio of the O₂Hb that are measured by employing Eq. (5.29) and Eq. (5.30) is considered fractional arterial oxygen saturation, as the COHb ratio and the MetHb ratio are taken into account during the calculations. However, it should be noted that the invasive measurements have a normal range for COHb%, RHb% and MetHb%. The maximum values of the COHb%, RHb%, and MetHb% were 3%, 3.95%, and 0.95% respectively.

Method-1:

Modified Lambert-Beer law was employed to compensate for the light scattering effect on the optical path length elongation. Two main equations are derived according to modified Lambert-Beer law and the principles of the pulse oximetry. These equations are Eq. (5.25) and Eq. (5.26). As to Eq. (5.26), it is introduced for the first time in order to measure the pre-mentioned physiological variables.

The use of light emitting diode having a wavelength of 1200 nm to indicate Δd was effective and reliable.

Method-1-part1 and Method-1-part2 are employed. The difference between the RMS errors of results of the two parts is not significant, but the estimated results by applying Method-1-part2 are correlated, in a better manner, to the reference laboratory measurements.

Method-2:

As a new trend, fuzzy expert systems were used to measure the pre-mentioned physiological variables in order to overcome defining some parameters (e.g. Δd) which are necessary to be calculated by applying the conventional methods, which are based on various optical equations.

Table 8-1 shows the results of the two proposed methods for the non-invasive measuring for the tHb concentration and the ratios of COHb, O₂Hb, MetHb, and RHb. The results of Method-2 that is based on a fuzzy expert system looks promising when compared to the other conventional method either part1 or part2. However, it needs more reference laboratory invasive measurements with a large range in order to build an accurate fuzzy rule base.

Table 8-1: Root Mean Square error (RMS) of the online test results for the proposed non-invasive methods

Method	RMS errors				
	tHb g/dl	COHb%	O ₂ Hb%	MetHb%	RHb%
Method-1-part1	0.75	0.569	1.371	0.181	0.961
Method-1-part1	0.63	0.611	0.499	0.239	0.954
Method-2	0.103	0.055	0.075	0.015	0.15

8.2.2 Invasive measuring

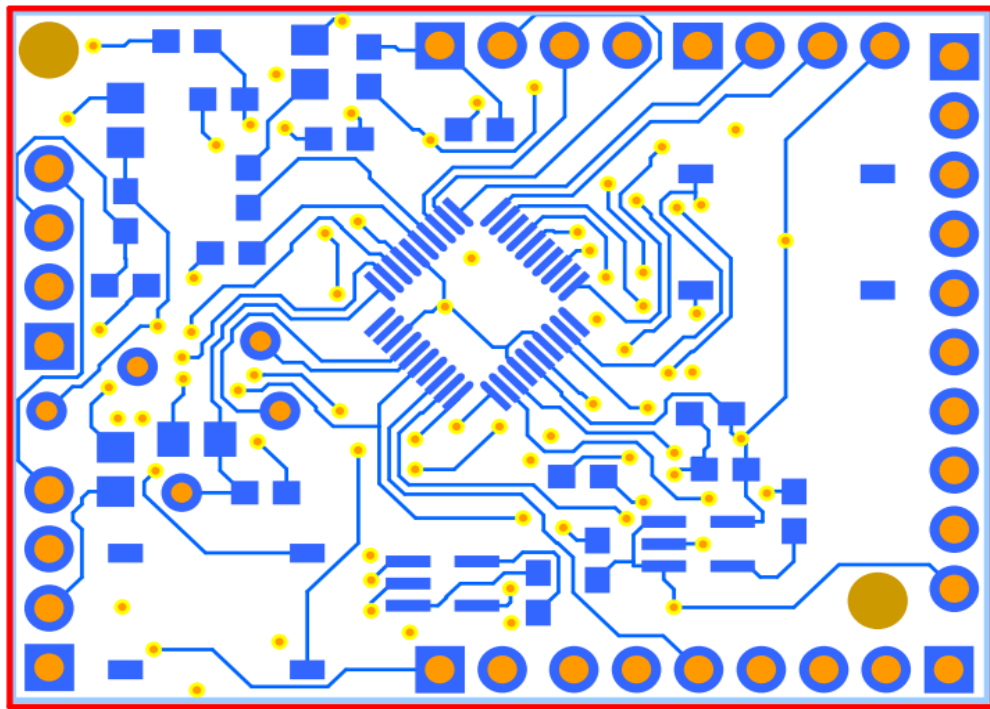
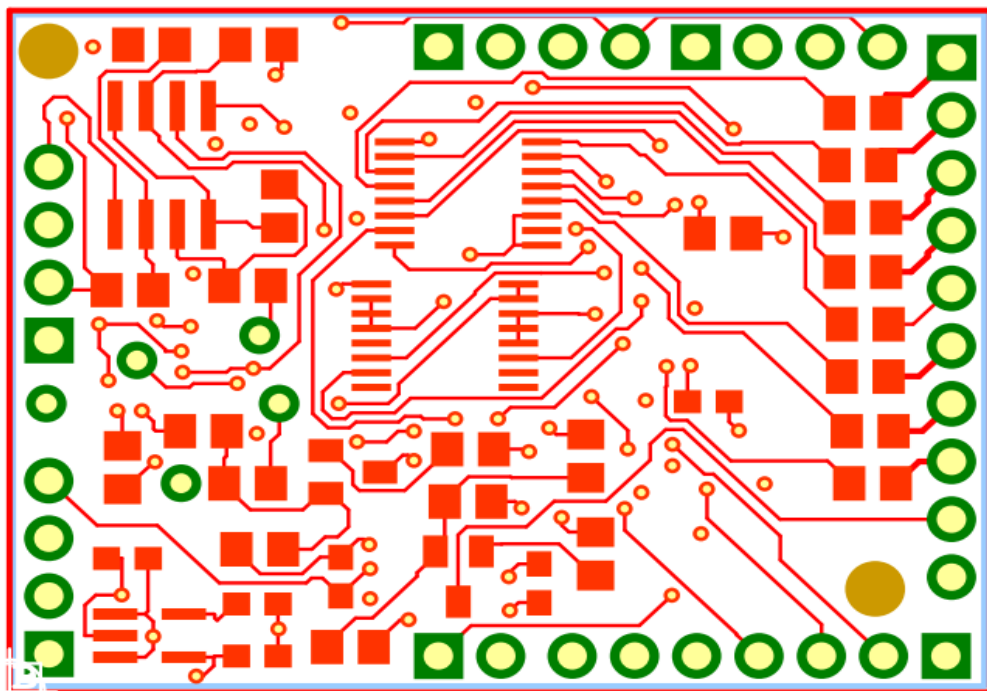
The present thesis developed a new algorithm in order to estimate the pre-mentioned physiological variables invasively using a few drops of blood.

This new trend of using the fuzzy expert systems to calculate the tHb concentration and the ratios of its four components according to the spectrophotometry principles has succeeded

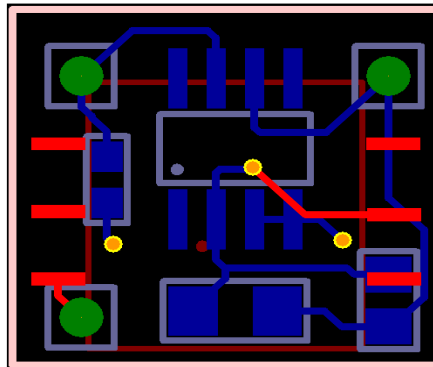
according to the feasibility study, which is conducted by the OPTI Medical Company research team after testing the developed new algorithms. In this respect, fuzzy techniques are a powerful general technology for information processing. The research is still continued in order to increase the accuracy of the measurements.

8.3 Future work

- Develop a reliable motion artifact filter without using any further sensors in order to overcome the motion artifact effect and increase the PPG signals quality.
- Design a new fingertip probe that reduces the sensitivity of the results to the finger position.
- Each online measurement using the developed optoelectronic measuring system needs 50 sec. to be conducted, as 30 sec. for recording the PPG signals and 20 sec. for the signals processing and the calculations. This duration can be reduced by reducing the time of the recorded signals to 10 sec instead of 30 sec. Therefore, each online measurement will need only 30 sec to calculate the physiological variables of interest and the patient will have to put his finger inside the fingertip probe for only 10 sec.
- Conduct new invasive measurements that have a large range and different cases to increase the measuring range of tHb concentration for method1 and also to build an accurate fuzzy rule base in order to develop a more reliable algorithm. This will give the expert system the power to make the decision in an accurate manner.
- Rewrite the algorithms in C language to be implemented in a Microcontroller instead of the LabVIEW environment in order to compact the non-invasive optoelectronic measuring system.
- The accuracy of the new developed algorithms of the invasive measuring can be improved by some modifications, which are based on the genetic algorithms which can accurately parameterize the fuzzy membership functions.

Appendix : The printed circuit layouts**1- Layout of the developed optoelectronic printed Circuit for PPG signals extraction****The layout top surface****The layout bottom surface**

2- Layout of the developed transimpedance amplifier printed Circuit



References

- [Adv11] Advance medical and health products, <http://oximeter.holisticphysio.com/indexE.html>, accessed on 10-Feb-2011.
- [Alb07] Alberts B., 2007. "Leukocyte functions and percentage breakdown". Molecular Biology of the Cell. NCBI Bookshelf, 04-14.
- [All07] Allen J., 2007. Photoplethysmography and its application in clinical physiological measurement, Topical Review. *Physiol. Meas*, Vol. 28, PP. 1-39.
- [Alt11] Altered states net, <http://altered-states.net/barry/update227/index.htm>, accessed on 10-Feb-2011.
- [Bar87] Barker S.J. and Tremper K.K., 1987. Pulse oximetry: applications and limitations *Int. Anesthesiol. Clinics*, Vol. 25, PP. 155-175.
- [Bar87-] Barker S.J. and Tremper K.K., 1987. The effect of carbon monoxide inhalation on pulse oximetry and transcutaneous PO₂. *Anesthesiology*, Vol. 66 (5), PP. 677-679.
- [Bar89] Barker S.J. and Tremper K.K., and Hyatt J., 1989. Effects of methemoglobinemia on pulse oximetry and mixed venous oximetry. *Anesthesiology*, Vol. 70, PP. 112-117.
- [Bel01] Belal S.Y., Taktak A.F.G., Nevill A.J., and Spencer S.A., 2001. A fuzzy system for detecting distorted plethysmogram pulses in neonates and pediatric patients., *Physiological Measurement*, Vol. 22 (2), PP. 397-412.
- [Bel02] Belal S.Y., Taktak A.F.G., Nevill A.J., Spencer S.A., Roden D., and Bevan S., 2002. Automatic detection of distorted plethysmogram pulses in neonates and pediatric patients using an adaptive-network-based fuzzy inference system. *Artificial Intelligence in Medicine*, Vol. 24, PP. 149-165.
- [Beu06] Beutler E., 2006. Disorders of hemoglobin structure: sickle cell anaemia and related abnormalities. In: Lichtman M.A., Beutler E., Kipps T.J., Seligsohn U., Kaushansky K., Prchal J.T. (eds.). *Hematology Williams*. New York: McGraw-Hill, PP. 667-700.
- [Bic05] Bickler P.E., Feiner J.R., and Severinghaus J.W., 2005. Effects of skin pigmentation on pulse oximeter accuracy at low saturation. *Anesthesiology*; Vol.102, PP. 715-719.
- [Bir09] Birnbaum S., 2009. Pulse oximetry: identifying its applications, coding, and reimbursement. *Chest.*, Vol. 135(3), PP. 838-841.
- [Bol02] Bolz A. and Urbaszek W., 2002. *Technik in der Kardiologie*. Berlin: Springer.
- [Bre04] Brecht H.P.F., Prough D.S., Petrov Y.Y., Petrova I.Y., Deyo D. J., and Esenaliev R.O., 2004. Accurate, noninvasive measurement of total hemoglobin concentration with optoacoustic technique, *Proceedings of the 26th Annual International Conference of the IEEE EMBS*, PP. 1-5.
- [Cas03] Casillas J., Cordon O., Herrera F., L. and Magdalena, 2003. *Accuracy Improvements in Linguistic Fuzzy Modeling*. Berlin, Springer.

- [Cha05] Chan G., Middleton P., Lovell N.H., and Celler B.G., 2005. Extraction of photoplethysmographic waveform variability by low pass filtering: Proc. 27th Annual International Conference of the IEEE EMBS, 1st-4th Sept, Shanghai, China.
- [cha74] Challoner A.V.J. and Ramsay C.A., 1974. A photoelectric plethysmograph for the measurement of cutaneous blood flow, *Phys. Med. Biol.* Vol. 19(3), PP. 317-328.
- [Che01] Chernecky C.C. and Barbara J.B., 2001. *Laboratory Tests and Diagnostic Procedures*. 3rd ed. Philadelphia: W. B. Saunders Company.
- [Cin08] Cintra M.E., Camargo H.A., and Monar M. C., 2008. Fuzzy feature subset selection using the Wang & Mendel method. *IEEE Eighth International Conference on Hybrid Intelligent Systems*, PP. 590-595.
- [Cla97] Clark S.A ., 1997. "Normal Transport Oxygen", in *Design of Pulse Oximeters*, J. G. Webster, Ed., Bristol, UK: IOP Publishing, PP. 1-12.
- [Coh05] Cohen D., 2005. The 5th Vital Sign, RT for Decision Makers in Respiratory Care. http://www.rtmagazine.com/issues/articles/2005-10_11.asp, accessed on 10-Jan-2011.
- [Cre11] <http://www.creagbrown.co.uk/anae/pulsox.htm>, accessed on 10-Feb-2011.
- [Dat09] ADUC7020- ARM7 Precision Analog Mikrocontroller (Data Sheet).
- [DeM07] DeMeulenaere S., 2007. Pulse oximetry: uses and limitations. *The Journal for. Nurse Practitioners - JNP*, May, PP. 312-317.
- [Dem98] Demtröder W., 1998. *Laser Spectroscopy*. Springer-Verlag, Berlin.
- [Esp08] http://ep.espacenet.com/advancedSearch?locale=en_EP, accessed on 10-Feb-2008.
- [Esp08] Espacenet database, <http://v3.espacenet.com/results?TI=hemoglobin&AB=noninvasive+fuzzy&sf=a&DB=EPODOC&PGS=10&CY=ep&LG=en&ST=advanced>, accessed on 10-Feb-2008.
- [Fei07] Feiner J.R., Severinghaus J.W., and Bickler P.E., 2007. Dark skin decreases the accuracy of pulse oximeters at low oxygen saturation: the effects of oximeter probe type and gender. *Anesth Analg*, Vol. 105(6), PP. 18-23.
- [Fen90] Fenton M., and Gayeski T.E.J., 1990. Determination of microvascular oxyhemoglobin saturations using cryospectrophotometry. *Am. J. Physiol.* Vol. 259, H1912-H1920
- [Fre08] <http://www.freepatentsonline.com/20070191697.pdf>, accessed on 10-Feb-2008
- [Gal89] Galdun J.P, Paris P.M, and Stewart R.D., 1989. Pulse oximetry in the emergency department. *Am J Emerg Med.*, Vol. 7(4), PP. 422–425.
- [Gan03] Ganong W.F, 2003., *Blood and the immune system*. In: *Review of medical physiology* (21th ed.) New York: Lange Medical Books/McGraw-Hill. P. 518.
- [Gan05] Gang L., Yan W., Ling L. Yuliang L., Xiaoxia L., and Stephen L., 2005. Dynamic Spectrum: a Brand-new Non-invasive Blood Component Measure Method, *Proceedings of the IEEE Engineering in Medicine and Biology 27th Annual Conference Shanghai, China, September*, PP. 1-4.

- [Gan06] Gan K.B., Zahedi E., and Mohd Ali M.A., 2006, Feasibility of Fetal Photoplethysmography Signal Extraction Using Adaptive Noise Cancellation. Proc. 3rd Kuala Lumpur Int. Conf. Biomedical Eng., Kuala Lumpur, PP. 413-419.
- [Geh02] Gehring H., Hornberger, C., Matz, H., Konecny, E., and Schmucker, P., 2002. The effects of motion artifact and low perfusion on the performance of a new generation of pulse oximeters in volunteers undergoing hypoxemia: *Respir. Care*. Vol. 47, PP. 48–60.
- [Gol00] Goldman J.M., Petterson M.T., Kopotic R.J., and Barker S.J., 2000. Masimo signal extraction pulse oximetry. *J Clin Monit Comput.*, Vol. 16, PP.475-483.
- [Gra96] Graham A., 1996, Plethysmography Safety, effectiveness and clinical utility in diagnosing vascular disease. *Health Technol Assess*, Vol. 7, PP. 1-46.
- [Guy06] Guyton A. C. and Hall J. E., 2006. Blood cells, immunity and blood Clotting. In: *Textbook of medical physiology* (11th ed.). Elsevier Inc., PP. 418-81.
- [Har02] Harris C., Hong X., Gan Q., 2002. Adaptive Modelling, Estimation and Fusion from Data, Springer, Berlin.
- [Hem11] Hemocue brochure, <http://www.vitaid.com/Default.asp?l=1&id=17>, accessed on 6 Mars 2011.
- [Her38] Hertzman, A. B., 1938. The Blood Supply of Various Skin Areas as Estimated by the Photoelectric Plethysmograph, *Am. J. Physiol.*, Vol. 124, PP. 328-340.
- [Hil00] Hill E. and Stoneham M.D., 2000. Practical Applications of Pulse Oximetry, *World Federation of Societies of Anesthesiologists*, Issue 11, Article 4.
- [Hir06] Hironori S., Kiyotaka I., Mitsuo U., Sunao T., and Tatsuo T., 2006. Noninvasive measurement of total hemoglobin and hemoglobin derivatives using multiwavelength pulse spectrophotometry -In vitro study with a mock circulatory system-, *Proceedings of the 28th IEEE EMBS Annual International Conference New York City, USA*.
- [Hon00] Hornberger C., Knoop P., Nahm W., Matz H., Konecny E., Gehring H., Bonk R., Frankenberger H., Meyfroidt G., Wouters P., Gil-Rodriguez J., Ponz L., Benekos K., Valais J., Avgerinos ,Karoutis A., Ikiades A., and Weininger S.,2000. A prototype device for standardized calibration of pulse oximeters, Vol. 16(3), PP. 161-169.
- [Hum04] Hummler H. D., Engelmann A., Pohlandt F., Högel J., and Franz A.R., 2004. Accuracy of pulse oximetry readings in an animal model of low perfusion caused by emerging pneumonia and sepsis. *Intensive. Care. Med.*, Vol. 30, PP. 709-713.
- [Joh03] Johansson A., 2003. Neural network for photoplethysmographic respiratory rate monitoring. *Med Biol Eng Comput*, Vol. 41, PP. 242-248.
- [Joh93] John R.E. and Peacock J.E., 1993. Limitation of pulse oximetry. *The Lancet*, Vol. 341(8852), PP. 1092-1093.
- [Jub06] Jubran A., 2006. Pulse oximetry In: MR Pinsky (ed) *Applied Physiology in Intensive Care Medicine*, Springer-Verlag Berlin Heidelberg, PP 29-32.
- [Jub98] Jubran A., 1998. Pulse oximetry. In: Tobin MJ (ed) *Principles and practice of intensive care monitoring*, McGraw-Hill, New York, pp 261–287.

- [Kam02] Kamat V., 2002. PULSE OXIMETRY. *Indian J. Anaesth.*, Vol.46 (4), PP. 261-268.
- [Kam89] Kamal A.A., Harness J.B., Irving G., and Mearns A.J., 1989. Skin hotoplethysmography-a review *Comp. Method.Prog. Biomed.*, Vol. 28, PP. 257–269.
- [Käs99] Kästle S., 1999. Ein Algorithmus zu zuverlässigen Verarbeitung von Pulsoximetrie-Signalen bei schwierigen Störverhältnissen. Logos Berlin, PP. 274-278.
- [Kea04] Keates R.A.B, 2004. Lecture 2, 3, 4. Chem 3560: Structure and Function in Biochemistry. Department of Chemistry and Biochemistry: University of Guelph. <http://www.chembio.uoguelph.ca/educmat/chm356/index.htm>. February 2005, accessed on 10-Feb.-2011.
- [Kee01] Kee, J.L.F., 2001. *Handbook of Laboratory and Diagnostic Tests*. (4th ed.). Upper Saddle River, NJ: Prentice Hall.
- [Kha06] Khattab A.D., Rawlings B., Ali I.S., 2006. Care of patients with haemoglobin abnormalities: history and biology. *Br J Nurs*, Vol. 15, PP. 994-998.
- [Kje00] Kjeldsberg, C., 2000. *Practical Diagnosis of Hematologic Disorders* (3rd ed.). Chicago: ASCP Press.
- [kno06] Knorr B.R., McGrath S.P., Blike G.T., 2006. Using Neural Networks to Identify Airway Obstructions in Anesthetized Patients based on Photoplethysmography, Bioengineering Conference, Proceedings of the IEEE 32nd Annual Northeast.
- [Kno08] Knorr B.R., McGrath S.P., Blike G.T., 2008. Identifying Airway Obstructions Using Photoplethysmography (PPG). *J Clin Monit Comput.* Jan 25; The abstract only.
- [Kra05] Kraitl J., Ewald H., and Gehring H., 2005. An optical device to measure blood components by a photoplethysmographic Method, *J. Opt. A: Pure Appl. Opt.* Vol.7, S318–S324.
- [Kue94] Kuensten J.T., Norris K., 1994. Spectrophotometry of human hemoglobin in the near infrared region from 1000 to 2500 nm. *J. Near Infrared Spectrosc.*, Vol. 2, PP. 59-65.
- [Kye02] Jeon K.J., Kim S.J., Park K.K., Kim J.W., Yoon G., 2002. Noninvasive total hemoglobin measurement, *Journal of Biomedical Optics*, Vol. 7(1), PP. 45–50.
- [Lom11] Lomw Linde University Clinical center, <http://lomalindahealth.org/health-library/condition-guides/28/000210.htm>, accessed on 5-Feb-2011.
- [Lyn06] Lynn L.A. and Lynn E. N., 2006. System and method for sound and oximetry integration, US 2006/0155206 A1.
- [Lyn07] Lynn L.A. and Lynn E. N., 2007. System and method for SPO2 instability detection and quantification, US 2007/0191697 A1.
- [Lyn07] Lynn L.A., 2007. System and method for CO2 and oximetry integration, US 2007/0129647 A1.
- [Man07] Mannheimer P.D., 2007. The Light-Tissue Interaction in Pulse Oximetry, *Anesth Analg.*, 105(6 Suppl), PP. 10-17.
- [Mar05] Mark,T. A. (us), 2005. Multi-domain motion estimation and plethysmographic recognition using fuzzy neural-nets, WO2005/020798 A3.

- [Mar92] Mardirossian G. and Schneider R. E., 1992. Limitations of Pulse Oximetry, *Anesth Prog.*, Vol. 39, PP.194-196.
- [Mas02] Mason L., 2002. Signal Processing Methods for Non-Invasive Respiration Monitoring, This thesis is submitted to the Department of Engineering Science, University of Oxford, in partial fulfillment of the requirements for the degree of Doctor of Philosophy.
- [Mat35] Matthes K, 1935. Untersuchungen über die sauerstoffsättigung des menschlichen arterienblutes. *Arch. Exp. Pathol. Pharmacol.*, Vol. 179, PP. 698-711.
- [MBR11] MPR Company, <http://www.mbr-os.com/index.htm?de/studien.htm>, accessed on 6-Mars-2011.
- [McG96] McGovern J.P., Sasse S.A., Stansbury D.W., Causing L.A., and Light R.W., 1996. Comparison of oxygen saturation by pulse oximetry and co-oximetry during exercise testing in patients with COPD, *Chest.*, Vol. 109(5), PP.1151-1155.
- [Med11] Mediaid Pulse Oximetry.
http://www.mediaidinc.com/Contact/Mediaid_iPOX_OxiBroch_w-models.pdf, accessed on 10-Feb-2011.
- [Men92] Mendelson, Y. Pulse oximetry, 1992. Theory and applications for noninvasive monitoring. *Clin Chem.*, Vol. 38, PP.1601-1606.
- [Mig02] Miguel J., and Higuera L., 2002. Handbook of optical Fibre Sensing Technology. *John Wiley&Sons Ltd.*
- [Moy94] Moyle J.T.B., 1994. Pulse oximetry In: Hahn CEW, Adams AP (eds) Principles and Practice Series. BMJ Publishing Group, London.
- [Nag05] Nagre, A. and Y. Mendelson, 2005. Effects of motion artifacts on pulse oximeter readings from different facial regions, *Proc. IEEE 31st Ann. Northea. Bioeng. Con.*, PP. 220-222.
- [Nat11] Natsche M., 2011. Diplomarbeit: Einsatz des modifizierten Lambert-Beer-Gesetzes mit Fuzzy-Interpolation und kubischer Hermite-Interpolation zur Berechnung der Konzentrationen von Hämoglobinkomponenten.
- [Nef88] Neff T.A., 1988. Routine oximetry: a fifth vital sign? *Chest.*, Vol. 94, PP. 227a-227.
- [Nic04] Nicklin S., Wickramasinghe Y.A., Spencer S. A., 2004. Neonatal intensive care monitoring. *Current Pediatrics*, Vol. 14, PP. 1-7.
- [Nij07] Nijm G.M., Sahakian A.V., Swiryn S., and Larson A.C., 2007. Comparison of Signal Peak Detection Algorithms for Self-Gated Cardiac Cine MRI: Proceedings of the IEEE Computers in Cardiology Conf.
- [Nop10] Noppeney T. and Nüllen H., 2010. *Varikose: Diagnostik-Therapie-Begutachtung*, Publisher: Springer, PP. 83-86.
- [Old07] Old J.M., 2007. Screening and genetic diagnosis of haemoglobinopathies. *Scand J Clin Lab Invest.*, Vol. 67, PP. 71-86.

- [Oml11] OMLC Structure of Heme, <http://omlc.ogi.edu/spectra/hemoglobin/hemestruct>, accessed on 5-Feb-2011.
- [Pee01] Peeters R.T.H., 2001, Cavity Enhanced Absorption Spectroscopy, Thesis Katholieke Universiteit Nijmegen, ISBN 90-9014628-8.
- [Phu01] Phuong N.H., and Kreinovich V., Fuzzy logic and its applications in medicine. *Int-J-Med-Inf.*, Vol.62, PP. 165-173.
- [Pil07] Pilt K., Meigas K., Lass J., and Rosmann M., 2007. Signal processing methods for PPG module to increase signal quality: IFMBE Proc. vol. 16.
- [Pre78] Perutz M.F., 1987. Hemoglobin Structure and Respiratory Transport. *Scientific American*, Vol. 239(6).
- [Psc11] PSC-New Blood, <http://www.psc.edu/science/Ho/Ho.html#hemoglobin>, accessed on 5-Jan-2011.
- [Rus96] Rusch T.L., Sankar R., Scharf, J.E., 1996. Signal processing methods for pulse oximetry. *Comput. Biol. Med.*, Vol. 26, PP. 143–159.
- [Sea99] Sears D.W. 1999. Overview of Hemoglobin's Structure/Function Relationships. <http://tutor.lscf.ucsb.edu/instdev/sears/biochemistry/tw-hbn/hba-overview.htm>, accessed on 1-Jan-2011.
- [Sel07] Selim S., Gregory C., John M., and Gregory J., 2007. Non-invasive determination of hemoglobin by digital photography of palpebral conjunctiva, *The Journal of Emergency Medicine*, Vol. 33(2), PP. 105–111.
- [Sev92] Severinghaus J.W., Kelleher J.F., 1992. Recent developments in pulse oximetry. *Anesthesiology*. Vol. 76, PP. 1018-1038.
- [Sha06] Shafqat K., Jones D.P., Langford R.M., and Kyriacou, P.A., 2006. Filtering techniques for the removal of ventilator artefact in oesophageal pulse oximetry. *Medical and Biological Engineering and Computing*, Vol. 44, PP. 729-737.
- [Shu06] Shmukler M, 2006. "Density of Blood". In: *The Physics Factbook*, 10-04.
- [Sik09] Sik Shin H., Lee C., Lee M., 2009. Adaptive threshold method for the peak detection of photoplethysmographic waveform. *Computers in Biology and Medicine*, Vol. 39(12), PP. 1145-1152.
- [Sol04] Soltane M., Ismail M., Abdul-Rashid Z.A., 2004. Artificial Neural Networks (ANN) Approach to PPG Signal Classification, *Proc. International Conference on Informatics (ICI-2004)*, Turkpp., PP.146-151.
- [Ste03] Stetson P.F., 2003. Determining heart rate from noisy pulse oximeter signals using fuzzy logic. *Fuzzy Systems, FUZZ* . The 12th IEEE International Conference ((Adv. Dev. Group, Nellcor-Tyco Healthcare, Pleasanton, CA, USA)).
- [Str10] Strategic test, http://strategic-test.se/support/download/an-02_measuring%20dynamic%20specifications.pdf, accessed on 10-Feb-2010.

- [Tak06] Takla G., Petre J.H., Doyle D.J., Horibe M., and Gopakumaran B., 2006. The Problem of Artifacts in Patient Monitor Data During Surgery: A Clinical and Methodological Review. *Anesth. Analg.*, Vol. 103, PP. 1196-1204.
- [Tak85] Takagi T. and Sugeno M., 1985. "Fuzzy identification of systems and its applications to modelling and control," *IEEE Transactions on Systems, Man, and Cybernetics*, vol. SMC-15, PP. 116-132.
- [Tall06] Tallitsch R., Martini F., Timmons M., 2006. Human anatomy (5th ed.). San Francisco: Pearson/Benjamin Cummings, P. 529.
- [TbM11] Technical bulletin MASIMO. Accuracy of Noninvasive Spot-Check Testing of Total Haemoglobin with the Masimo Pronto-7™, accessed on 1- Mars-2011.
- [The07] Theodorsson E., Birgens H., Hagve T.A., 2007. Haemoglobinopathies and glucose-6-phosphate dehydrogenase deficiency in a Scandinavian perspective. *Scand J Clin Lab Invest*, Vol. 67, PP. 3-10.
- [Tim01] U. Timma, G. Leena, E. Lewisa, D. McGrathb, J. Kraitlc and H. Ewaldc, 2010. Non-Invasive Optical Real-time Measurement of Total HemoglobinContent, Proc. Euroensors XXIV, September 5-8, Linz, Austria.
- [Tit97] Tittle M. and Flynn M.B., 1997, Correlation of pulse oximetry and co-oximetry. *Dimens Crit Care Nurs*, Vol. 16, PP.88-95.
- [Tor06] Torres A., and J. Nieto, 2006. Fuzzy logic in medicine and bioinformatics. *J Biomed Biotechnology*, 1-7.
- [Unb09] [http://www.unboundmedicine.com/medline/ebm/mesh/ebm/classic?in=kw|Hemoglobinometry\[MH\]&in=jn|&in=au](http://www.unboundmedicine.com/medline/ebm/mesh/ebm/classic?in=kw|Hemoglobinometry[MH]&in=jn|&in=au), accessed on 10-Feb-2008.
- [Unb10] <http://www.patentstorm.us/patents/search-results.html?search=noninvasive+hemoglobin+measurements>, accessed on 10-Feb-2008.
- [Unc11] SI Units for Clinical Data, http://www.unc.edu/~rowlett/units/scales/clinical_data.html, accessed on 10-Feb-2011.
- [Van01] Van de Louw A, Cracco C, Cerf C, Harf A, Duvaldestin P, Lemaire F, Brochard L ,2001. Accuracy of pulse oximetry in the intensive care unit. *Intensive Care Med*, Vol. 27, PP. 1606-1613.
- [Vil99] Villanueva. R., Bell C., Kain Z.N., and Colingo K.A., 1999. Effect of peripheral perfusion on accuracy of pulse oximetry in children: *J. Clin. Anesth.*, Vol. 11, PP. 317-322.
- [Wan03] Wang L., 2003.The WM method completed: a flexible fuzzy system approach to data mining. *IEEE International Conference on Fuzzy Systems*, Vol.11, PP. 768-782.
- [Wan92] Wang L.X., Mendel and J.M., 1992. Generating fuzzy rule by learning from examples, *IEEE-Transactions on Systems, Man, and Cybernetics*, Vol. 22(6), PP. 1414-1427.

- [Wea01] Weatherall D.J, Clegg J.B, Higgs D.R, et al., 2007. The hemoglobinopathies. In: Scriver, CR, Beaudet AL, Sly WS, Valle D, Childs B, Kinzler KW, Vogelstein B (eds.). The Metabolic and Molecular Bases of Inherited Disease. New York: Mc Graw-Hill; PP. 4571-664.
- [Wea06] Weatherall D.J., 2006. Disorders of globin synthesis: the thalassemias. In: Lichtman M.A., Beutler E., Kipps T.J., Seligsohn U., Kaushansky K., Prchal J.T. (eds.). Hematology Williams. New York: McGraw-Hill, PP. 644-66.
- [Web06] Webster J., 2006. Encyclopedia of Medical Devices and Instrumentation, 2nd edition, Vol. 5, p. 239, New York: John Wiley & Sons.
- [Web09] John Webster, 2009.
Medical Instrumentation: Application and Design, 4thEd, Ed., Wiley and Sons.
- [Web95] Weber, W.; Elfadel, IM.; Barker, SJ., 1995. Low-Perfusion Resistant Pulse Oximetry: Journal of Clinical Monitoring, Vol. 11, Issue 4.
- [Web97] Webster J G 1997. Design of Pulse Oximeters (Bristol: Institute of Physics Publishing).
- [Web98] Webster J G 1998.
Medical Instrumentation: Application and Design, 3th Ed, Ed., Wiley and Sons.
- [WHO00] World Health Organization, 2000, Turning the tide of malnutrition: responding to the challenge of the 21st century. Geneva: WHO, (WHO/NHD.007).
- [WHO01] Water Sanitation and Health (WSH) repared for World Water Day 2001. WHO/WSH/WWD/DFS.07
http://www.who.int/water_sanitation_health/diseases/anemia/en/, accessed on 15-Feb-2011.
- [WHO02] World Health Organization, 2002. The world health report 2002—reducing risks, promoting healthy life; WHO.
- [Wie97] Wieben O., 1997. "Light Absorbance in Pulse Oximetry", in Design of Pulse Oximeters, J. G. Webster, Ed., Bristol, UK: IOP Publishing, PP. 40-55.
- [Wik11] Wikipedia. http://en.wikipedia.org/wiki/File:Hb_saturation_curve.png, accessed on 6-Mars-2011.
- [Wip09] Wipo search,
<http://www.wipo.int/tools/en/gsearch.html?cx=000395567151317721298%3Aaqrs59qtb0&q=noninvasive+hemoglobin++measurement+fuzzy&cof=FORID%3A11#500>, accessed on 10-Feb-2008.
- [Wuk88] Wukitsch M.W., Petterson M.T., Tobler D.R. and Pologe J.A. 1988 Pulse oximetry: analysis of theory, technology, and practice, J Clin Monit, Vol. 4 (4), PP. 290-301.
- [Xu08] Xu L., Meng M.Q., Liu R., Wang K., 2008. Robust Peak Detection of Pulse Waveform Using Height Ratio, 30th Annual International IEEE EMBS Conference Vancouver, Canada, PP. 20-24.
- [Yel83] Yelderman M., New W., 1983. Evaluation of pulse oximetry, Anesthesiology, Vol. 59, PP. 349-352.

- [Yoo05] Yoon G., Kim S.J., Jeon K.J., 2005. A Robust design of finger probe in non-invasive total hemoglobin monitor, *Med. Biol. Eng. Comput.*, Vol. 43, PP. 121-125.
- [Zad02] Zadeh L., 2002. From computing with numbers to computing with words-from manipulation of measurements to manipulation of perceptions. *Int. J. Appl. Math. Comput. Sci.*, Vol. 12(3), PP. 307–324.
- [Zbi08] Zbiba K, 2008. Diplomarbeit: Miniaturisierung eines Pulshemometers.
- [Zij00] Zijlstra W.G, Buursma A., and Van Assendelft O.W, 2000. Visible and near infrared absorption spectra of human and animal haemoglobin, VSP: Utrecht, ISBN 90-6764-317-3, accessed on 10-Feb.-2011.

Acknowledgements

I kneel humbly to **God** thanking HIM for showing me the right path, without his help my efforts would have gone astray.

First of all, I wish to express my deep gratitude and thanks to my advisor Prof. Dr. rer. nat. Armin Bolz for the fact that he gave me the opportunity to work in his group and for encouraging, discussions, and suggestions which gave me a direction and inspiration.

I would like to thank the Egyptian Government for the financial support of my scholarship to carry out this work at Karlsruhe Institute of Technology in Germany.

I would like also to express my sincere thanks to Prof. Dr. rer. nat. Josef Guttmann (Uni. Klinik Freiburg) for being the second referee of my thesis.

Many thanks are to OPTI Medical Company in USA which supplied the institute by a large amount of the invasive measurements and also tested the developed algorithms that were developed during this work.

Deep appreciation and thanks is felt to all of my colleagues at the institute of biomedical engineering for their help, fruitful discussions, and guidance throughout the work. I'm also grateful to the students who worked with me for their master thesis.

Apart from the scientific issues, my sincere thanks to Mrs. Irene Günter who was always available and helpful regarding the treatment of administrative issues.

Last but not least, all my love and thanks to my lovely parents and family for their great support, encouragement during my study here alone in Germany. I would like to express my great thanks to all of my friends in Germany and Egypt. Also my great thanks to Prof. Nabila El Rabiee (MU FEE-Egypt) for her help and encouragement.

Publications list and Awards:

Journal Articles:

N. M. El-Rabaie, H. A. Awad, and K. T. Abo-Alam, "Arterial oxygen control using the enhanced fuzzy neural scheme," *Al Azher University Engineering Journal, AUEJ*, vol. 7, no. 1, January, 2004, 45-59

Conferences Contributions:

Abo Alam, K., Abdallah, O. and Bolz A., "New Estimation Approach for Total Hemoglobin Concentration Based on a Fuzzy Expert System" 11th World Congress of Medical Physics and Biomedical Engineering - ISBN-10: 3642038972, Munich, Germany, 2009.

Abo Alam, K., Abdallah, O. and Bolz A., Signal Processing Module to improve Photoplethysmography Signal Quality and Extract its Main Features, in Biomed Tech (BMT), Rostock, 2010

Abo Alam, K., Abdallah, O. and Bolz A., Robust estimation approach for a compact hemoglobin components analyzer based on fuzzy expert systems, in Biomed - The Eighth IASTED International Conference on Biomedical Engineering, Innsbruck, 2011

Abdallah, O., Abo Alam, K. and Bolz, A., "Towards Noninvasive Monitoring of a total Hemoglobin Concentration and Fractional Oxygen Saturation Based on Earlobe Pulse Oximetry", 4th European Congress for Medical and Biological Engineering – ISBN: 978-3540892076, Antwerp, Belgium, 2008.

Abdallah, O., Natsheh, M., Abo Alam, K., Qananwah, Q., Al Nabulsi, A., Bolz, A., Concentrations of hemoglobin fractions calculation using modified Lambert-Beer law and solving of an ill-posed system of equations, SPEI 2010, Brussels, Belgium.

Abdallah, O., Qananwah, Q., Abo Alam, K., Bolz, A., Towards noninvasive method for the detection of pathological tissue variations by mapping different blood parameters, SPEI 2010, Brussels, Belgium.

Abdallah, O., Piera Tarazona, A., Martinez Roca, T., Boutahir, H., Abo Alam, K. and Bolz, A., "Photoplethysmogram Signal Conditioning by Monitoring of Oxygen Saturation and

Diagnostic of Cardiovascular Diseases”, 4th European Congress for Medical and Biological Engineering – ISBN: 978-3540892076, Antwerp, Belgium, 2008.

O. Abdallah, A. Piera Tarazona, T. Martínez Roca, K. Abo Alam and A. Bolz, adaptive motion artifact filter for photoplethysmogram extraction, 3rd International Conference on Bio-inspired Systems and Signal Processing, Valencia (Spain), 2010.

Symposiums Abstracts Contributions:

Abo Alam, K., O. Abdallah, H. Boutahir, A. Bolz, Photoplethysmograms Extraction to Investigate Non-invasive Total Hemoglobin Sensor, 1st KIT Ph.D Symposium on, Karlsruhe, Germany, 2009.

Abo Alam, K., Abdallah, O. and Bolz A., Robust estimation approach for a compact hemoglobin components analyzer based on fuzzy expert systems, 2nd KIT Ph.D Symposium, Karlsruhe, Germany, 2010.

Awards:

Award of the father of Prof. Dr. Eng. Mohamed Ibrahim that is granted to the Top Graduate Student of the Year 1999. Faculty of Electronic Engineering, Minoufia University, Egypt.

Curriculum Vitae

Personal Data:

Name Kawther Abo Alam
Place of birth El-Menoufia, Egypt
Nationality Egyptain
E-mail address Kawtheraboalam@yahoo.com

University Education:

At El-Menoufia University, Faculty of Electronic Engineering.

Duration	Certificate	Approval Date
1994-1999	B.Sc. of Electronic Engineering, Automatic Control & Measurements Eng. Dept.	May 1999 With excellent and honored degree.
1999-2000	M. Sc. Courses	October 2000
2000-Jan. 2005	M. Sc. Degree	January 2005

The Topic of M.Sc. Thesis:

(Fuzzy Neural Control for Hypoxemia)

Employment:

Employer	Duration	Position
Industrial Electronics and Automatic Control Dept., Faculty of Electronic Eng., El- Minoufia University, Egypt.	13.05.2000 till 14.03.2005	Demonstrator
Industrial Electronics and Automatic Control Dept., Faculty of Electronic Eng., El- Minoufia University, Egypt.	15.03.2005 till 09.02.2007	Assistant lecturer
Biomedical Engineering Institute, Karlsruhe Institute of Technology, Germany.	30.09.2007 till now	Ph.D Student Research Assistance

